Homochirality via Supramolecular Catalysis

Combining Covalent and Non-Covalent Chemistry to Amplify Enantiomeric Excess in a Hydrogenation Reaction

van Basten, Jule

Award date:
2022

Title: Homochirality *via* Supramolecular Catalysis: Combining Covalent and Non-Covalent Chemistry to Amplify Enantiomeric Excess in a Hydrogenation Reaction.

Name: Jule van Basten

Composition of assessment committee: E.W. Meijer, A.R.A. Palmas, I.A.W. Filot

Size: 45 ECTS

Date: 23-09-2021

Track: Molecular Systems and Materials Chemistry

This graduation project was established in accordance with the rules of the TU/e Code of Scientific Conduct

Department of Chemical Engineering and Chemistry

Molecular Science & Technology

Master thesis

Homochirality *via* Supramolecular Catalysis

Combining Covalent and Non-Covalent Chemistry to Amplify Enantiomeric Excess in a Hydrogenation Reaction

Author
Jule van Basten
0938221

Supervisor
Prof. Dr. E.W. Meijer
Dr. T. Schnitzer

Advising Committee
Prof. Dr. Ir. A.R.A. Palmans
Dr. Ir. I.A.W. Filot

September 15, 2021

Abstract

The origin of homochirality in life still is a point of debate. While the significance of homochirality has been studied in more detail, the question of how life became homochiral remains one of the big challenges of the 21st century. E.g. chiral initiators, such as polarized light, might have accounted for low enantio imbalances (*ee* <2%) in the first organic molecules. However, to realize high enantioenrichment, as seen in biological compounds, an amplification pathway is needed. In this thesis we propose a new strategy to use a catalytically active supramolecular scaffold to amplify enantioselectivity. We will explore a supramolecular helical assembly based on benzene-1,3,5-tricarboxy amides (BTAs) as catalyst for a stereoselective hydrogenation reaction. For this purpose, we designed a system, in which the reaction product of the hydrogenation is the stimulus that biases the helical screw-sense of the supramolecular scaffold. As such, the enantiomeric excess of the product is reflected in the screw sense of the supramolecular helix. Resulting in an autocatalytic amplification system.

In chapter 1, an introduction in asymmetric chemistry is given. The use of chiral metal/ligand complexes as well as supramolecular scaffolds in catalytic asymmetric hydrogenation reactions is analyzed. We review most proficient strategies used so far to amplify enantioselectivity and combine these findings in our strategy to realize high enantioenrichement. Opposed to previously reported strategies, in our system the substrate will be part of the catalytic BTA scaffold and converted to the product it can bias the helical screw-sense of the supramolecular stacks. Hereby, the enantioselective product will amplify its own formation without the need of a chiral ligand and metal.

In chapter 2, the synthesis of four different BTAs is discussed, which later serve as achiral substrate, achiral comonomer or enatiopure product in the catalytic supramolecular system.

In chapter 3, the self assembly properties of BTAs into helical supramolecular polymers is investigated. The solubilization effect of different solvents is studied with respect to the stability of the homopolymers. We found that all homopolymerizations are described by cooperative polymerization mechanisms. Furthermore, the limits of chiral amplification is examined via 'Sergeants-and-Soldiers' principle. The experiments showed that the newly designed BTA monomers follow the previously established rules of amplification.

In chapter 4, the asymmetric hydrogenation of substrate BTAs is examined. As the hydrogenation of substrate BTAs has not been reported in literature, first optimized reaction conditions for the reduction were established. A literature study identified metal precursors and chiral ligands used in the optimization. The conducted reaction condition screenings showed that an increase in pressure, amount of chlorinated solvent and higher catalyst loading all increase the conversion. Besides, for all but one ligand, good catalytic reactivity is observed. Remarkably, even triphenylphosphine showed excellent reactivity (>99%) in the hydrogenation reactions. This result motivated synthesis of asymmetric ligand BTA, which was successfully tested in the hydrogenation of substrate BTA (38% conversion).

The last chapter focuses on irreproducibility issues encountered throughout the experiments performed for this project – both in the characterization of the assemblies and the hydrogenation reactions. The water content of the solvents, impurities, samples volumes, and hydrogenation pressure and source were identified as dominant factors that caused not reproducible results.

This thesis ends with a conclusion on the current state of progress for the asymmetric hydrogenation using a supramolecular catalyst for amplification. Furthermore, next steps such as, possible methods to determine enantioselectivity and testing the catalytic BTA scaffold in presence of small enantio imbalance are recommended. Following these suggestions, we envision that a catalytic supramolecular system might be established which can amplify small enantio imbalances as e.g. present in the early days of life which might ultimately bring us a step closer to answer the question *'how life became homochiral?'*.

Contents

1 Introduction

1.1 Chirality and Asymmetric Synthesis

Organic compounds are all around us. These molecules are composed of covalently linked carbon and hydrogen atoms.[1] The chemical bonds that connect the atoms provide the molecules with chemical energy, a key for the chemical processes of life. Different relative arrangement of the atoms to each other, yet connected by the same amount of bonds leads to altering of the structure and the chemical energy of a molecule. This is especially important for isomers, molecules possessing the same chemical formulas, but having different structural arrangement.

In chemistry two types of isomers are known, constitutional isomers and stereoisomers.[1–3] In constitutional isomerism the connectivity between atoms is altered. in contrast to stereoisomers, where the connectivity of the atoms is the same but their placing in space differs. One differentiates two types of stereoisomers: enantiomers and diastereoisomers. While enantiomers are stereoisomers, which relate to each other as mirror images, diastereoisomers are all stereoisomers that are not enantiomers.

Enantiomers are particularly fascinating as they are different types of molecules, but contain the same chemical energy.[1] Molecules that are enantiomers to each other are chiral. The word chiral is derived from the greek $\chi\epsilon\iota\rho$ (kheir) "hand" and similar to a hand, they are non imposable. Amino acids are typical examples of chiral molecules (Fig. 1.1). They contain so called stereogenic center: a (in this case) carbon atom that bears four different substituents. The substituents take a tetrahedral shape, so if a molecule is turned 180° it would not have the same spatial arrangement as its enatiomer. Similar to hands when the left hand is placed atop the right hand there is no way our thumbs can be placed directly over each other.

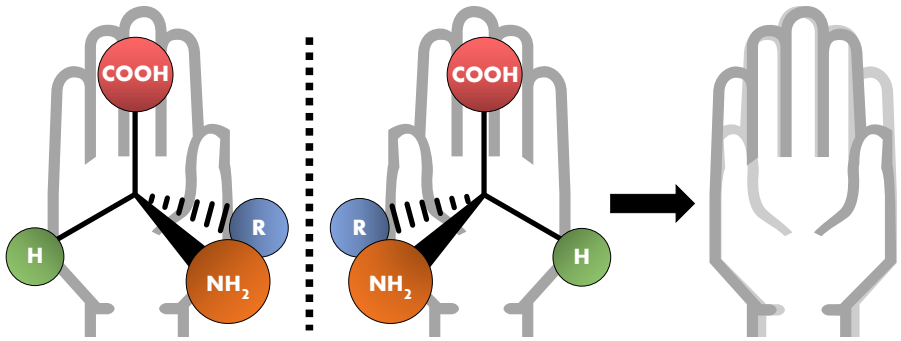

Figure 1.1: *Two enantiomers of general amino acid (left), which are non superimposible mirror images of one another, represented by hands (right).*

Chirality is a property not solely ascribed to molecules with a stereogenic center.[1, 3] A special class of isomers possess axial chirality as stereogenic element. For example, in substituted biaryl compounds rotation about the aryl-aryl bond would interconvert enantiomers but the barrier of rotation about that bond is so large that enantiomers do not interconvert. This is called atropisomerism.[1] This group of molecules that lack point chirality can be considered helical and have shapes related to screws or propellers.

Despite enantiomers sharing the same physical properties (e.g. boiling point, density and polarity) they are in fact distinct chemical entities.[1] Enantiomers can be differentiated by their optical activity. A chiral molecule is optically active, as plane polarized light that passes through a solution of one enantiomer, is rotated. If one enantiomer rotates the light clockwise the other would rotate the light counter clockwise. These two enantiomers will besides rotating linear polarized light also show differential absorption of left- and right-handed circular polarized light. This is related to their chiroptical property and can be measured by circular dichroism (CD) spectroscopy. This fact is used to distinguish enantiomers without having to identify their exact chemical structure. The common stereo descriptors used to describe the handedness of a stereogenic center are (R) and (S) (rectus and sinister) and (M) and (P) (minus and plus) for atropisomers.[1] A set of optically active enantiomers can have a net optical activity of zero if these enantiomers are present in a 1:1 mixture. Such a mixture is called a racemate. The ratio of of enantiomers is expressed by the enantiomeric excess, *ee*. It is the difference between the major enantiomer over the minor enantiomer, Eq. (1).[2]

$$ee\,(\%) = \frac{R-S}{R+S} \times 100\% \tag{1}$$

In the early 19^{th} century Jean Baptiste Biot[4] discovered that a tartaric acid solution rotates plane polarized light clockwise. In that time, Biot also found an optical inactive form of tartic acid, racemic acid. He concluded that this change in direction was in fact a rotation of light, and that its basis was of molecular origin. Hereby he identified optical activity.[5]

A decade later, Louis Pasteur[6] studied crystalline forms of tartaric and racemic acid. He found that, under certain conditions, crystals originating from racemic acid formed two distinct enantiomorphic crystals. With tweezers he separated the crystals, and found that a solution of one group of crystals rotated plane polarized light clockwise, while a solution of the other group rotated it counterclockwise.[5, 7] In this way, Pasteur used crystallization – a strategy that could be recognized as supramolecular chemistry – to enantiomerically pure products. From that point on, crystallization was further developed as a strategy to obtain purify steroisomers of a product. Only in the mid 20^{th} century, new strategies, such as asymmetric synthesis, were developed that used stereoselective covalent reactions to obtain a single stereoisomer of a compound of interest.

1.1.1 Asymmetric Synthesis

In 1960s, the groups of Knowles, Noyori and Sharpless reported on their pioneering work in the asymmetric synthesis of α-amino acids, secondary alcohols and epoxides, respectively.[8–11] Although the enantiomeric excesses of the obtained products were (compared to modern standards) low, these were the first examples of using enantiomerically pure catalysts to yield reaction products with ~15% enantiomeric excess. To highlight the importance of these findings, in 2001, William S. Knowles, K. Barry Sharpless and Ryoji Noyori were awarded with the Nobel Prize in chemistry for *"their work on chirally catalysed hydrogenation reactions and chirally catalysed oxidation reactions."*[12]

Knowles discovered that a complex formed between rhodium(I) and phosphanes could catalyze asymmetric hydrogenation of functionalized olefins.[8, 13] Phosphorus, like carbon, can be chiral when four or three (the lone pair on phosphorus is also a substituent) different substituents are attached. He used these chiral phosphines (Scheme 1a) as ligands in the asymmetric synthesis of phenylacetic acid derivatives and α-amino acids. They were monodentate ligands combined with Rh(III).

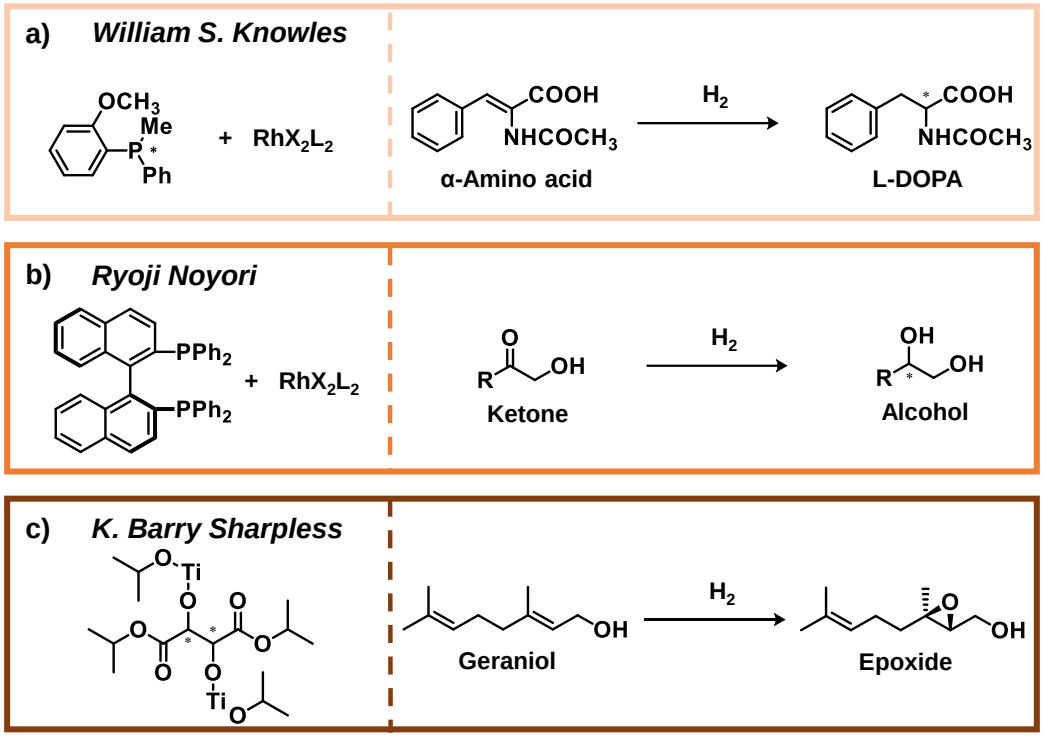

Scheme 1: *Asymmetric hydrogenation reactions of (a) α-amino acid to L-DOPA with chiral rhodium(I)/phosphine catalyst as proposed by Knowles and (b) unsubstituted ketone to a secondary alcohol with chiral rhodium(III)/BINAP catalyst as proposed by Noyori. (c) Asymmetric epoxidation reaction with chiral titanium(IV)/tartate diester complex as proposed by Sharpless.*

Noyori focussed on the development of more stereoselective catalysts.[14] He introduced chiral, atropisomeric binaphthylphosphine (BINAP) ligands which yielded chiral catalysts with ruthium(I)

(Scheme 1b).[15, 16] It was a C_2-symmetric bisphosphane ligand and the chirality in BINAP was the result of the carbon backbone. The angle between two naphthyl groups is approximately 90° creating opposite placement for the phosphine groups. These catalysts were successfully used in the the asymmetric hydrogenation of functionalized ketones, olefins and enamines.[17, 18]

In the same period Sharpless started his work of asymmetric epoxidation on geraniol, a trisubstituted olefin with two C-C double bonds.[9, 19] It presented a huge challenge to regio- and enantioselective oxidate geraniol, as it is possible to synthesize four different monoepoxides. Remarkably, Sharpless found that the same chiral organic molecule - tartaric acid - which had previously been enantiomerically pure isolated by Pastuer, served as ligand for asymmetric epoxidationn reactions. Herein, a chiral tartrate diester bonded to titanium(IV) forms the catalytic complex (Scheme 1c). The stereochemistry of chiral diisopropyl tartrate determines the stereoselectivity of the asymmetric epoxidation reaction of allylic alcohol substrates. [20, 21]

Since the development by Knowles and Noyori, asymmetric hydrogenations established as one of the most powerful tools to synthesize enantiomerically enriched compounds. Yet, the catalysts developed focused on the reduction of carbonyl compounds and imines providing chiral alcohols and amines. But, in paricular the reduction of C-C double bonds is desired as alkenes would serve as starting materials for chiral hydrocabon scaffolds.

In 1993, Andreas Pfatz reported on iridium complexes with a phosphanodihydrooxazole (PHOX) ligand as efficient stereoselective catalyst for the hydrogenation of alkenes (Fig. 1.2).[22] He showed the remarkable capacities of this catalyst as they were able to hydrogenate a wide variety of functionalized and unfunctionalized olefins as well as iminies with high conversion and stereoselectivity (>95%, >85% *ee*).[23–27] Even tocopherol and farnesol derivatives containing multiple double bonds were obtained in high yield and stereoselectivity (>99%, >98% *ee*) (Fig. 1.2).[28, 29]

The high reactivity of the developed Ir catalysts stimulated research on the underlying reaction mechanism. Multiple pathways for iridium catalyzed hydrogenations are observed depending on hydrogen pressure, substrate and temperature.[30] Of the numerous mechanisms possible the general consent is distinction between two pathways.[31] Both pathways start with a solvated Ir(III)-dihydride complex (species I in figure 1.2) followed by exchanging solvent molecules with olefin and hydrogen (species II). The last step is a reductive elimination (species III). The mechanisms differentiate between the transition states. The coordinated hydrogen can either undergo oxidative addition to an iridium-olefin-hydride complex followed by reductive elimination of saturated hydrocarbon (orange mechanism) or methathesis reaction with the olefin also followed by reductive eliminiation (blue mechanisms).[23, 31–33]

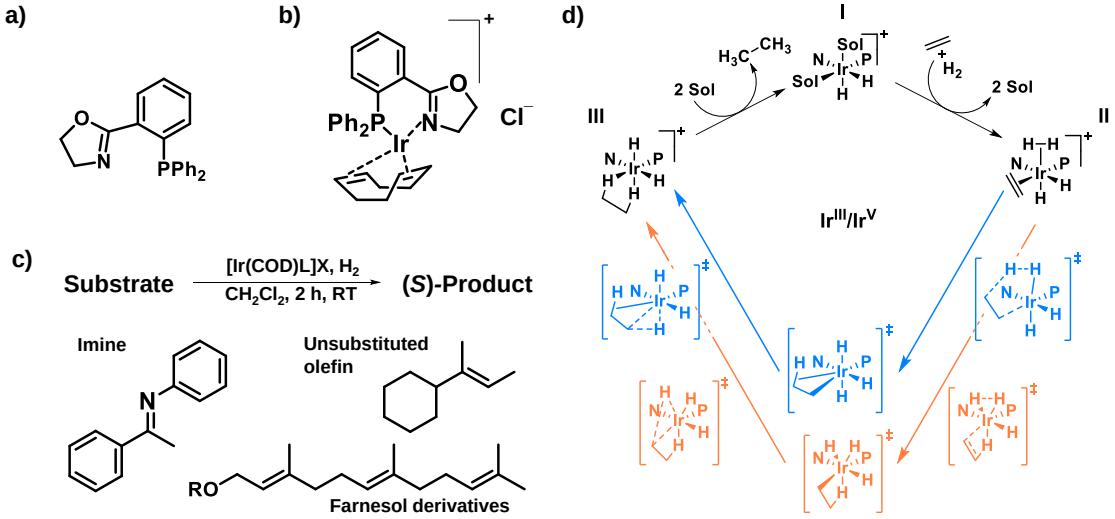

Figure 1.2: *A) General PHOX ligand. B) Representation of iridium/PHOX catalyst. C) Substrate classes hydrogenated by Ir/PHOX catalyst. COD = cyclooctadiene, L = ligand, X = halide anion. D) Catalytic cycle for iridium/phosphinooxazoline catalyzed hydrogenation of unfunctionalized olefins as proposed by P. Brandt (blue cycle)[34] and Burgers and Hall (orange cycle)[32]. Sol = solvent molecule. Figure adjusted from [31].*

After years of research scientists are now able to perform stereoselective reactions resulting in formation of almost enatiopure compounds. The catalytic mechanisms involved in these reactions were elucidated, which led to even higher enantioselectivities for the chiral catalysts. This shows us that catalytic asymmetric hydrogenation reactions are a powerful tool to induce chirality from an

achiral substrate.

1.2 Homochirality in Nature

Life is homochiral. Hence, all chiral molecules occur in one preferred handedness: D-sugars in DNA or RNA and L-amino acids in proteins.[1] As all amino acids are chiral, enzymes are also chiral, which produce all these chiral natural products. So nature distinguishes between two enantiomers of a given molecule because enzymes act as asymmetric catalyst governing the formation of only one enantiomer of these chiral products.[1, 35]

It remains unknown how life became homochiral. Miller and Urey showed how molecules essential for life, such as alanine and aspartic acid, could emerge from the prebiotic environment.[36, 37] Yet, they were all racemic mixtures of D and L enantiomers. While this was an important step in understanding the origin of life, it is not clear how enantiomerically pure compounds, required for homochirality, arose. This requires amplification of small enantio imbalances.

Chiral initiators, such as circular polarized light, asymmetric photoselection or parity violation could have accounted for small enantio imbalances (*ee* <2%) in these chiral prebiotic molecules.[38–40] Several routes can lead to the generation of high enantiomeric excess from achiral mixtures with small quantities of chiral impurities.[35]

One of the first reported examples is the crystallization of tartaric acid by Pasteur, in which he obtained a racemic mixture of D and L crystals, which he then separated with a pair of tweezers.[5, 6] Similarly, amino acids show such crystallization behavior. When a water solution, with very small excess of one enantiomer is allowed to evaporate slowly this enantiomer is amplified in the bulk of the crystals.[41–43] Some experiments even showed an amplification of the enantiomeric excess from 1% to 90%.[43]

Physical forces such as grinding can also result in amplification of asymmetry in crystals.[35] In 1999 such an example was provided by Kondepudi.[44] A solution of sodium chlorate ($NaClO_3$) in water was crystallized with and without stirring. The first series provided $NaClO_3$ as racemate. The second series produced $NaClO_3$ crystals in one form, either D or L (>99.7% *ee*). More examples followed of this symmetry breaking process and were also applied to intrinsically chiral molecules. For a set of chiral molecules that are (I) conglomerates, (II) crystalline and (III) can be racemized in solution, it was shown that grinding of these solutions over time results in enantiopure crystals.[45, 46]

Another route for amplification is based on chemical processes. Before experiments were performed F.C. Frank designed a reaction mechanism in which he demonstrated how to tilt the racemic equilibrium and yield one enantiomer in particular.[47] Of major importance in amplification is asymmetric autocatalysis. Frank used as definition for asymmetric autocatalysis *"A chemical substance which is a catalyst for its own production and an anti-catalyst for the production of its optical antimer."* Meaning that the configuration of the chiral centre of the autocatalyst must be the same as that of the product. So within this reaction mechanism initial enantio imbalances in combination with asymmetric autocatalysis creates a self-reproducible system amplifying the enantiomeric excess.

To this date the most remarkable example that exhibits asymmetric autocatalytic behavior is the Soai reaction, an enantioselective alkylation.[48] Soai and coworkers studied the enantioselective addition of diisopropylzinc to pyrimidine aldehydes to form chiral pyrimidyl alkanols (Fig. 1.3).[48, 49] In this autocatalytic pyrimidyl system several consecutive autocatalytic rounds were ran, in each round the product of the previous round is used as autocatalyst (species 1 in Fig. 1.3). After four rounds the enantiomeric excess was increased to 88%, which means they observed amplification of asymmetry (Fig. 1.3).

Optimization of the substituent at the 2-position resulted in (*S*)-2-(*tert*-butylethynyl)-5-pyrimidyl alkanol which improved both the yield and the enantioselectivity (>99% and >99.5% *ee*).[50–52] After three consecutive rounds they observed an enantioenrichment of 0.00005% to almost enantiopure product > 99.5% for this alcohol.

To further unravel the origin of the amplification, Soai and coworkers performed mechanistic studies.[53–56] The catalytic cycle begins with dimerization of the zinc aloxides, forming higher ordered aggregates. Starting from both enantiomers the configuration of this species can be *RR*, *SS* and *SR*, *RS*. The homodimers *RR* and *SS* are catalytically active, the heterodimers *RS* and *SR* are inactive. The equilibrium constant for the formation of the heterodimers is much higher compared to that of the homodimers. As a result, the minor enantiomer of the catalyst is "trapped" as inactive heterodimer, while the major enantiomer can form catalytically active homodimer. Therefore, only enantiomerically pure homodimer catalyst is responsible for the product formation leading to amplification of the enantiomeric excess of the alcohol. In each step in the catalytic

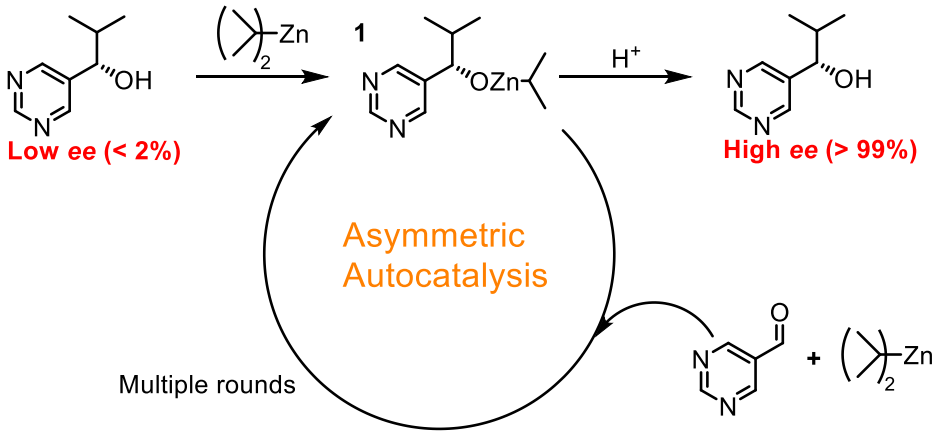

Figure 1.3: *Reaction scheme of asymmetric autocatalysis of pyrimide-5-carboxyaldehyde. Figure adapted from [48].*

cycle all stereocenters have the same configuration. Hereby, the configuration of the final product is predetermined. So starting from a small imbalance with an excess of the (*S*)-product, this will be product that is amplified.

1.3 Supramolecular Polymers and Catalysis

The Soai reaction shows that generation of homochirality from racemic mixtures is possible.[52] This implies that amplification of chirality is fundamental to comprehend homochirality in nature. Supramolecular polymers, which can be seen as dynamical aggregates, proved effective in understanding amplification of chirality in e.g. biopolymers.[57] These assemblies have the properties of covalently linked polymers but are held together *via* non-covalent interactions such as hydrogen bonding, π-interactions, charge transfer interactions and hydrophobic interactions.[1]

Because non-covalent interactions have a dominant role in the assembly there is dynamic equilibrium between the monomers in solution and the monomer in the polymer.[58] Therefore, under thermodynamic control, spontaneous assembly of the building blocks is achieved if suitable conditions are applied.[59] This implies that e.g. changing the temperature, varying the solvent, either assembled or disassembled state can be reached.

A supramolecular building block which is studied in great detail are benzene-1,3,5-tricarboxyamides (BTAs).[57–65] This C_3-symmetric monomer comprises three *meta* substituted C-centered amide groups attached to an aromatic benzene core (Fig. 1.4). Wherein the nature of the side chains (R in figure 1.4) regulates solubility. Each amide bond can contribute to intermolecular hydrogen bonding, which together with π-stacking govern self-assembly into stable supramolecular helical aggregates. Concentration, solubility and temperature as well as secondary interactions determine the length and stability of these aggregates.[57]

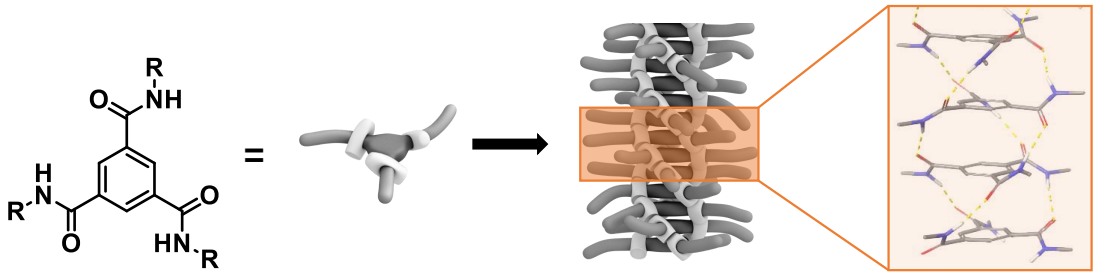

Figure 1.4: *Structure of benzene-1,3,5-tricarboxy amide where R represents side chains which can be altered (left). Illustration of benzene-1,3,5-tricarboxyamides assembled into supramolecular P-helix (middle). BTA monomers with intermolecular hydrogen bonds (right). Figure adopted from [59].*

The synthesis of symmetric C=O-cetered BTAs proceeds *via* an one-step condensation reaction of trimesoic acid chloride with preferred amine.[59] The nature of the side-chains can range from aliphatic to aromatic, polar to apolar and chiral to achiral. If such a side-group contains a stereogenic center close to the benzene ring, the handedness of the helix, *M* or *P*, is determined by the chirality of the side chain.[65] An achiral side chain would result in equal ratios of left- and right-handed helices.[66] This can be investigated with CD spectroscopy, as a racemate would not provide a CD signal. The sign of the CD signal describes the helicity of the helix and the signal magnitude represents the net helicity of all BTA stacks.[67]

Two principle can be applied to govern the handedness of the helix. The first principle that can be applied to supramolecular polymers is so called Sergeant-Soldiers (S&S) principle. It was initially reported in 1989 on covalent polymers, by Green and coworkers.[68] In 1997, it was for the first time reported for an extended-core disc-shaped supramolecular polymer and later for smaller C_3-symmetric BTAs.[69, 70]. In a S&S experiment, supramolecular polymers containing mostly achiral monomers, "soldiers", are controlled by a small fraction of chiral monomers, "sergeants". The soldiers have no preferred helicity as there is no stereocenter in the side chains, instead the helicity induced by the chirality of the sergeants dictate the helicity of the soldiers and thus the overall polymer. As a result, in a S&S experiments with a *S* configured stereogenic center (*S*)-BTA (Fig. 1.5) as sergeant and achiral BTA as soldier, shows a non-linear relation between fraction of sergeant and maximum cotton effect at 223 nm. For a 50 μM solution with only 10% sergeant, the same CD intensity at 223 nm is observed as for a 50 μM enantiomerically pure solution of sergeant (Fig. 1.5). This phenomenon is indicative for amplification of chirality.

The second principle are the majority rules (MR).[67] According the MR, the major enantiomer determines the helicity of stack. The minor enantiomer is either in solution or if incorporated it has to overcome two energetic barriers the helix reversal penalty (HRP) and the mismatch penalty (MMP). The HRP describes the energy penalty of helix reversal in a stack. The MMP penalizes the mismatch of the minor enantiomer if incorporated in a helix of opposite handedness. For BTAs a high constant HRP was observed and the MMP was found to be concentration and temperature dependent and related to the chemical structure of side chains. For a BTA molecule with a high MMP no amplification can arise as the minor enantiomer cannot be incorporated in the helical stacks of opposite helicity.[60, 71–73]

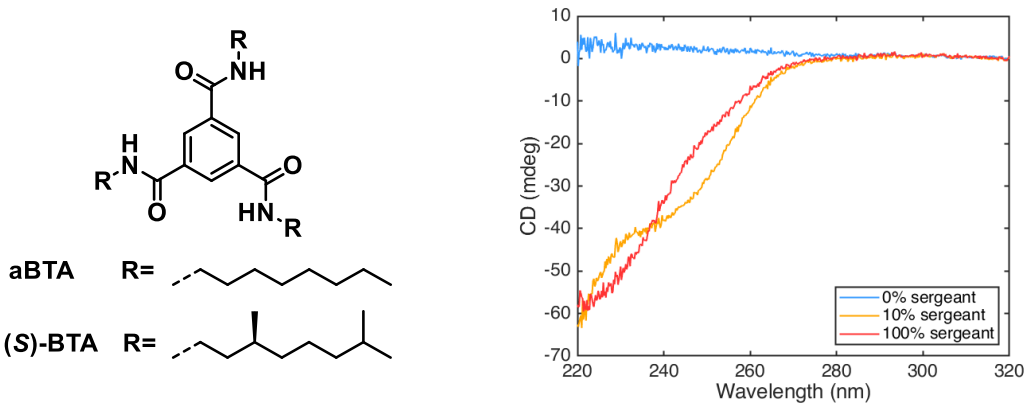

Figure 1.5: *S&S experiement of achiral aBTA and chiral (S)-BTA . CD spectrum of pure aBTA (blue line), pure (S)-BTA (red line) and of mixtures of aBTA and 10% (S)-BTA (orange line), where aBTA is soldier and (S)-BTA is sergeant.*

Later this non-linear behavior between fraction of sergeant and CD maximum cotton effect was observed for other BTA derivatives with different sergeant and soldier molecules.[64, 66, 67] An asymmetric BTA containing one chiral side chain was introduced, to study the influence of number of stereocenters per sergeant molecule on the S&S effect.[67] Even with one chiral tail a S&S effect was observed.

Both principles are clear examples how amplification can occur in supramolecular polymers. A small enantiomeric excess or fraction of sergeant governs the chirality on the supramolecular level and over a large dimension in space. This idea that a small fraction of sergeant molecules can dictate the helicity of supramolecular stacks was applied in the construction of ligand supramolecular asymmetric catalyst by the group of Raynal and Bouteiller.[74]

In 2013 Raynal and co-workers presented an asymmetric hydrogenation of dimethyl itaconate, with a BTA stack as supramolecular catalyst (Fig. 1.6).[74] They used an asymmetric BTA core functionalized with a diphenylphosphine group and two alkyl chains as BTA ligand. As rhodium

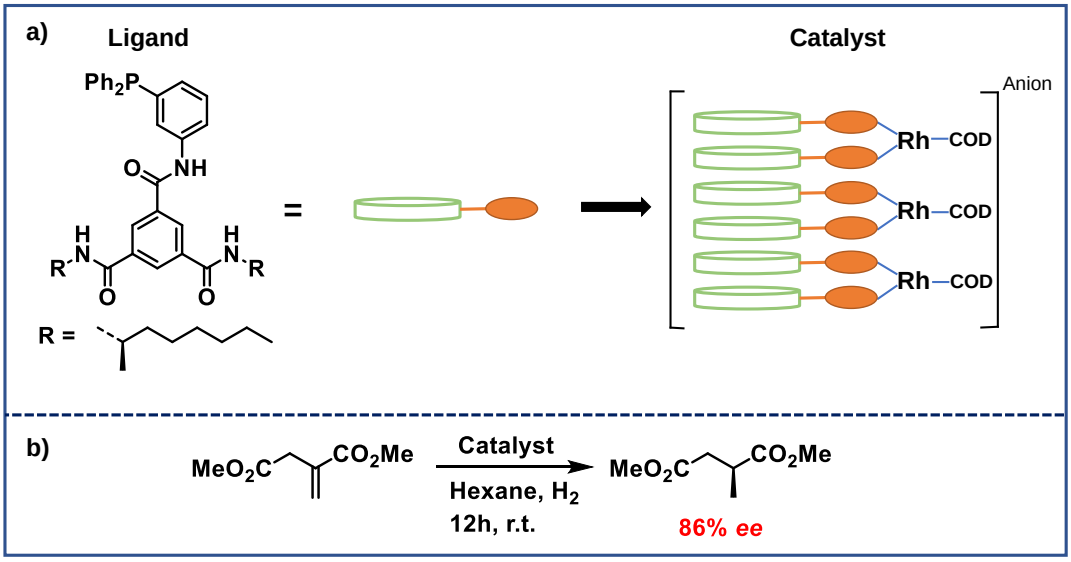

Figure 1.6: *A) Molecular structure and schematic representation of ligand BTA which assemble to form a supramolecular catalyst with rhodium, used in [74]. B) Asymmetric hydrogenation of dimethyl itaconate with the supramolecular catalyst, COD = cyclooctadiene, anion = tetrakis(3,5-bis(trifluoromethyl)phenyl)borate.*

has two free binding sides, two BTA ligands which are adjacently incorporated into the stack can bind to the metal center. Different ligands were obtained by altering the chirality of the alkyl side chains, which could be chiral 1-methylheptyl or (*n*)-octyl.

Within the catalyst they designed, the chiral supramolecular helix determines the enantioselectivity of the product as the stereogenic center in the monomer is far away from the catalyst. The metal is coordinated by two phosphines, which could place the phosphines in similar position as in the BINAP ligand.[16, 74] This is a result of the conformation of the amide bonds throughout the stack. They will slightly be twisted to support intermolecular hydrogen bonding, placing the phosphines the right distance apart to mimic BINAP.[59]

All supramolecular catalysts converted dimethyl itaconate with a typical conversion of >99% but with different enantioselectivities, the highest up to 86% *ee*.[74] Surprisingly when they tested the achiral ligand with a chiral BTA additive (2.5 mol%) an enantiomeric excess of 31% was observed. This implied that indeed the chirality of stack determines the enantioselectivity of the hydrogenation. Moreover, it suggests that taking advantage of the increased S&S-effect provide high enantioselectivities even if the BTA monomer that coordinates to the Rh is achiral.

They, therefore, examined the influence of an achiral BTA additive in further detail.[75, 76] It helped to increase the helical screw-sense excess, caused more evenly dispersion of BTA ligands over the stack increasing the enantioselectivity of the catalyst and reduced the defects present in the supramolecular stacks. But most importantly they created a system were S&S effect and MR are operative.

The results of these findings were combined in the copper catalyzed hydrosilation of 1-(4-nitrophenyl)ethanone (Fig. 1.7), were they show the significant influence of the achiral BTA additive.[76]. Here, the helicity is not proportional to the addition of achiral BTA additive but is amplified in presence of chiral comonomer (S&S effect). So, with low enantiomeric excess of chiral comonomer the asymmetry of the system can be amplified, thus increasing the selectivity of the reaction. Remarkably, the co-assembled system produced high enenatioselectivities (90% *ee*) even with low optical purity of sergeant (20% *ee*). Increasing the enantiomeric excess of the sergeant (>99%) yielded very high enantioselectivity with only 0.25 mol% sergeant (*ee* >90%, Fig. 1.7). Hence, only a small fraction of enantiomerically enriched sergeant is required to obtain high enantioselectivites.

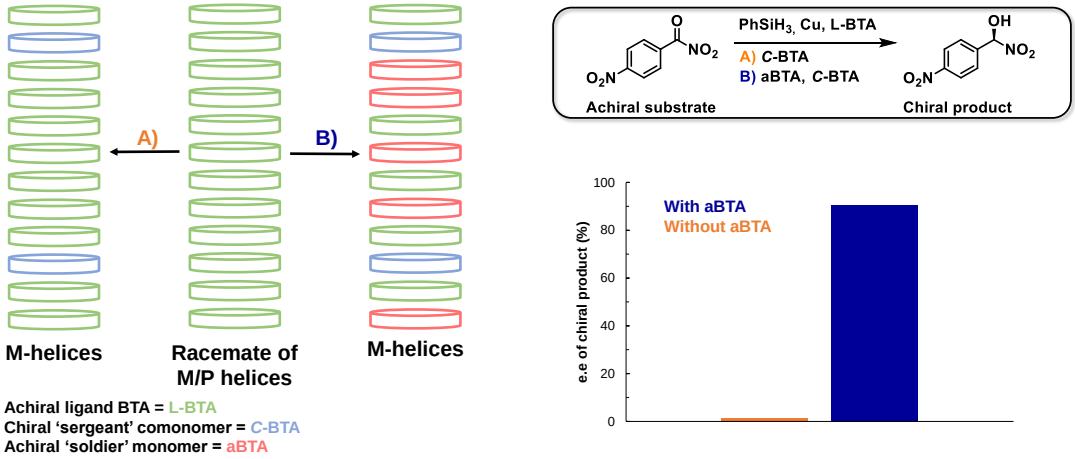

Figure 1.7: *Schematic scheme of copper catalyzed hydrosilylation on 1-(4-nitrophenyl)ethanone (achiral substrate) as proposed by [76]. Racemate of supramolecular stacks composed of 16 mM achiral ligand BTA (green). In reaction* ***A*** *80 µM of chiral sergeant* ***C****-BTA (blue) was added to the supramolecular stacks. In reaction* ***B*** *80 µM of chiral sergeant* ***C****-BTA (blue) and 16 mM of achiral 'soldier' aBTA (orange) was added to the supramolecular stacks. The addition of copper transformed these stacks to be used as chiral catalysts in the conversion of 1-(4-nitrophenyl)ethanone to 1-(4-nitrophenyl)ethanol. In reaction* ***A*** *the ee of the product was only 0.5%, while in reaction* ***B*** *the ee was 91%. This indicates how amplification of asymmetry on supramolecular scale can influence the ee of a hydrosylilation reaction.*

1.4 New Strategy to Amplify Asymmetry

Herein we propose a new strategy to utilize supramolecular polymers with catalytic activity to unravel new reaction with activity to amplify enantiomeric excess. We will combine a supramolecular helical assembly based on BTAs with a stereoselective hydrogenation reaction. Unlike the work done in the group of Raynal we will focus on the hydrogenation of a BTA substrate which can intercalate into the polymer. For this purpose, we designed a system, in which the reaction product of the hydrogenation is the stimulus that induces the helical screw-sense of the supramolecular scaffold. As such, the enantiomeric excess of the product is reflected in the enantiomeric excess of the supramolecular helix. The catalyst is attached to the BTA helix and its stereoselectivity depends on the chirality of the helix.

In the first step achiral BTA monomers form a racemate of M- and P-helices (Fig. 1.8). To one of the achiral BTA monomers an achiral catalyst (green) is attached. This catalyst can convert substrate (grey square) into product (grey plus). The grey square represents achiral BTA monomer composing the supermalocular stack. Because in the first step the catalyst is present as a racemate the product which is formed will also be racemic. In the second step an external stimulus (red plus) is introduced to the system, which is incorporated in the achiral BTA staks creating a slight enantiomeric excess of M-helices. The catalyst will now be enantioselective and convert the substrate to product ($ee>0$). The system is designed in such a way that the product of the reaction is also the external stimulus. Thus over time more chiral product is formed because a higher fraction of the helices is present as M-helices, which generate catalysts with higher enantioselectivity. As a consequence the formed product will be almost enantiomerically pure, which is indicated in step 3 and amplification of asymmetry is observed over time. So, the proposed system to test this new reaction consists of the following components: I achiral substrate; II enantiopure product; III achiral comononer; IV catalytic BTA.

So, if the product is formed with small bias of one enantiomer over the other this would result in biased conformation of helices over time. As a consequence, higher enantiomeric excess of helices will produce more product which favors this handedness of helix. The product will amplify its own formation and inhibit the formation of product with opposite handedness. Hence, in our system low conversion and low selectivity of the asymmetric hydrogenation reaction would succeed to cause amplification over time. Contrary to the systems designed by the group of Raynal.

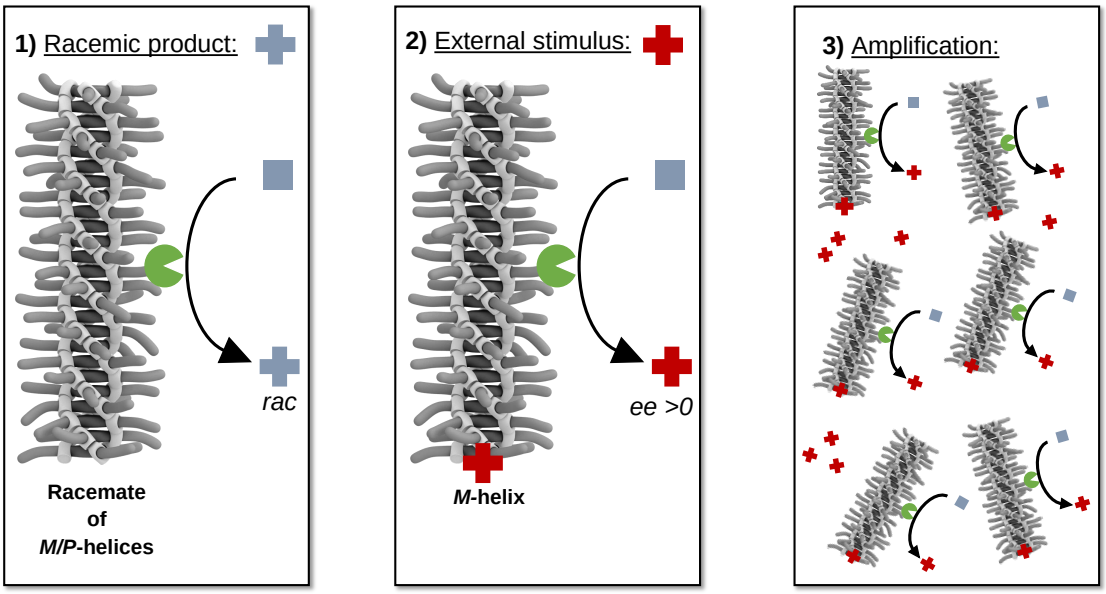

Figure 1.8: *A schematic overview of the system proposed in this work. A catalytically active supramolecular BTA polymer (gray stack) amplifies the enantioselectivity of a hydrogenation reaction. The BTA helices are composed of catalytic BTA (green), achiral substrate BTA (gray square) and achiral additive BTA. Step 1: The helices are present as racemate thus the formed product will be a racemate. Step 2: External stimulus (red square) will generate low enantiomeric excess of M helices, which will convert substrate to product as racemic mixture. The product is also the external stimulus. Step 3: Generated product will increase the enantiomeric excess of M helices and as a consequence the product will be amplified over time.*

References

(1) Anslyn, E. V.; Dougherty, D. A., *Modern physical organic chemistry*, 2006.

(2) Carey, F.; Sundberg, R. In *Advanced Organic Chemistry: Part A: Structure and Mechanisms*, 2007, pp 119–251.

(3) Bruice, P., *Organic Chemistry*, 2014.

(4) Biot, A. B. *Annales de Chim. et de Phys. L.* **1832**, *368*, 119–124.

(5) Derewenda, Z. S. *Acta Crystallographica Section A: Foundations of Crystallography* **2008**, *64*, 246–258.

(6) Pasteur, L. *C.r. hebd. Séanc. Acad. Sci. Paris* **1848**, *26*, 535.

(7) Gal, J. *Chirality* **2019**, *31*, 261–282.

(8) Knowles, W. S.; Sabacky, M. J. *Catalytic Asymmetric Hydrogenation employing a Soluble, Optically Active, Rhodium Complex*; tech. rep.; 1968.

(9) Sharpless, K. B.; Michaelson, R. C. *Journal of the American Chemical Society* **1973**, 6136–6137.

(10) Nozaki, H.; Moriuti, S.; Takaya, H.; Noyori, R. *Tetrahedron Letters* **1966**, *7*, 5239–5244.

(11) Nozaki, H.; Takaya, H.; Moriuti, S.; Noyori, R. *Tetrahedron* **1968**, *24*, 3655–3669.

(12) The Nobel Prize in Chemistry 2001, 2001.

(13) Knowles, W. S.; Sabacky, M. J.; Vineyard, B. D. *Annals of the New York Academy of Sciences* **1973**, *214*, 119–124.

(14) Kitamura, M. *Chirality* **2000**, *12*, 295–298.

(15) Kitamura, M.; Ohkuma, T.; Inoue, S.; Sayo, N.; Kumobayashi, H.; Akutagawa, S.; Ohta, T.; Takaya, H.; Noyori, R. *J. Am. Chem. Soc.* **1988**, *110*, 629–631.

(16) Noyori, R.; Takaya, H. *Accounts of Chemical Research* **1990**, *23*, 345–350.

(17) Noyori, R.; Ohkuma, T. *Angewandte Chemie - International Edition* **2001**, *40*, 40–73.

(18) Noyori, R. *Advanced Synthesis and Catalysis* **2003**, *345*, 15–32.

(19) Rossiter, B.; Katsuki, T.; Sharpless, K. *American Chemical Society* **1981**, 464–465.

(20) Woodard, S. S.; Finn, M. G.; Sharpless, K. *Journal of the American Chemical Society* **1991**, *113*, 113–126.

(21) Finn, M. G.; Sharpless, K. B. *Journal of the American Chemical Society* **1991**, *113*, 113–126.

(22) Von Matt, P.; Pfaltz, A. *Angewandte Chemie - International Edition* **1993**, *32*, 566–568.

(23) Brandt, P.; Hedberg, C.; Andersson, P. G. *Chemistry - A European Journal* **2003**, *9*, 339–347.

(24) Blankenstein, J.; Pfaltz, A. *Angewandte Chemie - International Edition* **2001**, *40*, 4445–4447.

(25) Smidt, S.; Zimmermann, N.; Studer, M.; Pfaltz, A. *Chemistry - A European Journal* **2004**, *10*, 4685–4693.

(26) Helmchen, G.; Pfaltz, A. *Accounts of Chemical Research* **2000**, *33*, 336–345.

(27) Lightfoot, A.; Schnider, P.; Pfaltz, A. *Angewandte Chemie - International Edition* **1998**, *37*, 2897–2899.

(28) Bell, S.; Wu, B.; Kaiser, S.; Menges, F.; Netscher, T.; Pfaltz, A. *Science* **2006**, *311*, 642–645.

(29) Wang, A.; Wüstenberg, B.; Pfaltz, A. *Angewandte Chemie* **2008**, *120*, 2330–2332.

(30) Hou, D. R.; Reibenspies, J. H.; Burgess, K. *Journal of Organic Chemistry* **2001**, *66*, 206–215.

(31) Källström, K.; Munslow, I.; Andersson, P. *Chemistry - A European Journal* **2006**, *12*, 3194–3200.

(32) Fan, Y.; Cui, X.; Burgess, K.; Hall, M. *Journal of the American Chemical Society* **2004**, *126*, 16688–16689.

(33) Cui, X.; Burgess, K. *Journal of the American Chemical Society* **2003**, *125*, 14212–14213.

(34) Brandt, P.; Hedberg, C.; Andersson, P. *Chemistry - A European Journal* **2003**, *9*, 339–347.

(35) Blackmond, D. G. *Cold Spring Harbor Perspectives in Biology* **2019**, *11*, 1–18.

(36) Miller, S. *Science* **1953**, *117*, 528–529.

(37) Parker, E. T.; Cleaves, H. J.; Dworkin, J. P.; Glavin, D. P.; Callahan, M.; Aubrey, A.; Lazcano, A.; Bada, J. L. *Proceedings of the National Academy of Sciences of the United States of America* **2011**, *108*, 5526–5531.

(38) Soai, K.; Kawasaki, T.; Matsumoto, A. *Accounts of Chemical Research* **2014**, *47*, 3643–3654.

(39) Gal, J. *Chirality* **2011**, *43*, 1–16.

(40) Feringa, B.; Delden, R. *Angew. Chem. Int. Ed.* **1999**, *38*, 3418–3438.

(41) Pizzarello, S.; Weber, A. L. *Science* **2004**, *303*, 1151.

(42) Kojo, S. *Symmetry* **2010**, *2*, 1022–1032.

(43) Breslow, R.; Levine, M. *Proceedings of the National Academy of Sciences of the United States of America* **2006**, *103*, 12979–12980.

(44) Kondepudi, D.; Kaufman, R.; Singh, N. *Science* **1990**, *250*, 975–976.

(45) Noorduin, W. L.; Vlieg, E.; Kellogg, R. M.; Kaptein, B. *Angewandte Chemie - International Edition* **2009**, *48*, 9600–9606.

(46) Noorduin, W. L.; Bode, A. A. C.; Van Der Meijden, M.; Meekes, H.; Van Etteger, A. F.; Van Enckevort, W. J. .; Christianen, P. C. .; Kaptein, B.; Kellogg, R. M.; Rasing, T.; Vlieg, E. *Nature Chemistry* **2009**, *1*, 729–732.

(47) Frank, F. C. *Biochimica et Biophysica Acta - General Subjects* **1953**, *11*, 459–463.

(48) Soai, K.; Shibata, T.; Morioka, H.; Choji, K. *Nature* **1995**, *378*, 767–768.

(49) Shibata, T.; Morioka, H.; Hayase, T.; Choji, K.; Soai, K. *J. Am. Chem. Soc.* **1996**, 471–472.

(50) Shibata, T.; Yonekubo, S.; Soai, K. *Angewandte Chemie (International ed. in English)* **1999**, *38*, 749–751.

(51) Soai, K.; Shibata, T.; Sato, I. *Accounts of Chemical Research* **2000**, *33*, 382–390.

(52) Sato, I.; Urabe, H.; Ishiguro, S.; Shibata, T.; Soai, K. *Angewandte Chemie International Edition* **2003**, *42*, 315–317.

(53) Micheau, J. C.; Coudret, C.; Cruz, J. M.; Buhse, T. *Physical Chemistry Chemical Physics* **2012**, *14*, 13239–13248.

(54) Ercolani, G.; Schiaffino, L. *Journal of Organic Chemistry* **2011**, *76*, 2619–2626.

(55) Schiaffino, L.; Ercolani, G. *Angewandte Chemie - International Edition* **2008**, *47*, 6832–6835.

(56) Trapp, O. *Frontiers in Chemistry* **2020**, *8*, 1–9.

(57) Palmans, A. R. A.; Meijer, E. W. *Angewandte Chemie - International Edition* **2007**, *46*, 8948–8968.

(58) Hartlieb, M.; Mansfield, E. D. H.; Perrier, S. *Polymer Chemistry* **2020**, *11*, 1083–1110.

(59) Cantekin, S.; de Greef, T. F. A.; Palmans, A. R. A. *Chemical Society Reviews* **2012**, *41*, 6125–6137.

(60) Cantekin, S.; Balkenende, D. W.; Smulders, M. M.; Palmans, A. R.; Meijer, E. W. *Nature Chemistry* **2011**, *3*, 42–46.

(61) Ten Eikelder, H. M. M.; Markvoort, A. l. J.; De Greef, T. F.; Hilbers, P. A. J. *Journal of Physical Chemistry B* **2012**, *116*, 5291–5301.

(62) Lafleur, R. P. M.; Lou, X.; Pavan, G. M.; Palmans, A. R. A.; Meijer, E. W. *Chemical Science* **2018**, *9*, 6199–6209.

(63) Smulders, M. M. J.; Buffeteau, T.; Cavagnat, D.; Wolffs, M.; Schenning, A.; Meijer, E. W. *Wiley InterScience* **2008**, *43*, 34–43.

(64) Smulders, M.; Nieuwenhuizen, M.; De Greef, T.; Van Der Schoot, P.; Schenning, A.; Meijer, E. *Chemistry - A European Journal* **2010**, *16*, 362–367.

(65) Stals, P. J. M.; Smulders, M. M. J.; Martín-Rapún, R.; Palmans, A. R. A.; Meijer, E. W. *Chemistry - A European Journal* **2009**, *15*, 2071–2080.

(66) Wilson, A. J.; Masuda, M.; Sijbesma, R. P.; Meijer, E. W. *Angewandte Chemie - International Edition* **2005**, *44*, 2275–2279.

(67) Wilson, A. J.; Van Gestel, J.; Sijbesma, R. P.; Meijer, E. W. *Chemical Communications* **2006**, 4404–4406.

(68) Green, M. M.; Reidy, M. P. *American Chemical Society* **1989**, 6452–6454.

(69) Palmans, A. R. A.; Vekemans, J. A. J. M.; Havinga, E. E.; Meijer, E. W. *Angew. Chem. Int. Ed.* **1997**, *36*, 2648–2651.

(70) Brunsveld, L.; Schenning, A. P. H. J.; Broeren, M. A. C.; Janssen, H. M.; Vekemans, J. A. J. M.; Meijer, E. W. *Chemistry Letters* **2000**, 292–293.

(71) Smulders, M. M. J.; Stals, P. J. M.; Mes, T.; Paffen, T. F. E.; Schenning, A. P. H. J.; Palmans, A. R. A.; Meijer, E. W. *Journal of the American Chemical Society* **2010**, *132*, 620–626.

(72) Smulders, M. M. J.; Filot, I. A. W.; Leenders, J. M. A.; Van Der Schoot, P.; Palmans, A. R. A.; Schenning, A. P. H. J.; Meijer, E. W. *Journal of the American Chemical Society* **2010**, *132*, 611–619.

(73) Filot, I. A. W.; Palmans, A. R. A.; Hilbers, P. A. J.; Van Santen, R. A.; Pidko, E. A.; De Greef, T. F. A. *Journal of Physical Chemistry B* **2010**, *114*, 13667–13674.

(74) Raynal, M.; Portier, F.; Van Leeuwen, P. W. N. M.; Bouteiller, L. *Journal of the American Chemical Society* **2013**, *135*, 17687–17690.

(75) Desmarchelier, A.; Caumes, X.; Raynal, M.; Vidal-Ferran, A.; Van Leeuwen, P.; Bouteiller, L. *Journal of the American Chemical Society* **2016**, *138*, 4908–4916.

(76) Li, Y.; Hammoud, A.; Bouteiller, L.; Raynal, M. *Journal of the American Chemical Society* **2020**, *142*, 5676–5688.

2 Molecular Design and Synthetic Route

2.1 Introduction

The BTA polymer that we will use for the catalytic hydrogenation will comprise of three different components: 1) aBTA, bearing three n-octyl chains. This BTA serves as achiral Soldier of the system. 2) (*S*)-BTA, a BTA that has three (*S*)-configured tetrahydrogeranyl units attached to the core. This serves as Seargent and can be used to bias the helical screw-sense of the polymer. 3) g BTA or aagBTA, which have either three geranyl side-chains (gBTA) or one geranyl and two octyl (aagBTA) side chains. These BTAs serve as substrate of the hydrogenation reaction and their olefinic side-chains can be hydrogenated forming the tetrahydrogeranyl chains as implemented in the Seargent BTAs.

The addition of a small fraction of sergeant, which is the product in the hydrogenation, will induce a minor bias of helical handedness in the stacks. Hereby, the first hydrogenation cycle of achiral substrate BTA will lead to a slight increase in enantiomeric excess of the product, increasing the helicity of the environment and of the catalyst further. In the next round this effect is increased, as more product of a single handedness will be formed. This will increase the helical screwsense of the BTA stacks and amplification can be observed over several rounds.

Selection of these compounds was based upon literature. The group of E.W. Meijer has studied the family of chiral BTAs extensively.[1–3] Therefore, the thermodynamic parameters and assembly properties of this BTA class are known. Based upon this information (*S*)-BTA (Fig. 2.1) seems promising to function as sergeant. Moreover, (*S*)-BTA must be a close representation of the achiral substrate BTA, but with a double bond at γ-position. Geranylamine, which is commercially available, has exactly these features. So, gBTA (Fig. 2.1) could be easily synthesized in a condensation reaction between 1,3,5-benzenetricarboxylic acid and three equivalents of geranylamine.

Hydrogenation of gBTA would produce not only (*S*)-BTA, but a total of 5 isomers can be formed. Making it much harder to determine the enantiomeric excess of the reaction. To hurdle this obstacle also an asymmetric substrate BTA was synthesized, aagBTA in Fig. 2.1. Raynal et al. used a BTA very similar to their sergeant as achiral co-monomer to increase stereoselectivity without increasing the mol% of their sergeant. Hence, aBTA was selected in our system (Fig. 2.1).[4]

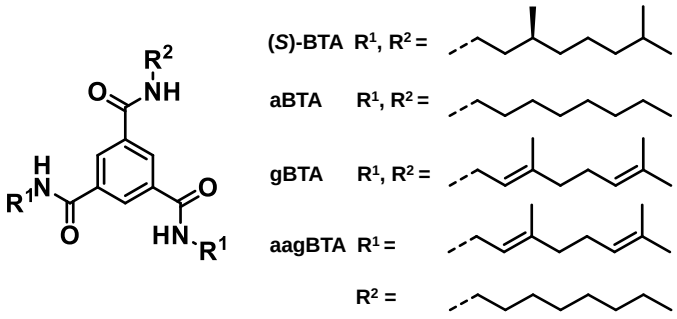

Figure 2.1: *Molecular structure of the different symmetrically and asymmetrically BTAs used in this thesis.*

2.2 Synthetic Approach

The C3-symmetric trialkyl-substitued 1,3,5-benzenetricarboxamide (BTAs, **1** in Scheme 2) were synthesized starting from trimeoisc acid chloride (1a in Scheme 2) and the corresponding amines (gBTA: geranyl amine, aBTA:(*n*)-octyl and (*S*)-BTA: (*S*)-3,7-dimethyloctylamine. The purity of the compounds was confirmed by ^{1}H-NMR and ^{13}C-NMR spectroscopy, MALDI-TOF mass spectroscopy and IR spectroscopy. These symmetric BTAs were synthesized using procedures described in literature.[5, 6]

The asymmetric BTA aagBTA, bearing two (*n*)-octyl chains and one geranyl chain was obtained in a four-step synthesis starting from trimethyl benzene-1,3,5-tricarboxylate (BTE, **2a** in Scheme 3). First, BTE was partially hydrolysed with sodium hydroxide yielding 5-methoxycarbonyl-benzene-1,3-dicarboxylic acid (**2b**). Then, the acid was activated using oxalyl chloride followed by amide coupling with achiral *n*-octylamine yielding methyl 3,5-bis-octylcarbamoyl)benzoate (**2c**). This intermediate was hydrolyzed with lithium hydroxide to 3,5-bis((octyl)carbamoyl)benzoic acid (**2d**). The last step was activation of acid with oxalyl chloride followed by amide coupling with

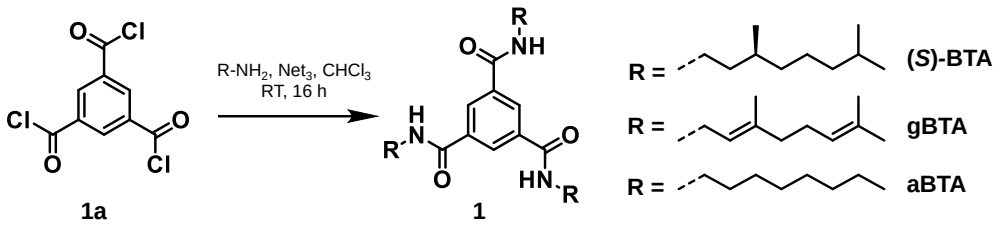

Scheme 2: *Synthetic route for (S)-BTA, gBTA and aBTA*

geranylamine yielded aagBTA. The purity of the compounds was confirmed by ^{1}H-NMR and ^{13}C-NMR spectroscopy, MALDI-TOF mass spectroscopy and IR spectroscopy.

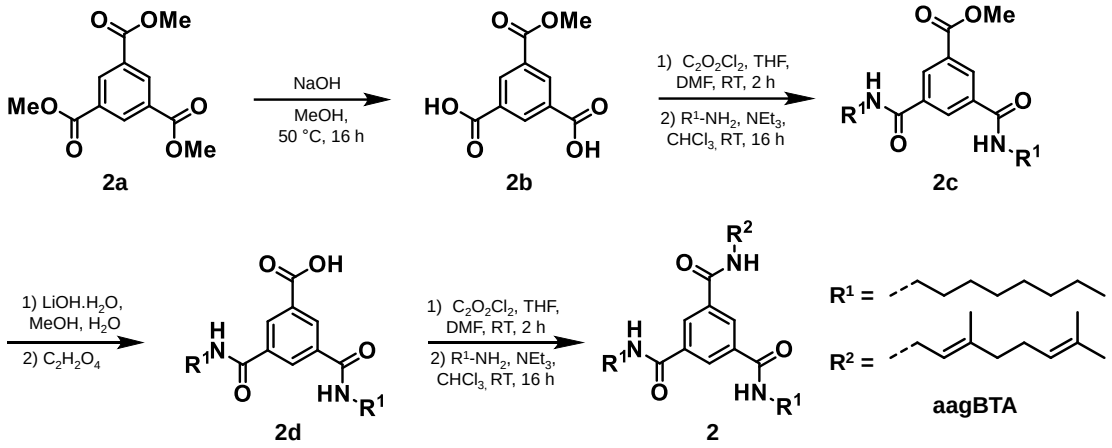

Scheme 3: *Synthetic route for aagBTA*

2.3 Experimental Section

2.3.1 Materials and Instrumentation

All chemicals were obtained from TCI, abcr or Sigma Aldrich and used as received. Solvents were purchased from Biosolve and deuterated solvents were obtained from Cambridge Isotopes Laboratories. aBTA was synthesized by my supervisor and the synthesis is described elsewhere.[7] Reactions were followed by thin-layer chromatography (TLC) using Mercks' $F60_{254}$ silica gel plates.

^{1}H-NMR and ^{13}C-NMR measurements were carried out on a Bruker 400 MHz Ultrashield spectrometer (400 MHz for ^{1}H, 100 MHz for ^{13}C and 162 MHz for ^{31}P). Proton and carbon chemical shifts are reported in ppm (δ) downfield from trimethylsilane (TMS). Phosphorus chemical shifts are reported in ppm (δ) using solvent resonance frequency of chloroform as internal standard. Splitting patterns are abbreviated as: singlet (s), doublet (d), triplet(t), quartet (q), multiplet (m), and broad singlet (br). Solvent peaks δ (ppm) = $CDCl_3$ 7.26, $(CD_3)_2SO$ 2.50, chloroform 7.26 and 8.32, dichloromethane 5.30 and 5.76, ethyl acetate 2.05 and 4.12 and 1.99 and 4.03, H_2O 1.56 and 3.33, THF 1.85 and 3.76 and 1.76 and 3.60.

MALDI-TOF MS measurements were recorded on a Bruker Autoflex Speed using α-cyano-4-hydroxycinnamic acid (CHCA) and 2-[(2E)-3-(4-tert-butylphenyl)-2-methylprop-2-enylidene]-malononitrile (DCTB) as matrices. All samples for MALDI-TOF MS were dissolved in chloroform. IR spectra were recorded on a PerkinElmer Spectrum Two FTIR spectrometer. Variable temperature IR spectroscopy was performed on a Bruker Tensor 27 GladiATR with temperature controller. Column chromatography was carried out on a Biotage Isolera One using Biotage Silica cartridges with eluents specified in the synthesis.

2.4 Synthetic Procedures

2.4.1 Symmetric BTAs

Synthesis of N,N',N"-Tris((S)-3,7-dimethyloctyl)benzene-1,3,5-tricarboxamide ((S)-BTA)
In a round bottom flask, triethylamine (417 mg, 4.12 mmol, 4.0 eq.) and (*S*)-dimethyloctylamine (574, 3.72 mmol, 3.6 eq.) were dissolved in chloroform (20 mL, stabilized with amylene), placed under argon and on an icebath. In another round bottom flask benzene-1,3,5-tricarbonyl trichloride (265 mg, 0.998 mmol, 1.0 eq.) was dissolved in chloroform (10 mL stabilized with amylene). This solution was then transferred to a dripping funnel and added dropwise to the solution of triethylamine and (*S*)-dimethyloctylamine in 15 min. The icebath was removed and the reaction mixture was stirred overnight. The reaction mixture was transferred to a separation funnel and washed thrice with demineralized water, followed by an aqueous solution of hydrogen chloride (1 mol/L) and brine (3×20 mL). The organic phase was dried over magnesium sulfate and filtrate was collected using a cellulose filter. The solvent was removed under vacuum which provided N,N',N"-Tris((*S*)-3,7-dimethyloctyl)benzene-1,3,5-tricarboxamide as a white solid (577 mg, 92% yield).[7]

^{1}H-NMR (400 MHz, Chloroform-d) δ (ppm) = 8.33 (s, 3H), 6.37 (s, 3H), 3.69 – 3.29 (m, J = 7.1, 6.7 Hz, 6H), 1.75 – 1.06 (m, 30H), 0.95 (d, J = 6.5 Hz, 9H), 0.87 (d, J = 6.6 Hz, 18H). ^{13}C-NMR (101 MHz, Chloroform-d) δ (ppm) = 135.23, 128.02, 39.25, 38.54, 37.14, 36.59, 30.77, 27.95, 24.64, 22.70, 22.60, 19.48. MALDI-TOF mass spectrometry: *m/z* ratio calcd. for $[C_{39}H_{70}N_3O_3]^+$ ($[M \cdot H]^+$) 628.54; observed 628.55, 650.54 $[M \cdot Na]^+$.

Synthesis of N,N',N"-Trisgeranylbenzene-1,3,5-tricarboxamide (gBTA)
A similar procedure was employed to the synthetic procedure of (*S*)-BTA.

The product was obtained as white solid (505 mg, 82% yield). ^{1}H-NMR (400 MHz, Chloroform-d) δ (ppm) = 8.35 (s, 3H), 6.33 (d, J = 5.3 Hz, 3H), 5.29 (t, J = 7.3 Hz, 3H), 5.10 (t, J = 6.8 Hz, 3H), 4.07 (t, J = 6.2 Hz, 6H), 2.25 – 1.91 (m, 13H), 1.73 (s, 9H), 1.69 (s, 10H), 1.61 (s, 10H). ^{13}C-NMR (101 MHz, Chloroform-d) δ (ppm) = 165.33, 141.15, 135.17, 131.89, 127.96, 123.78, 118.95, 39.53, 38.25, 26.38, 25.70, 17.73, 16.43. MALDI-TOF mass spectrometry: *m/z* ratio calcd. for $[C_{39}H_{58}N_3O_3]^+$ ($[M \cdot Na]^+$ 638.87; observed 638.43.

Synthesis of N,N',N"-Trisoctylbenzene-1,3,5-tricarboxamide (aBTA)
Obtained from supervisor. But purity was checked by MALDI-TOF MS.

MALDI-TOF mass spectrometry: *m/z* ratio calcd. for $[C_{33}H_{57}N_3O_3]^+$ ($[M \cdot H]^+$) 544.86; observed 544.45, 566.43 $[M \cdot Na]^+$.

2.4.2 Asymmetric BTAs

Step 1: Synthesis of 5-(methoxycarbonyl)isophthalic acid (2b) In a three-neck flask with reflux condensor trimethyl benzene-1,3,5-tricarboxylate (49.7 g, 197 mmol, 1.0 eq.) was dissolved in methanol (320 mL). In a round bottom flask sodium hydroxide (17.6 g, 440 mmol, 2.2 eq.) was dissolved in methanol (380 mL), this solution was then transferred to a dripping funnel and added dropwise (in 4 hours) to the solution of trimethyl benzene-1,3,5-tricarboxylate add stirred overnight at 50 °C. The reaction mixture was then cooled to RT and was washed with methanol (150 mL) and ether (200 mL) using a buchner funnel. The filtrate was concentrated and once more washed with ether (400 mL). The obtained solids were combined and dissolved in H_2O (670 mL) and acidified with oxalic acid to a pH of ∼2. Filtrate was collected using a cellulose filter and excess solvent was evaporated in vacuo to obtain crude product. The crude product was purified by silica column choromatography eluting with ($CHCl_3$:CHOOH:THF(unstabilized) 99.5:0.5:0-83.5:0.5:16 v/v) to afford product **2b** as white powder (25.1 g, 56% yield).

^{1}H-NMR (400 MHz, DMSO-d6) δ (ppm) = 8.67 (s, J = 6.1 Hz, 1H), 8.64 (s, J = 6.1 Hz, 2H), 3.93 (s, 3H).

Step 2: Synthesis of 3,5-bis((octyl)carbamoyl)benzoic methyl ester (2c)
In a round bottom flask under argon **2b** (1.75 g, 7.81 mmol, 1.0 eq.) was dissolved in THF (30 mL) and a drop of DMF was added. The reaction mixture was cooled on an ice bath. A solution of

oxalyl chloride (2.18 g, 17.2 mmol, 2.2 eq.) in THF (4 mL) was added dropwise to the solution of **2b** and was stirred for 2 hours. Excess oxalyl chloride was removed using a solvent trap, then THF was removed on a rotary evaporator and a orange-yellow mixture was obtained. In a round bottom flask coolend on icebath (*n*)-octylamine (2.23 g, 17.5 mmol, 2.2 eq.) and triethylamine (3.11 g, 30.7 mmol, 4.0 eq.) were dissolved in chloroform (45 mL) under argon. The acyl chloride was dissolved in chloroform (20 mL) and added dropwise to the solution of (*n*)-octylamine and triethylamine. The reaction mixture was stirred overnight at RT. he reaction mixture was transferred to a separation funnel and washed thrice with demineralized water, followed by an aqueous solution of hydrogen chloride (1 mol/L) and an aqueous $NaHCO_3$ (3×90 mL). The organic phase was dried over magnesium sulfate and filtrate was collected using a cellulose filter. The solvent was removed under vacuum which yielded crude product as a white powder. After two times recrystallization in ethyl acetate the final pure product **2c** was obtained (2.48 mg, 71% yield).[8]

^{1}H-NMR (400 MHz, Chloroform-d) δ (ppm) = 8.51 (s, 2H), 8.41 (s, 1H), 6.47 (d, J = 5.8 Hz, 2H), 3.96 (d, J = 1.8 Hz, 3H), 3.46 (q, J = 6.8 Hz, 4H), 1.63 (q, J = 7.1 Hz, 4H), 1.49 – 1.12 (m, 22H), 0.88 (t, J = 6.4 Hz, 6H).

Step 3: Synthesis of 3,5-bis((octyl)carbamoyl)benzoic acid (2d)
In a round bottom flask **2c** (2.50 g, 5.61 mmol, 1.0 eq.) was dissolved in methanol (48 mL). Water (3 mL) was added and subsequently lithium hydroxide monohydrate (0.627 g, 14.9 mmol, 2.59 eq.) and the solution was stirred overnight at room temperature. The solution was acidified with oxalic acid to a pH of ∼2 and the solid was removed using a buchner funnel. The solid was dissolved in chloroform (95 mL) and washed with water and brine (2 × 45 mL). The organic phase was dried over magnesium sulfate and filtrate was collected using a cellulose filter. The solvent was removed under vacuum which yielded crude product as a white powder (1.51 mg, 62% yield).

^{1}H-NMR (400 MHz, Chloroform-d) δ (ppm) = 8.53 (d, J = 29.2 Hz, 3H), 7.52 (s, 2H), 3.74 – 3.06 (m, 4H), 1.49 – 1.03(m, 24H), 0.85 (t, J = 6.4 Hz, 6H).

Step 4: General Synthesis of aagBTA
In a round bottom flask under argon **2d** (1.50 g, 3.36 mmol, 1.0 eq.) was dissolved in THF (24 mL) and a drop of DMF was added. The reaction mixture was cooled on an ice bath. A solution of oxalyl chloride (0.52 g, 4.10 mmol, 1.1 eq.) in THF (4 mL) was added dropwise to the solution of **2d** and was stirred for 2 hours. Excess oxalyl chloride was removed using a solvent trap, then THF was removed on a rotary evaporator and a orange-yellow mixture was obtained. In a round bottom flask cooled on icebath geranylamine (0.59 g, 3.85 mmol, 1.1 eq.) and triethylamine (0.64 g, 6.32 mmol, 2.0 eq.) were dissolved in chloroform (40 mL) under argon. The acyl chloride was dissolved in chloroform (15 mL) and added dropwise to the solution of geranyl and triethylamine. The reaction mixture was stirred overnight at RT. he reaction mixture was transferred to a separation funnel and washed thrice with demineralized water, followed by an aqueous solution of hydrogen chloride (1 mol/L) and an aqueous $NaHCO_3$ (3×90 mL). The organic phase was dried over magnesium sulfate and filtrate was collected using a cellulose filter. The solvent was removed under vacuum which yielded crude product as a white powder. Recrystallization in ethyl acetate and drying resulted in the final pure product (1.03 mg, 54% yield).[8]

^{1}H-NMR (400 MHz, Chloroform-d) δ (ppm) = 8.35 (s, 3H), 6.48 (t, J = 5.8 Hz, 2H), 6.37 (t, J = 5.3 Hz, 1H), 5.29 (t, J = 7.4 Hz, 1H), 5.09 (t, J = 7.3 Hz, 1H), 4.07 (t, J = 6.2 Hz, 2H), 3.46 (q, J = 6.8 Hz, 4H), 2.09 (dp, J = 24.4, 8.1, 7.3 Hz, 4H), 1.78 – 1.52 (m, 9H), 1.45 – 1.18 (m, 20H), 0.88 (t, J = 6.5 Hz, 6H). ^{13}C-NMR (100 MHz, Chloroform-d) δ (ppm) = 165.68, 135.29, 135.13, 131.88, 127.97, 123.77, 118.97, 40.41, 39.53, 38.26, 31.80, 29.55, 29.27, 29.19, 27.00, 26.39, 25.70, 22.64, 17.73, 16.42, 14.09. MALDI-TOF mass spectrometry: *m/z* ratio calcd. for $[C_{35}H_{58}N_3O_3]^+$ ($[M \cdot H]^+$) 567.88; observed 568.47.

References

(1) Stals, P. J. M.; Smulders, M. M. J.; Martín-Rapún, R.; Palmans, A. R. A.; Meijer, E. W. *Chemistry - A European Journal* **2009**, *15*, 2071–2080.

(2) Smulders, M. M. J.; Stals, P. J. M.; Mes, T.; Paffen, T. F. E.; Schenning, A. P. H. J.; Palmans, A. R. A.; Meijer, E. W. *Journal of the American Chemical Society* **2010**, *132*, 620–626.

(3) Palmans, A. R. A.; Meijer, E. W. *Angewandte Chemie - International Edition* **2007**, *46*, 8948–8968.

(4) Li, Y.; Hammoud, A.; Bouteiller, L.; Raynal, M. *Journal of the American Chemical Society* **2020**, *142*, 5676–5688.

(5) Brunsveld, L.; Schenning, A. P. H. J.; Broeren, M. A. C.; Janssen, H. M.; Vekemans, J. A. J. M.; Meijer, E. W. *Chemistry Letters* **2000**, 292–293.

(6) Wilson, A. J.; Masuda, M.; Sijbesma, R. P.; Meijer, E. W. *Angewandte Chemie - International Edition* **2005**, *44*, 2275–2279.

(7) De Windt, L. N.; Kulkarni, C.; Ten Eikelder, H. M.; Markvoort, A. J.; Meijer, E. W.; Palmans, A. R. *Macromolecules* **2019**, *52*, 7430–7438.

(8) Raynal, M.; Portier, F.; Van Leeuwen, P. W. N. M.; Bouteiller, L. *Journal of the American Chemical Society* **2013**, *135*, 17687–17690.

3 Characterization of Assembly Properties

3.1 Introduction

In order to use the mixture of different BTA components as supramolecular catalysts, it is essential to understand the assembly behaviour of each individual component. Elucidating the assembly behavior and related parameters reveals the stability of the supramolecular BTA helices, which regulates the catalytic reactivity. To observe amplification in the final system, it is essential to observe an S&S effect between achiral BTAs and sergeant BTA. The enentiomeric excess of the supramolecular helices will control the selectivity of the catalyst.

We therefore started our investigation by determining the optimal solvent for the supramolecular homopolymerization of each BTA, which should reveal optimal assembly conditions. This is of major importance for the supramolecular catalyst as the self-assembly of the compounds will determine the catalytic reactivity. These optimal conditions are characterized by the trade-off between the solubilizing ability of the solvent and strength of the intermolecular hydrogen bonds in the solvent.[1] Higher solubilizing ability lowers the strength of the intermolecular hydrogen bonds and thus decreases the stability of the assembly. To confirm if all BTAs are aggregated in the selected solvent, variable temperature infrared (VT-IR) spectroscopy was used.

Second, we describe the supramolecular polymerization in more detail by identification of several thermodynamic parameters. The dynamicity of the monomers in solution and monomers in the BTA stack will reveal if the assembly mechanism is cooperative. Cooperative effects are involved when monomers self-assemble in longer and more stable chiral supramolecular aggregates.[2–4] It is important to obtain long stable supramolecular stacks as it determines the catalytic reactivity. Temperature-dependent UV/vis spectroscopy measured for different concentrations provide a fast and conclusive approach to find these parameters.

Last, to amplify the chirality of the helical stacks, S&S effect should be observed between achiral soldiers (aBTA, aagBTA and gBTA) and chiral sergeant ((*S*)-BTA). Thus a non-linear effect should be observed between the fraction of sergeant and the observed helicty of the stacks, which can be supported by CD spectroscopy. Because, the selectivity of the catalyst is governed by the enantiomeric excess of the helices.

3.2 Solubilization Effect on Assembly Properties

As aagBTA and gBTA have not been described in the literature before, we started with a solubility study of the BTAs. Both aBTA and (*S*)-BTA are well soluble in alkanes such as e.g. methylcyclohexane (MCH) and typically studied therein.[5] We therefore studied the solubility of aagBTA and gBTA in MCH.

Samples were prepared by dissolving approximately 5 mg compound in 4 mL MCH, followed by heating to 80 °C and stirring for 4 hours and sonicated for 2 hour for additional solvation. aagBTA showed a higher solubility then symmetric gBTA, which can be attributed to solubility of the flexible (*n*)-octyl side chains.[6] Similarly, the low solubility of gBTA can be attributed to the three rigid geranyl side chain, making interactions with solvent molecules less favoured. As pure MCH did not sufficiently dissolve the gBTA, we explored decalin as a typically better solvent for BTAs. However reproducibility issues were encountered which will be further explained in Section 5. Next, we focused on solvent mixtures of MCH and 1,2-Dichloroethane (DCE) as these have better solubilizing properties. However, as DCE is known to weaken the H-bonds of the polymer, only a limited amount can be used to solubilize the BTA. This fine balance between solibilizing and weakening of the polymer affords careful optimization of the MCH/DCE ratio.

UV/vis spectroscopy can be used to differentiate between assembled and disassembled polymer. The absorption spectrum of assembled supramolecular stacks differs from the monomeric spectrum.[7] A shoulder, if present, will shift to lower wavelengths and an intensity decrease is observed in the aggregated phase at the wavelength characteristic for aggregation. This wavelength is determined by measuring a BTA sample at several temperatures, as these two phases are apparent at different temperatures. At high temperature, the BTAs will be molecularly dissolved, providing a distinct absorption spectrum, while low temperature favors aggregated BTAs.[8] However, if a molecule is not soluble in a given solvent this change will not be observed. The same holds for a very good solvent then the monomers will be moleculary dissolved and no change in absorption spectrum will be observed between high and low temperature. The different absorption spectra of these two structural phases can be used to determine which ratio of DCE solubilizes the gBTA molecules but does not interfere with assembly formation.

For measurements, samples of 50 μM were first heated to 80 °C and slowly cooled to 20 °C. If absorption spectrum at 20 °C are similar to those at 80 °C the MCH/DCE ratio is not suited for our experiments.

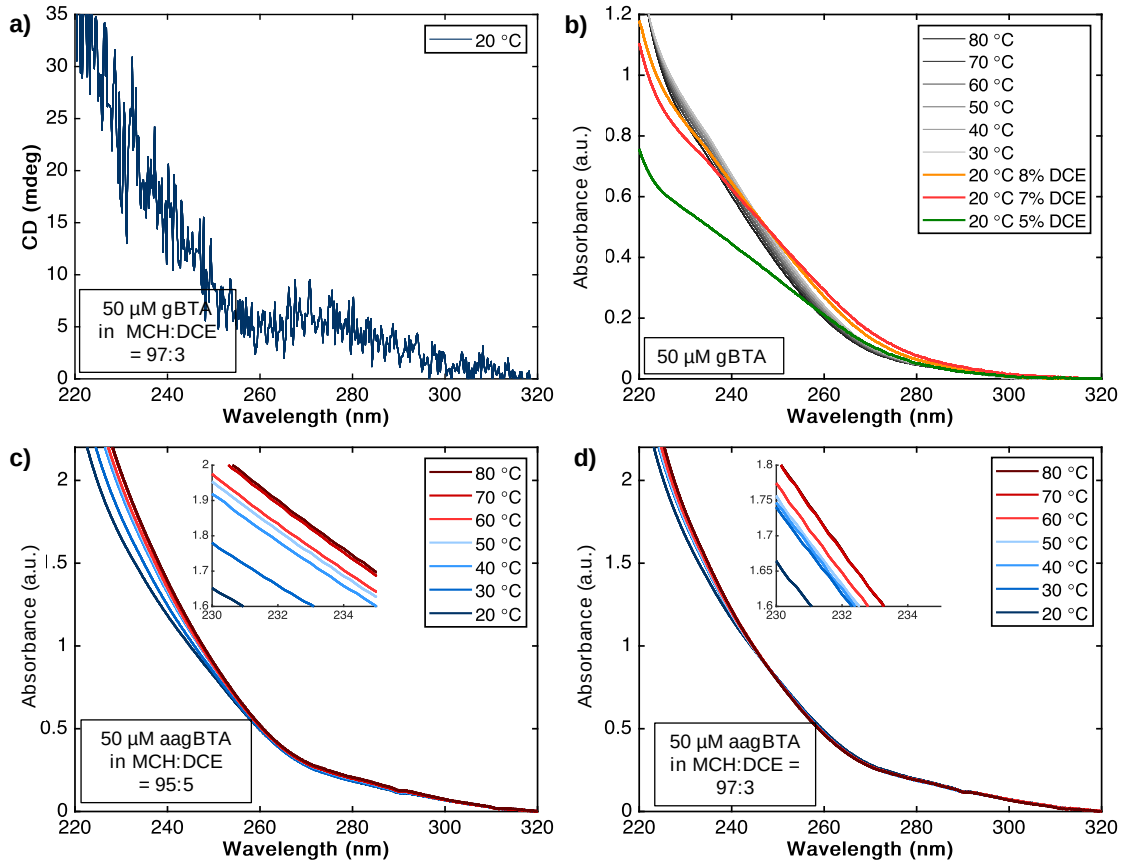

Figure 3.1: *CD and absorption spectra for 50 µM solution of gBTA and aagBTA. (a) CD spectrum of gBTA in MCH with 3 vol% DCE. Melting curves for (b) gBTA in 5%, 7% and 8% DCE (v/v), (c) aagBTA in 5% DCE (v/v) and aagBTA in 7% DCE (v/v).*

In solutions with 1% or 3% DCE (v/v), gBTA was not fully dissolved, which was supported by the changes in absorption spectra. When measuring the same sample a day later or when a new sample was prepared from the same stock solution and measured different absorption spectra were observed. In Section 5 this will be elaborated. Furthermore, gBTA showed a CD signal with a local maximum at 270 nm. We attributed this to the formation of aggregates indicating that at low vol% of DCE individual supramolecular stacks are not sufficient dissolved but form larger aggregates (Fig. 3.1a).

Then, mixtures containing 5, 7 and 8% DCE (v/v) were tested. The maximum intensity of the absorption spectrum at 20 °C for higher vol% DCE is increased and the shoulder, at 230 nm, shifts upwards to 240 nm (Fig. 3.1b) for increasing amounts of DCE. Both indicating that gBTA becomes molecularly dissolved at 8% DCE (v/v). For aagBTA a similar trend was observed, only the maximum intensity at 30 °C and 40 °C also increases for higher volume precent DCE, observed for wavelengths bewow 240 nm (Fig. 3.1c),Fig. 3.1d). This implies that aagBTA is already moleculary dissolved at lower volume percent DCE. Thus the supramolecular polymer formed by gBTA is more stable in the presence of higher amounts of DCE then aagBTA. We attribute this to the side chains. Furthermore, the temperatures that such changes in the absorption spectra are visible differ for gBTA and aagBTA. While for supramolecular stacks composed of gBTA it occurs at 20 °C and for aagBTA at 40 °C. This suggests that aagBTA stacks are more stable at higher temperatures.

For both compounds 5% DCE (v/v) in MCH is a good solvent mixture. A clear change in maximum intensity is observed between 20 °C and at 80 °C at wavelengths below 240 nm for aagBTA and for gBTA this is observed for wavelengths below 265 nm. This change indicates that the monomers are sufficient solubalized but that the intermolecular hydrogen bond strength has not decreased that polymerization is not possible. This solvent mixture was selected for all further studies if not mentioned otherwise.

Infrared (IR) spectroscopy has been identified as a sensitive tool to examine the intermolecular hydrogen bonding between neighbouring molecules in the same supramolecular stack.[5, 6] Vibrations for C═O stretching at ≈ 1640 cm^{-1}, amide II at ≈ 1560cm^{-1} and N—H stretching at ≈ 3240 cm^{-1}, which indicate intermolecular hydrogen bonding.[5, 9] The amide II transition consists of a combination of N—H in-plane bending and C—N stretching. In variable temperature IR (VT-IR) the temperature is slowly increased from 25 °C to 210 °C. In 5% DCE (v/v) MCH at 25 °C all molecules are self-assembled into supramolecular stacks according to the solubility investigation, thus these vibrations should be visible, while at 210 °C all molecules are molecularly dissolved and these vibrations should be decreased and shifted. This finding will support the hypothesis that intermolecular hydrogen bonding are present in solvent mixture of 5% DCE in MCH.

The indicative N—H stretching is observed for all BTAs, but for aagBTA and aBTA the peak is shifted towards higher wavenumber (≈ 3300 cm^{-1}) and a shoulder is observed at ≈ 3340 cm^{-1} (Fig. 3.2a-d; Section 8.1). For the amide II vibration a similar trend is observed, but the peak is shifted to ≈ 1530 cm^{-1} for aagBTA and gBTA. Furthermore, C═O stretching vibration is observed for all BTAs at ≈ 1640 cm^{-1} (Fig. 3.2e-h; Section 8.1). This indicates that intermolecular hydrogen bonds are formed between neighbouring molecules.

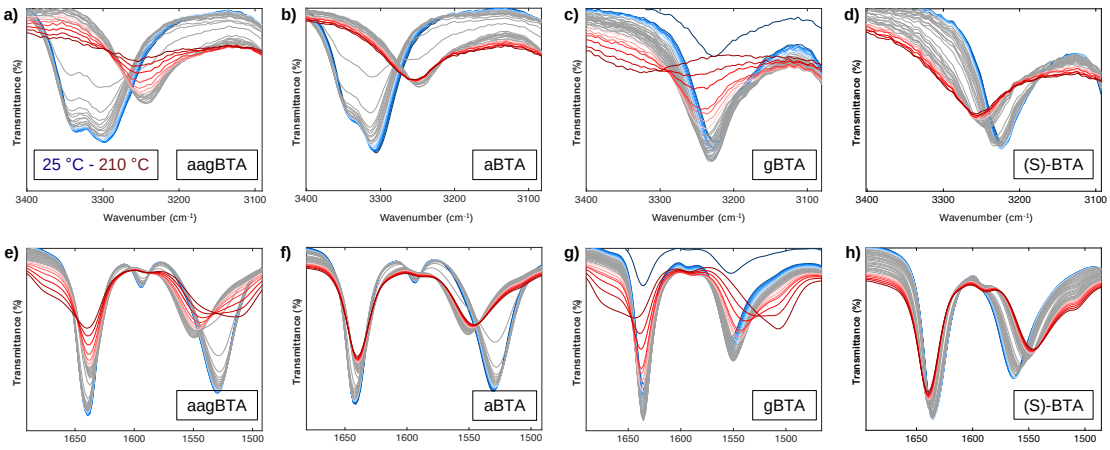

Figure 3.2: *VT-IR spectra at 25 °C to 210 °C, measured every 5 °C, in C = O stretching and amide II region for (a) aagBTA, (b) aBTA, (c) gBTA and (d) (S)-BTA. VT-IR spectra in N - H stretching region for (d) aagBTA, (e) aBTA, (f) gBTA and (g) (S)-BTA.*

3.3 Thermodynamic Analysis of Supramolecular Polymerization

3.3.1 Quantifying the Thermodynamic Parameters

The self-assembly mechanisms in BTAs have been extensively studied.[2, 3, 10] Temperature dependent UV/vis spectroscopy is applied to follow the degree of aggregation over a temperature range. Usually 'cooling curves' are obtained to plot a particular wavelength, distinctive for assembly, as function of temperature. The rate of cooling should be slow, allowing the system to remain under under thermodynamic control as a consequence, so no hysteresis in the heating-cooling cycle should be visible. These cooling curves can be fitted to a one-component mass-balance (MB) model to quantify the thermodynamic parameters. Details of the model used in this thesis can be found in Section 8.2.1.[4, 11]

Only isodesmic and cooperative polymerization mechanisms play a role for the self-assembly of our BTAs.[11] In isodsemic polymerization a single association constant (K) dictates the assembly pathway. For each consecutive addition of monomer to the growing chain the Gibbs free energy (ΔG) is reduced by the same amount.[1, 4] In contrast to isodesmic polymerization, cooperative polymerization happens in two distinct phases, the nucleation phase followed by the elongation phase. Each phase is characterized by its own thermodynamic parameters that describe the equilibrium, (K_n, ΔH_n, ΔS_n) for the nucleation phase and (K_e, ΔH_e, ΔS_e) for the elongation phase. Separation between these two phases occurs at the elongation temperature (T_e).

In the MB model the extend of cooperativity is described by the cooperativity factor ($\sigma = K_n/K_e = exp(\Delta H_{np}/(RT))$.[3] The more positive ΔH_{np} becomes, which is defined as ΔH_e - ΔH_n, the bigger the σ will become and thus a lesser cooperative system. In the special case were $\Delta H_e = \Delta H_n$, then σ equals 1, an isodesmic system is represented.

3.3.2 Cooperativity in the Supramolecular System

Before examination of the amplification properties, the homopolymerization of the monomers is investigated. Cooperative mechanism within the system cause high internally ordered supramolecular stacks.[2, 3, 10] This feature is especially important for our supramolecular molecular catalyst where the reactivity and stereoselectivity are not only determined by a metal/ligand complex but are also influenced by the stability and helicity of the stack.

The dominant element stabilizing the assembly are the triple helical hydrogen bonds between monomers. For each monomer a rotation of the dihedral angle (θ), between benzene core and carbonyl of the amide (Fig. 3.3b), is necessary to achieve a favourable geometry for intermolecular hydrogen bonds, which are essential of the polymerization.[1] In this structure the strength of intermolecular hydrogen bonding is optimal. The torsion angle greatly influences the cooperativity.[3, 6, 12] The optimal dihedral angle for BTAs bearing linear side chains has been found to be 35°, while for branched side chains an angle of 45° has been determined. But is also depended on the solvent nature, e.g. linear or branched.

The cooperativity factor, σ, quantifies the extend of cooperativity for such MB models. In 2017 the range for the σ of a large BTA family was determined. Isodesmic polymerization in methylcyclohexane corresponds to a σ of 1 and decreases to 10^{-6} for very cooperative polymerization.[3] The solvent and side chains influence the values.

In order to follow the assembly and disassembly over a range of temperatures, typically the change in absorption at 223 or 230 for (S) and aBTA is followed, as these wavelengths are characteristic for aggregation.[3] Absorption spectra at 20 °C for each component were first measured and indicated that these wavelengths are also suitable for aagBTA (Fig. 3.3a). For gBTA it became clear from the solubility study that 230 and 260 nm are characteristic for aggregation. Therefore, each component was followed at those three wavelengths. Only the wavelength for which the spectrum displayed the most significant change is shown.

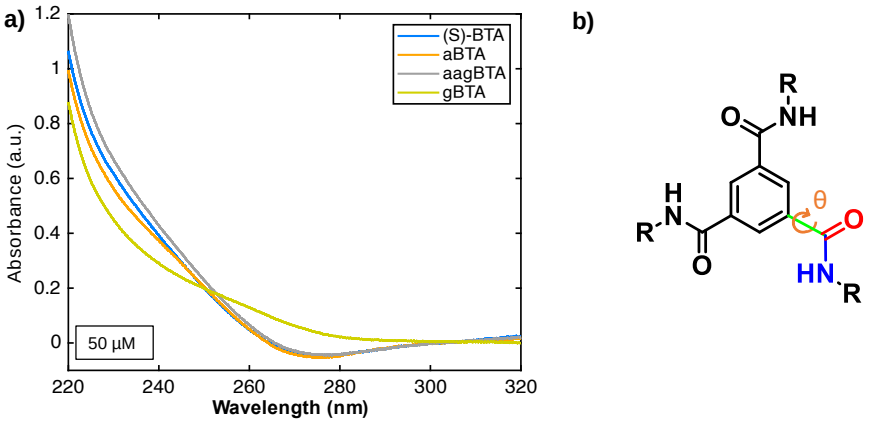

Figure 3.3: *a) Absorption spectra at 20 °C in 5% DCE (v/v) MCH for (S)-BTA (blue), aBTA (orange), aagBTA (gray) and gBTA (green). b) Dihedral angle (θ) between the carbonyl group of the amide and the benzene core.*

Four solutions for each BTA were prepared with concentrations of 20, 30, 40 and 50μM. The wavelength characteristic for aggregation for the BTAs was followed *via* temperature dependent UV/vis spectroscopy. These solutions were heated to 80 °C and slowly cooled, δT = 0.5 °C/min, to ensure the polymerization remained under thermodynamic control. Fitting these curves with the MB model gives the thermodynamic parameters, for details see Section 8.2.2.

In the resulting cooling curves obtained from such experiments (Fig. 3.4), two phases can be observed: a nucleation phase where all molecules are molecularly dissolved (marked by the straight line) and an elongation phase where the polymer grows. The separation between these two phases occurs at the elongation temperature, T_e. The T_e represents the formation of critical nucleus size to allow elongation. At this phase separation the equilibrium is concentration en temperature dependent.[10] Moreover, a lower T_e represents earlier formation of aggregates. For low concentrations the decrease in energy for polymerization is bigger then for high concentrations. Thus for lower concentrations the T_e shifts to lower temperatures, which is also observed here.

In the measured concentration range the T_e is highest for aBTA, where an decrease from 56.7-41.2 °C was observed, followed by (S)-BTA 47.4-33.7 °C and was significantly lower for aagBTA 38.4-30.8 °C and gBTA 36.6-30.2 °C. This is attributed to the tails in each BTA. Normally a longer

tail results in better solubility which lowers the T_e. But at a certain tail length there is stabilization *via* Van der Waals forces, which lowers the T_e. All side chains have the same length but differ in substituents on the alkane chain. The (*S*)-stereogenic tail in (*S*)-BTA and geranyl tail in gBTA and aagBTA is branched with one methyl group, as a result more solvent molecules interact with the aliphatic chain leading to better solubility, which lowers the T_e (Fig. 3.4 and Fig. 3.5a) compared to aBTA. The T_e's for gBTA and aagBTA were significantly lower, indicating a lower stability. Thus the evolution of the T_e for the compounds is gBTA>aagBTA>(*S*)BTA>aBTA. The signal decrease at higher temperature is a result of concentration decrease. The absolute amount of monomers stays constant but the sample volume increases at higher temperature lowering the concentration thereby decreasing the signal.

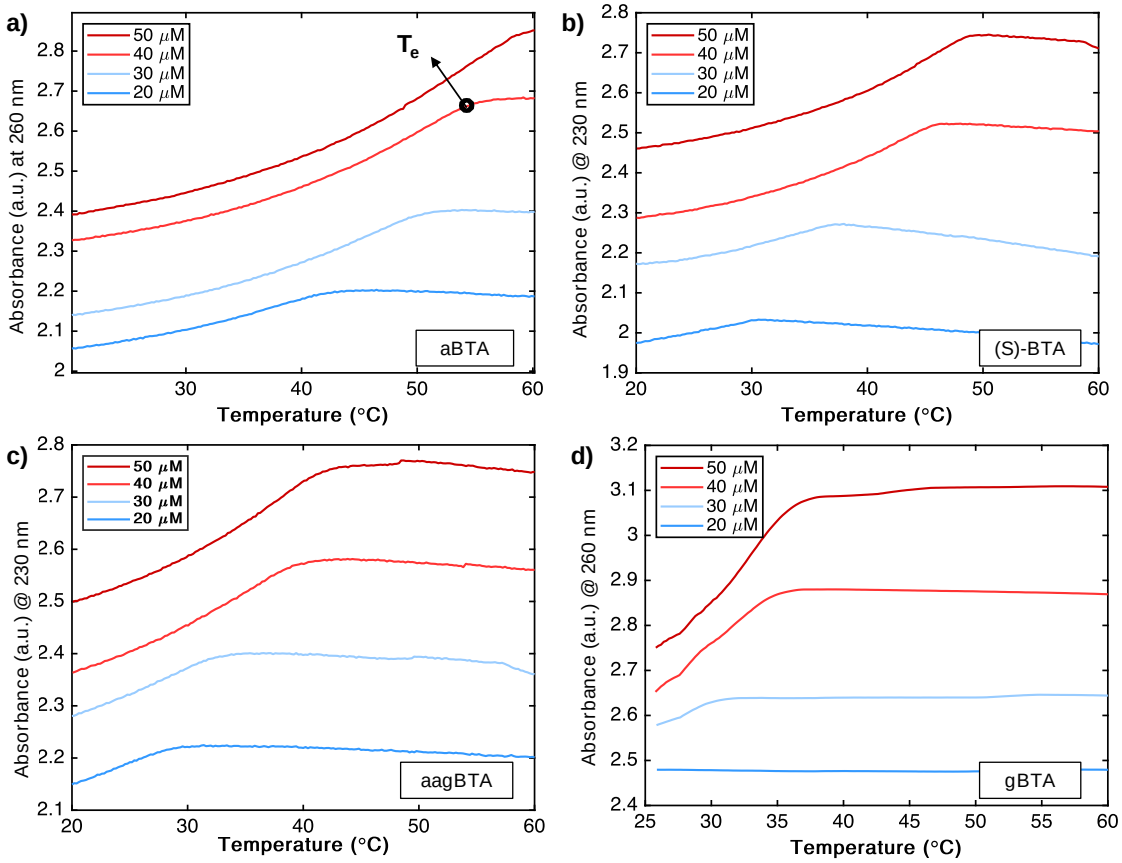

Figure 3.4: *Concentration dependent cooling curves in MCH with 5 vol% DCE for a) aBTA, b) (S)-BTA, c) aagBTA and d) gBTA. The elongation temperature, T_e, indicated at the transition between nucleation phase (linearly increasing line) and elongation phase (straight line) for aBTA.*

The cooperativity of the self-assembly is dictated by the nucleation penalty, σ=exp(ΔH_{np}/(RT)). δH_{nuc} values derived from absorption data was largest for (*S*)-BTA (-33.1±9.9 kJ mol^{-1}), followed by aBTA (-20.0±0.4 kJ mol^{-1}), gBTA (-17.8±7.3 kJ mol^{-1}) and smallest for aagBTA (-16.4pm2.4 kJ mol^{-1}) (Fig. 3.5b). Correspondingly, the self-assemblies of (*S*)-BTA were most cooperative (σ=1.55 × 10^{-6}), subsequently aBTA (σ=3.12 × 10^{-4}) and gBTA (σ=1.04 × 10^{-3}) and least cooperative was aagBTA (σ=2.40 × 10^{-3}) (Fig. 3.5c).

This support our hypothesis that the cooperativity is determined by the side chain and implies that the rigidity of the geranyl chains, caused by the two double bonds, lowers the cooperativity. The standard deviation for the ΔH_{np} (±7.3 kJ mol^{-1}) is very high for gBTA (Fig. 3.5b). Actual values for the cooperativity therefore range from 1.44 × 10^{-2} to 3.84 × 10^{-3}. This could indicate that gBTA is actually less cooperative then aagBTA, which is expected as gBTA has two more rigid side chains.

The δH_{nuc} for (*S*)-BTA (-38.6 kJ mol^{-1}) and aBTA (-19.2 kJ mol^{-1}) were reported in MCH. For aBTA this is corresponds to the value found here but for (*S*)-BTA there is a large deviation, which can be attributed to the large standard deviation of ± 9.9 kJ mol^{-1}. Besides, chlorinated solvents, such as DCE, are expected to lower the cooperativity.[7] In a previous study the cooperativity for (*S*)-BTA (3.0 × 10^{-6}) and aBTA (3.8 × 10^{-5}) in MCH were reported, therefore the σ values obtained are in accordance with literature.[3]

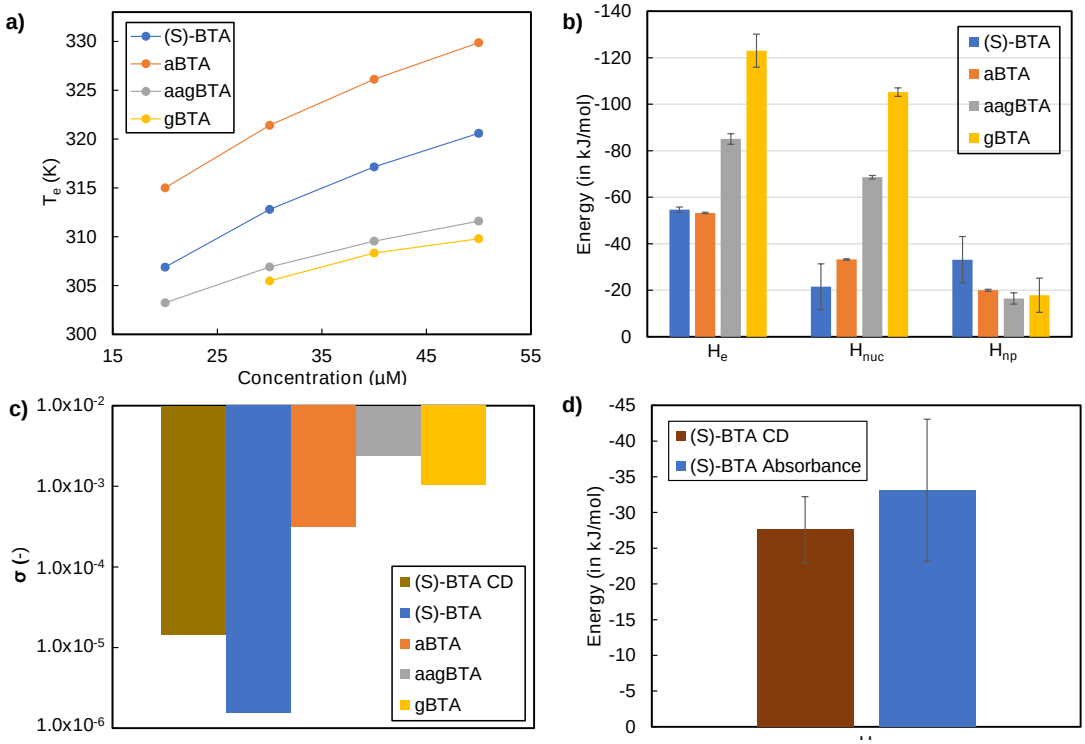

Figure 3.5: *For (S)-BTA, aBTA, aagBTA and gBTA a) thermodynamic parameters at 293 K, b) concentration dependent elongation temperature and c) cooperativity factor at 293 K. d) Difference in thermodynamic parameters when CD spectra or absorption spectra are used to fit the MB model.*

Our group found that (*S*)-BTA assembles very cooperative, so they looked at an explanation and found that the amide torsion is the reason, which is 45 ° for (*S*)-BTA in MCH.[3, 12] Previous work in this group elucidated that the position of methyl substituent affects the θ, thereby influencing the cooperativity to a large extend.[3] Thus, it is not unlikely that introducing rigid double bonds in side chains also affects the θ. Thus explaining the decrease in cooperativity of 10 and 100 times in aagBTA and gBTA respectively. Additionally, the three geranyl side chains of gBTA are much more rigid with their twofold double bond then the two flexible C_8-alkane chains of and one geranyl chain of aagBTA. Which also supports our hypothesis that the cooperativity of gBTA is lower then aagBTA.

Besides, the cooperativity in MCH for asymmetric $(C_8)_2$-(*R*)-BTA ($\sigma = < 10^{-8}$) is lower then symmetric (*R*)-BTA ($\sigma = 3.7 \times 10^{-6}$) and aBTA ($\sigma = 3.8 \times 10^{-4}$).[3] With that in mind it could explain why the cooperativity for aagBTA is actually higher then gBTA. The fact that the cooperativity is is not lower then aBTA is because aagBTA still has one very rigid geranyl side chain, which increases the cooperativity.

3.3.3 Evaluation of the model

The MB model is used to fit the thermodynamic parameters based on CD cooling curves. We wanted to compare the fitted results of CD and absorption cooling curves. In our system the only chiral molecule is (*S*)-BTA thus this molecule was used as reference. The δH_e was very similar for the thermodynamic parameters fitted for CD curves (-53.9±1.3 kJ mol^{-1}), but the δH_{nuc} increased while the error also became smaller (-26.3±4.4 kJ mol^{-1}). As a result the δH_{np} (δH_{np}=δH_e-δH_{nuc}) and the standard deviation of the δH_{np} decreased (-27.6±4.6 kJ mol^{-1} Fig. 3.5d). Calculated σ value (1.45×10^{-4}) of CD cooling curves give therefore a better representation of the actual value. This indicates that the σ value for all BTAs might be actually lower. However, the cooperativity determined by fitting absorption data lies within the error of the cooperativity as determined by CD spectra.

3.3.4 Hysteresis

When cooling a sample the monomers go from molecularly dissolved to aggregated state and the opposite occurs when heating a sample. In principle identical curves should be obtained for both experiments when the system is under full thermodynamic control. However, for cooperative

systems this is often not the case and hysteresis is observed.[13] Hysteresis is a clear sign of kinetic traps involved in the self-assembly. Then, the system is no longer only under thermodynamic control and the fitted thermodynamic parameters need to be interpreted with caution.[1]

The heating and cooling curves for gBTA do not overlap, this is also visible on the T_e which is 20 °C for cooling and 40 °C for heating (Fig. 3.6). This hysteresis indicates that kinetic traps are involved in the self-assembly. aBTA is known to show no hysteresis in heating cooling experiments in MCH. To investigate if the solvent mixture (MHC/DCE) might lead to the hysteresis, we studied aBTA in the same mixture. The overlap of the curves is not perfect but this can be ascribed to small environmental changes (Fig. 3.6b). As mentioned before hysteresis is a sign of kinetic barriers in the system. Because these kinetic barriers are present, the fit of the model to experimental data is not good which can result in a large error bar for the fitted parameters.

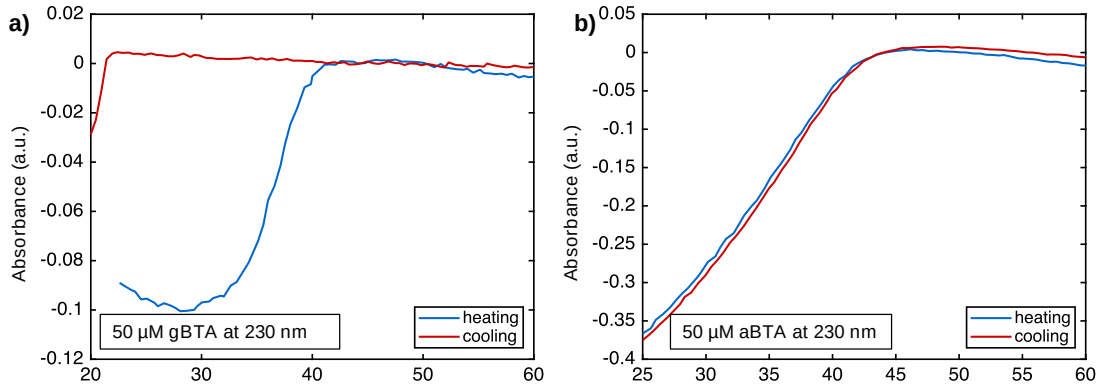

Figure 3.6: *A 50 µM solution was first heated to 80 °C, cooled down to 20 °C and heated to 80 °C. Hysteresis effect observed for gBTA (a), indicated by the change in T_e for cooling and heating curve. As comparison for aBTA (b) heating and cooling curves were measured.*

3.4 Amplification Properties

The selectivity of the catalyst will be governed by the enantiomeric excess of the helices. It is essential that the formed product, (*S*)-BTA, can induce S&S effect on molecules in the stacks which are already present. Only then can a small fraction of (*S*)-BTA bias the helical srewsense creating an enantio-enriched environment of the catalyst. As a result, the stereoselectivity of the catalyst is improved and will direct the formation of more (*S*)-BTA. This symbolizes amplification of asymmetry where the product is an autocatalyst for its own production.

We investigated this *via* the S&S principle for aBTA, aagBTA and gBTA and used (*S*)-BTA as sergeant. To measure this effect, the CD spectra of multiple samples with varying, from 0% to 100%, fraction of sergeant were measured while the total concentration of BTA molecules was kept constant at 50 µM (Fig. 3.7a-c,f). For (*S*)-BTA and aBTA a S&S effect was already confirmed in MCH and cyclohexane.[7, 14] Yet, it has not been investigated if (*S*)-BTA and aBTA follow a S&S principle in the solvent mixture 5% DCE (v/v) in MCH . Also, it is unknown if gBTA and aagBTA can serve as soldier in a S&S experiment with (*S*)-BTA.

For aBTA (Fig. 3.7a) two different CD spectra can be observed. For lower fractions of sergeant a type I CD spectrum, with a max CD signal at 220 nm and a shoulder at ∼245 nm is apparent. For higher fractions of sergeant a type II CD spectrum, with a maximum absorption at 224 nm is visible. The transition from type I CD spectrum to type II CD for aBTA is observed at ∼0.4 fraction of sergeant. For both aagBTA and gBTA (Fig. 3.7b, 3.7c respectively) the shape of the spectrum (max cotton effect at 223 nm) does not change with increasing amounts of sergeants. The shape of CD spectrum is similar for low and high fractions of sergeant.

The difference between type I and type II CD spectrum can be a result from different θ in the stacks. Previous results in literature showed a CD spectrum resembling type I CD spectrum for a θ of 35° and CD spectrum resembling type II for a θ of 45°.[6, 12] This suggests that at fractions below 0.4 sergeant the conformation of the supramolecular stacks favor a θ of 35° and above a θ of 45°. Branched side chains, present in e.g. (*S*)-BTA and gBTA induce a θ of 45 ° , while linear side chains in aBTA adopt a θ of 35 °.[6] Therefore, mixtures of aBTA/(*S*)-BTA show type I and II CD spectra while mixtures of aagBTA/(*S*)-BTA and gBTA/(*S*)-BTA only show type II CD spectrum.

Normalizing the Cotton effect provided the net helicity as function of fraction sergeant (Fig. 3.7d). A net helicity of 1 is observed at 0.1 fraction sergeant for aBTA and aagBTA,

indicating a clear S&S effect. This is in line with results previously reported in literature were S&S effect was measured for aBTA and (*R*)-BTA in MCH.[5, 14] In contrast for gBTA the relation between fraction of sergeant and net helicity is linear. Very low T_e (34 °C at 50 μM) indicate that the stacks form at low temperature. Therefore, (*S*)-BTA might not be incorporated in the the stacks and are unable to direct the handedness of helices.

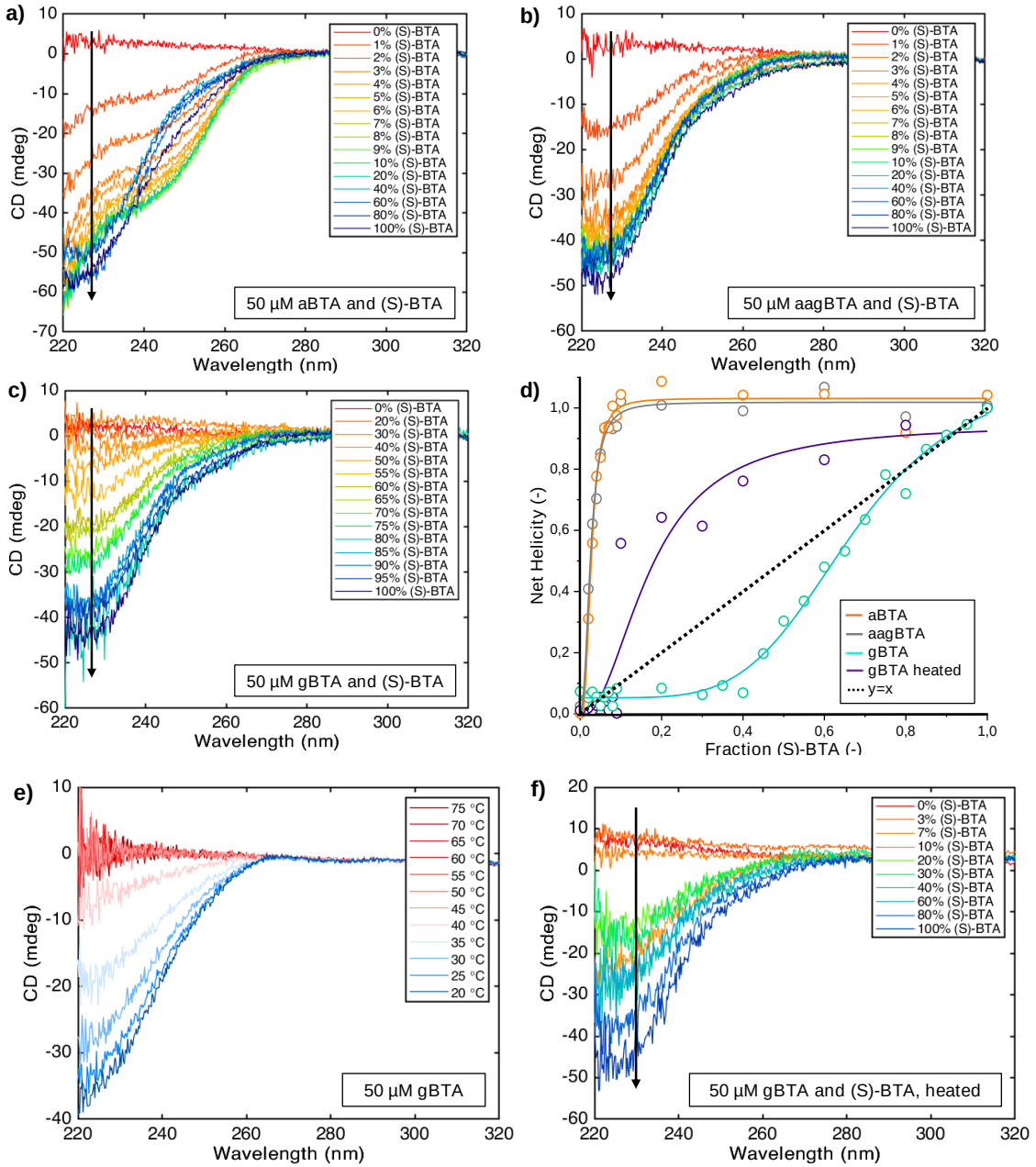

Figure 3.7: *S&S effect measured at total concentration of 50 µM at 20 °C for aBTA (a), aagBTA (b) and gBTA (c) with varying fraction of (S)-BTA. (d) The net helicity at 224 nm is plotted as function of fraction (S)-BTA. A linear relationship indicates no S&S effect. (e) Heating the sample to 75°C followed by slowly cooling indicates a temperature dependency of CD signal for 50 µM solution of gBTA with 20% (S)-BTA. f) New S&S effect for gBTA and (S)-BTA measured if all samples are first heated to 75°C. Measured for 50 µM solution at 20 °C.*

To test this theory, samples containing mixtures of gBTA and (*S*)-BTA were heated to 80 °C and cooled to 20 °C. The CD spectrum was measured every 10 °C. Heating the samples to 80 °C ensures all molecules are molecularly dissolved. Because the samples are cooled slowly (*S*)-BTA can be incorporated in the stacks and steer the screw-sense of the helices. When the sergeant fraction was below 0.2, no S&S effect was visible. Above 0.2 a clear S&S effect was visible (Fig. 3.7e), suggesting that indeed (*S*)-BTA can not be incorporated in gBTA stacks at low temperatures. The S&S experiment was therefore repeated but all samples were heated in a sand bath of 80 °C before measuring. As a result for fractions of sergeant above 20% a S&S effect is observed (Fig. 3.7f).

All experiments were performed with the same sergeant, namely (*S*)-BTA, which has three chiral side chains. If aagBTA is selected as achiral substrate BTA in the final system, this will be hydrogenated to a chiral BTA with not three but one chiral side chain. Thus only one stereocenter is present to bias the handedness of the helices. As a consequence the MMP will be lower and the S&S effect will become more linear.[7] Wilson et al. showed that, to reach a net helicity of 1, the fraction of such an asymmetric sergeant is much higher, almost ∼0.35, compared to a fraction of ∼0.10 for a symmetric sergeant. In our final system this implies that the stereoselectivity of the hydrogenation reaction must be higher if aagBTA is used as substrate compared to gBTA.

3.5 Conclusion

It was found that a mixture of 5% DCE (v/v) in MCH is a good binary solvent system to solubalize (*S*)-BTA, aBTA, aagBTA and gBTA to prevent aggregation but preserve intermolecular hydrogen bonding strength required for self-assembly. Temperature dependent UV/vis spectroscopy was used to determine the elongation temperature which increased in the order of gBTA<aagBTA<(*S*)-BTA<aBTA for 20 to 50 uM solutions. This is in analogy to the cooperativity of the polymerization which decreases in the order from (*S*)-BTA (1.55×10^{-6})<aBTA (3.12×10^{-4})<gBTA (1.04×10^{-3})<aagBTA (2.40×10^{-3}). Furthermore, the limits of chiral amplification were examined *via* means of a S&S experiment for achiral soldiers aBTA, aagBTA and gBTA with chiral sergeant (*S*)-BTA. It was established that all soldiers show strong amplification of chirality. For gBTA it was necessary to disrupt the equilibrium of the assemblies by increasing the temperature before measurement at 20 °C. The S&S effect was strongest for aBTA and aagBTA, were only a fraction of 0.10 sergeant was enough to induce a net helicity of 1. For gBTA no strong S&S effect is observed, but heating the samples increases the non-linear relation between fraction of sergeant and helicity. This indicates, that the envisioned catalytic BTA polymer can serve as a promising platform to study ampification *via* hydrogenation reaciton.

3.6 Experimental Section

3.6.1 Materials and instrumentation

Solvents were purchased from Biosolve and deuterated solvents were obtained from Cambridge Isotopes Laboratories. BTAs were synthesized as described in Section 2.4 and used without any further purification.

UV/Vis, circular dichroism (CD) and linear dichroism (LD) measurements were performed on a Jasco J-815 spectropolarimeter, for which the sensitivity, time constants, scan rates and temperature were chosen appropriately. Corresponding temperature depended measurements were performed with a Jasco PFD-425S/15 Peltier type temperature controller with a temperature range of 263–393 K and adjustable temperature slope. All spectroscopic measurements were recorded in cells with an optical path length of 1 cm. The Spectrophotometer is equipped with a multi-cells holder for 6 samples and the temperature controlled was set on the holder station.

3.6.2 Methods

Sample preparation
Weighing enough material of each component to make a stock solution of roughly 1 mM in the solvent selected for each measurement. Samples were then prepared by diluting the stock solution to give the desired concentration.

Jasco J-815 spectropolarimeter parameter settings
Melting curves were recorded with following parameters: sensitivity standard, response time 0.125s, band width 1 nm, scanning speed 100 nm/min, wavelength 220-320 nm, temperature gradient 1.0 °C/min, halt temperature ramping during measurement.

Cooling curves were recorded with following parameters: sensitivity standard, response time 0.125s, band width 1 nm, scanning speed 100 nm/min, wavelength 230 nm for (*S*)-BTA and aagBTA and 260 nm for aBTA and gBTA, temperature gradient 0.5 °C/min, no halt temperature ramping during measurement.

S&S experiments were recorded with following parameters: sensitivity standard, response time 0.125s, band width 1 nm, scanning speed 100 nm/min, wavelength 220-320 nm, temperature 22 °C.

References

(1) De Greef, T. F. A.; Smulders, M. M. J.; Wolffs, M.; Schenning, A. P. H. J.; Sijbesma, R. P.; Meijer, E. W. *Chemical Reviews* **2009**, *109*, 5687–5754.

(2) De Windt, L. N.; Kulkarni, C.; Ten Eikelder, H. M.; Markvoort, A. J.; Meijer, E. W.; Palmans, A. R. *Macromolecules* **2019**, *52*, 7430–7438.

(3) Kulkarni, C.; Meijer, E. W.; Palmans, A. R. A. *Accounts of Chemical Research* **2017**, *50*, 1928–1936.

(4) Zhao, D.; Moore, J. S. *Organic and Biomolecular Chemistry* **2003**, *1*, 3471–3491.

(5) Stals, P. J. M.; Smulders, M. M. J.; Martín-Rapún, R.; Palmans, A. R. A.; Meijer, E. W. *Chemistry - A European Journal* **2009**, *15*, 2071–2080.

(6) Nakano, Y.; Hirose, T.; Stals, . M.; Meijer, E. W.; Palmans, A. R. A. *Chemical Science* **2012**, *3*, 148–155.

(7) Wilson, A. J.; Van Gestel, J.; Sijbesma, R. P.; Meijer, E. W. *Chemical Communications* **2006**, 4404–4406.

(8) Cantekin, S.; de Greef, T. F. A.; Palmans, A. R. A. *Chemical Society Reviews* **2012**, *41*, 6125–6137.

(9) Brunsveld, L.; Schenning, A. P. H. J.; Broeren, M. A. C.; Janssen, H. M.; Vekemans, J. A. J. M.; Meijer, E. W. *Chemistry Letters* **2000**, 292–293.

(10) Smulders, M.; Nieuwenhuizen, M.; De Greef, T.; Van Der Schoot, P.; Schenning, A.; Meijer, E. *Chemistry - A European Journal* **2010**, *16*, 362–367.

(11) Ten Eikelder, H. M. M.; Markvoort, A. l. J.; De Greef, T. F.; Hilbers, P. A. J. *Journal of Physical Chemistry B* **2012**, *116*, 5291–5301.

(12) Nakano, Y.; Markvoort, A. J.; Cantekin, S.; Filot, I. A. W.; Ten Eikelder, H. M. M.; Meijer, E. W.; Palmans, A. R. A. *Journal of the American Chemical Society* **2013**, *135*, 16497–16506.

(13) Hartlieb, M.; Mansfield, E. D. H.; Perrier, S. *Polymer Chemistry* **2020**, *11*, 1083–1110.

(14) Smulders, M. M. J.; Stals, P. J. M.; Mes, T.; Paffen, T. F. E.; Schenning, A. P. H. J.; Palmans, A. R. A.; Meijer, E. W. *Journal of the American Chemical Society* **2010**, *132*, 620–626.

4 Asymmetric Hydrogenation

4.1 Introduction

In the designed BTA system, a hydrogenation of aagBTA or gBTA will be the core for the stereo-ampification. As the target for the hydrogenation reactions are olefinic double bonds, the Ir catalyzed hydrogenation systems developed by Pfaltz will be exploited. As the hydrogenation of aagBTA and gBTA has not been reported in literature, screening was performed to find out what type of catalyst, pressure and solvent would perform best. The selected ligands are bidentate ligands, allowing them to bind with two donor atoms the metal (Section 4.1), and all are previously reported in literature to hydrogenate olefins. [1–3] Ligands are among other things characterized by their donor atoms. A bidentate ligand which has two phosphorus donor atoms, is denoted as a P,P-type ligand, while a ligand indicated as N,P-type possesses a nitrogen and phosphorus atom as donor atoms.

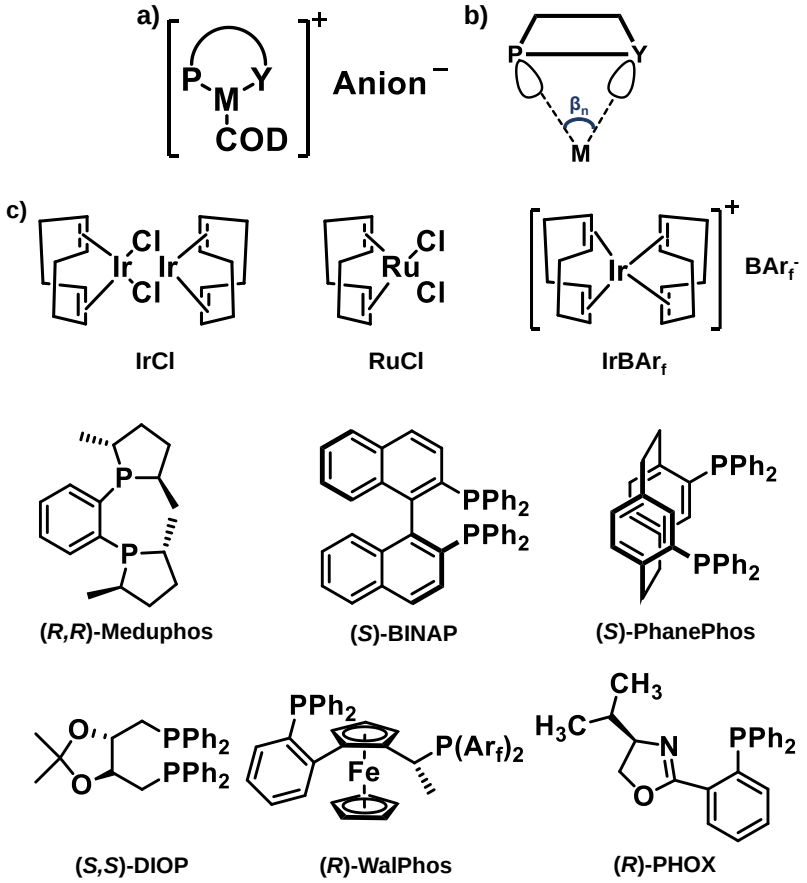

Figure 4.1: *a) General structure of chiral catalyst, 'Y' can be a nitrogen or phosphorus atom depending on the ligand, 'M' represents the metal. (b) Representation of bite angle, β_n, with lone pairs on donor atoms. c) Molecular structure of all metal precursors and chiral ligands used in this thesis. Abbreviations: MP = metal precursor; COD = cycloocta-1,5-diene; BAr_f^- = tetrakis(3,5-bis(trifluoromethyl)phenyl)borate; L = ligand; Ph = phenyl; Ar_f = 3,5-bis-(difluoromethyl)phenyl.*

In addition to the donor element on the ligands, the properties of the resulting metal complex are also influenced by the substituents on the donor atoms, the structure of the bridge between the donor atoms and the length of the bridge between them.[4] The length of bridge determines the distance between donor atoms when bonded to the metal. A factor which describes this distance better is the bite angle, β_n (Fig. 4.1b), as this angle can be estimated from the crystal structures of the ligands or corresponding metal complexes using X-ray crystallography. It describes the angle of the preferred ligand backbone i.e. the angle between ligand-metal-ligand denoted as L-M-L.[5] A structure of a five membered ring between L-M-L forms the most stable complexes.[6] In octahedral or square planar complexes this holds when the metal preferred angle is 90° and in tetrahedral complexes this angle will be enlarged to 109°.[6, 7]

A broad class of ligands was selected, with different substituents, donor atoms or bridges be-

tween the donor atoms: (-)-1,2-Bis[(2*R*,5*R*)-2,5-dimethylphospholano]benzene (**(*R,R*)-MeduPhos**) an atropisomeric ligand, with two phospolane rings that are connected *via* a phenyl bridge (Fig. 4.1c); (*S*)-(-)-2,2'-Bis(diphenylphosphino)-1,1'-binaphthyl (**(*S*)-BINAP**), a ligand that has previously shown to be effective in e.g. the hydrogenations performedn by Noyori; (*S*)-(+)-4,12-Bis(diphenylphosphino)-[2.2]-paracyclophane (**(*S*)-PhanePhos**), an atropisomeric ansa ligand which is constituted of two diphenylphosphine groups; (4*S*,5*S*)-(+)-4,5-Bis(diphenylphosphinomethyl)-2,2- dimethyl-1,3-dioxolane (**(*S,S*)-DIOP**), a ligand which is also composed of two diphenylphophine groups but these are connected *via* a bridged 1,3-dioxlane group, these are chiral C_2 symmetric ligands without stereogenic center, while the following ones bear a stereocenter. (*R*)-(-)-1-[(*R*)-2-(2'-Di-Ph-phosphino-Ph)ferrocenyl]ethyldi(bis-3,5-trifluoromethyl-Ph)phosphine (**(*R*)-WalPhos**), is an asymmetric diposphine ligand, where a diphenylphosphine group is bridged to a trifluoromethylphenyl phosphine group *via* ferrocene; (*R*)-(+)-2-[2-(Diphenylphosphino)phenyl]-4-isopropyl-2-oxazoline (**(*R*)-PHOX**), a N,P-type ligand, where a diphenylphosphine group is bridged to an oxazoline group via a phenyl ring.

For the screening two metal precursors bis(1,5-cyclooctadiene)diiridium(I) dichloride (**IrCl**) and Dichloro(1,5-cyclooctadiene)ruthenium(II) (**RuCl**) were compared. Chloride ions are the coordinating counter-ions, which will be replaced by the chiral ligand and cyclooctadiene (COD) is a ligand which will be replaced when the olefinic double bond is inserted. Ir(I) can be twice coordinated by the chiral ligand, while ruthenium(II) is mono coordinated. The last part of the screening focuses on the influence of the coordinating counter ion, therefore Bis(cyclooctadiene)iridium(I) tetrakis(3,5-bis(trifluoromethyl)phenyl)borate (**IrBAr$_f$**) was studied as precursor for the hydrogenation reactions as well. $BAr_f{}^-$ is much weaker coordinating counter-ion then Cl^-, which according to literature showed higher reactivity in hydrogenation reactions.[8, 9]

Ru complexes typically require an coordinating group next to an olefinic C=C bond, a lower reactivity compare to Ir complexes is expected.[10] But, a farnesol derivative, a molecule that is structurally very similar to the geranyl side chain, was hydrogenated with a Ru(II)/BINAP complex to >99% conversion and 96% *ee*.[11] In addition, chiral N,P-type ligands in combination with iridium have shown to achieve high enantioselectivity and reactivity for the group of unfunctionalized olefins. A particularly versatile ligand, which has been used for the hydrogenation of multiple types of olefins are phosphinooxazoline (PHOX) type ligands (**L4** in Fig. 4.1c). This ligand formed, with Ir(I), a catalytic complex and the group of Pfatlz were able to hydrogenate γ-Tocotrienyl Acetate giving >99% conversion and >98% enantiomeric excess.[10] Moreover, they demonstrated the hydrogenation of farnesol stereoisomers, with >99% conversion and 99% enantiomeric excess.[11, 12]

Hydrogenation reactions are mostly carried out in dichloromethane (DCM), but toluene and 1,2-dichloro-ethane (DCE) have also been reported with similar enantioselectivity and reactivity for the hydrogenation of unsubstituted olefins.[4, 10, 13] As toluene and MCH are both hydrocarbons and DCE has previously been reported in literature as a successful solvent, it was anticipated that the hydrogenation of gBTA and aagBTA could be accomplished in the selected solvent mixture of MCH and 5% DCE (v/v). Even though the hydrogenation of farnesol derivatives containing three double bonds were carried out at 50 bar, the screening was performed at 1 bar, because this decreases the required time to perform the screening.[11] An additional advantage of performing the hydrogenation at 1 bar is that the hydrogenation can be followed in real time with CD spectroscopy. Hereby the need to use a chiral HPLC column to separate the stereoisomers would be eliminated.

It is important to note that the goal of the hydrogenation is not to reach very high enantioselectivity and reactivity, but to produce enough chiral product in the first round to amplify the small enantio imbalance present in the stacks. Then, in the next round the enantioselectivity of the catalyst will be enhanced further, which will generate more chiral product.

4.2 Method to Determine the Conversion

In order to set up a screening of various ligands and conditions it is essential to establish a reliable method to determine the conversion of the hydrogenation reaction. to probe whether ^{1}H-NMR spectroscopy would be a feasible method to do so, we studied the ^{1}H-NMR spectrum of (*S*)-BTA and gBTA. Fortunately, three distinct signals of the side chains, that of the amide NH (blue box in Fig. 4.2 at $\delta = 6.30$), the α-CH_2 group (red box in Fig. 4.2 at $\delta = 4.10$) and the olefinic CH signals (gray box in Fig. 4.2 at $\delta = 5.30$ and $\delta = 5.05$) are well separated and shift or disappeared upon reduction.

The signal of the amide NH shifts to $\delta = 6.35$ and the α-CH_2 shifts to $\delta = 3.50$ and transforms to a multiplet. The olefinic signals completely disappear upon full reduction, otherwise integration of these peaks to one or three for aagBTA and gBTA respectively, can be used to determine the

conversion. Because gBTA has three symmetric side chains lower conversions were determined with less error in comparison to aagBTA.

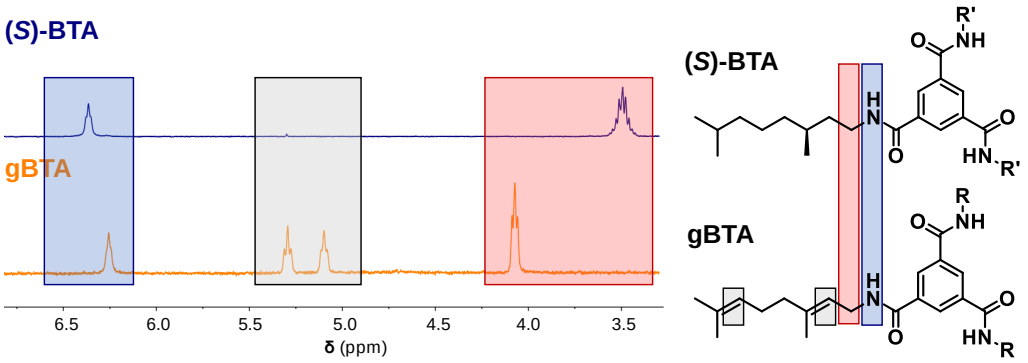

Figure 4.2: *Structure and* ^{1}*H-NMR spectrum of (S)-BTA and gBTA. Blue box indicates the proton signal of amide, red box indicates* α *protons to amide and gray box indicates the olefinc protons.*

Determining the enantioselectivity of the hydrogenation reaction is extremely challenging as the interaction with the chiral stationary phase in the HPLC columns will only minutely differ between the two enantiomers - formed after hydrogenating aagBTA - as those are very apolar and mainly consist of aliphatic chains. Although multiple separation attempt with different solvents and columns (chiracel-OD column, chiralpak IC, chiralpak AD and chiralpak AY in (n)-hexane/isopropanol 90/10 and hexane/ethanol 90/10) were tested no separation was observed. The screening focuses on finding the catalyst which can hydrogenate the substrates. Hence, the enantiomeric excess of the screening reactions was not determined.

4.3 Screening for Optimal Reaction Conditions

The results from the solubility study indicated that aagBTA and gBTA self-assemble at 20 °C into supramolecular stacks when 5% DCE (v/v) in MCH is the solvent mixture (Section 3.2). As the amount of polar solvent influences the conversion for homogeneous hydrogenation reactions, is it important to 1) find the MCH/DCE ratio compatible with the hydrogenation and 2) optimize the other reaction conditions, metal/ligand complex, pressure, catalytic loading that the hydrogenation can be performed in the solvent mixture of 5% DCE in MCH. Because, such conditions would allow to monitor the hydrogenation reaction in *situ* with e.g. CD spectroscopy.

Moreover, the S&S experiment conducted in 5% DCE (v/v) in MCH (Section 3.4) showed that a net helicity of 1 is reached when 10% of (S)-BTA sergeant is present in stacks constituted of aBTA or aagBTA. Thus the optimized reaction conditions, which reach higher conversion, would have the additional positive effect that the product is more enantioselectively formed which would induce a higher degree of bias of the helicity of the supramolecular stacks and thus higher degree of amplification would be observed in the final hydrogenation system.

All reactions were performed at 20 °C and all each reaction condition was tested at least two times, to obtain more reliable results. Furthermore, as IrCl is a dimer, it can per IrCl molecule bind two ligand molecules, whereas RuCl and IrBAr$_f$ are both monomers, thus each can only bind one ligand molecule per RuCl or IrBAr$_f$ molecule, giving a ratio of metal/ligand for IrCl 1/2 and for RuCl and IrBAr$_f$ 1/1. As aagBTA contained only a third of the reducible olefinic groups compared to gBTA only 10 mol% catalyst compared to 30 mol% for gBTA were used.

4.3.1 Initial Experiments for the Hydrogenation of gBTA

The initial reactions were carried out in a solvent mixture of 1% DCE (v/v) in MCH with 30 mol% of the catalytic complex. Reaction mixtures of gBTA were hydrogenated with a hydrogen balloon - at 1 bar. The solutions were stirred at room temperature for 24 hours, after which no conversion was observed (Table 1, entry 1-12). To analyze if the hydrogen balloon caused the low conversions and to decrease (small) H_2 pressure differences between samples, triethylsilane (Et_3SiH) was tested as hydrogen source for the same conditions. Unfortunately, all conversions were below the detectable limit (Table 2, entry 1-6). This suggested that typical assembly conditions do not seem compatible with the hydrogenation at 1 bar or with Et_3SiH. We therefore tested the hydrogenation in conditions that are typical for hydrogenations conditions - 5 bar and pure DCM.

Remarkably, when changing the solvent to pure DCM in the presence of 30 mol% IrCl/(*S,S*)-DIOP and 5 bar hydrogen quantitative conversion of gBTA was observed (Table 3, entry 1). Here a catalytic IrCl complex was used as the group of Platz suggest that its more promising then RuCl complexes.[8, 10–12, 14] This demonstrated that the hydrogenation of gBTA was possible at 5 bar H_2. Yet, as we are interested to perform the reaction in *situ* and monitor the hydrogenation reaction in real time with e.g. CD spectroscopy, lower pressure is required to limit the use of a high pressure apparatus. Thus the same reaction conditions were tried, but with only 1 bar H_2, which provided product **2** with 10% conversion (Table 3, entry 2).

Table 1: *Investigation of the reactivity of catalysts IrCl/L and RuCl/L for the enantioselective hydrogenation of gBTA*

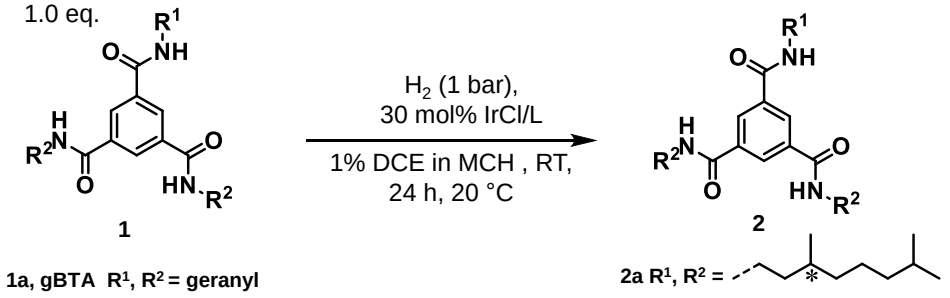

Entry	Cat.	Conv.(%)[a,b]	Entry	Cat.	Conv.(%)[a,b]
1	IrCl/(*R,R*)-MeduPhos	<5	7	RuCl/(*R,R*)-MeduPhos	<5
2	IrCl/(*S*)-BINAP	<5	8	RuCl/(*S*)-BINAP	<5
3	IrCl/(*S*)-PhanPhos	<5	9	RuCl/(*S*)-PhanPhos	<5
4	IrCl/(*S,S*)-DIOP	<5	10	RuCl/(*S,S*)-DIOP	<5
5	IrCl/(*R*)-WalPhos	<5	11	RuCl/(*R*)-WalPhos	<5
6	IrCl/(*R*)-PHOX	<5	12	RuCl/(*R*)-PHOX	<5

[a]The average conversion is listed, the full table can be found in Section 8.3 Table 14.

[b]Conversion of <5% indicates below detectable limit.

Table 2: *Investigation of the reactivity of catalysts IrCl/(R)-PHOX with Et_3SiH as hydrogen donor in the enantioselective hydrogenation of gBTA*

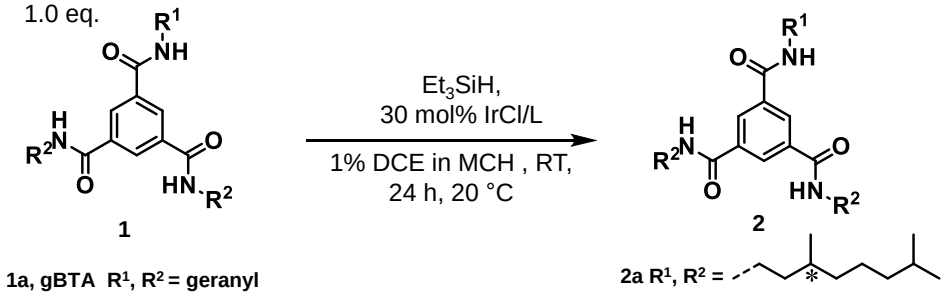

Entry	Cat.	Conv.(%)[a,b]	Entry	Cat,	Conv.(%)[a,b]
1	IrCl/(*R,R*)-MeduPhos	<5	4	IrCl/(*S,S*)-DIOP	<5
2	IrCl/(*S*)-BINAP	<5	5	IrCl/(*R*)-WalPhos	<5
3	IrCl/(*S*)-PhanPhos	<5	6	IrCl/(*R*)-PHOX	<5

[a]The average conversion is listed, the full table can be found in Section 8.3 Table 15.

[b]Conversion of <5% indicates below detectable limit.

4.3.2 Reproducibility in the Hydrogenation Reaction

To monitor the hydrogenation reaction in *situ*, not only a pressure of 1 bar is required, but also a solvent wherein the BTAs self-assembly into supramolecular stacks. Therefore, the solvent was changed from DCM to DCE and the ligand was changed (*R*)-PHOX, which is reported in literature to hydrogenate triple unsubstituted olefin similar to the geranyl amide side chain in DCM and DCE (Fig. 1.2).[10] Indeed, the obtained average conversion, 15%, was higher compared to

Table 3: *Influence of pressure and solvent for catalyst IrCl/(S,S)-DIOP for the enantioselective hydrogenation of gBTA*

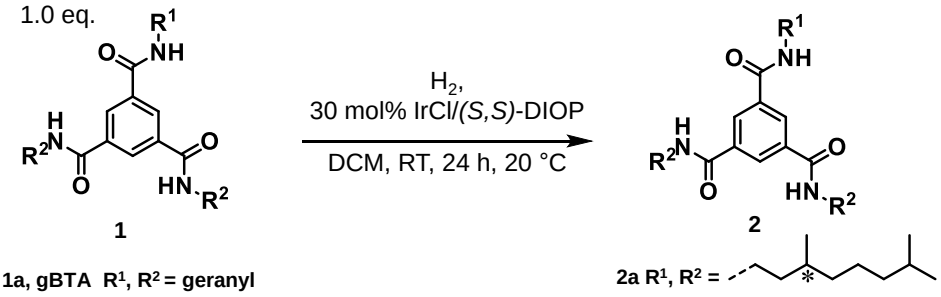

Entry	Pressure (bar)	Conv.(%)
1	5	>99
2	1	10

IrCl/(*S,S*)-DIOP complex (10%) for the same catalytic loading (30 mol%), but the conversion fluctuated between experiments(Table 4, entry 1-3). To determine the origin of the reproducibility issues, several reactions conditions were tested (Table 12 in Section 5.3). It was found that the hydrogen balloon was not air tight, hence there was partial exchange with air, which formed an air layer above the solution hereby causing irreproducibility and low conversions. The investigation which provided these results will be elaborated in Section 5.3.

In the new hydrogenation set-up the empty volume in the sample is filled with hydrogen, instead of a hydrogen balloon functioned as hydrogen source. This empty volume (15 cm^3) is large enough to provide the catalyst with enough hydrogen to fully hydrogenate gBTA. For the same reaction conditions, DCE with 30 mol% IrCl/(*R*)-PHOX, conversions of 39% for gBTA were obtained (Table 4, entry 4). As this reduction with the new set-up in DCE was successful, we decided to focus again on optimization of the asymmetric hydrogenation, at 1 bar. We therefore repeated the original screening, however started with optimization of the solvent as we suggest that is the most dominant factor influencing the conversion.

Table 4: *Influence of pressure and solvent for catalysts IrCl/(R)-PHOX and IrCl/(R)-PHOX for the enantioselective hydrogenation of gBTA*

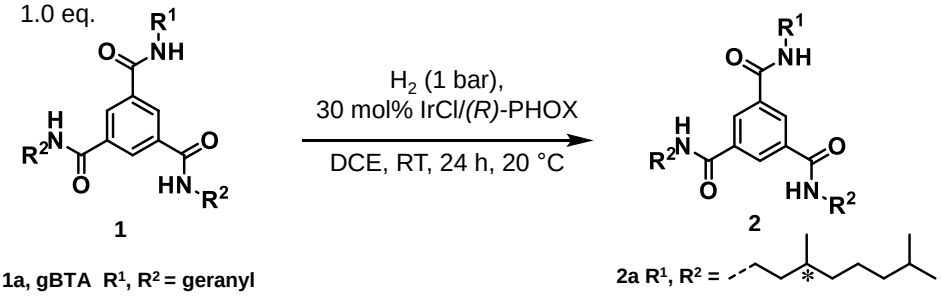

Entry	Conv. (%)
1	23
2	<5[a]
3	11
4	39

[a]Conversion of <5% indicates below detectable limit.

4.3.3 Influence of Volume Percent DCE

In order to reach the final aim of the project – the amplification of enantiomeric excess using the supramolecular catalyst – it is essential to be able to perform the hydrogenation reaction under conditions at which the BTAs are assembled (5% DCE (v/v) in MCH). Thus the ratio of MCH/DCE needs to be optimized as such that the hydrogenation can occur but there is self-assembly. To

evaluate the relation between polarity of the solvent and conversion in the hydrogenation of gBTA and aagBTA reaction mixtures containing pure DCE, MCH/DCE ratios of 20/80, 50/50, 80/20, 90/10, and pure MCH were tested in combination with IrCl/(*R*)-PHOX catalyst at 1 bar. As this catalyst hydrogenated gBTA in the first screening it was expected that it could also hydrogenate aagBTA successfully.

First, the influence of the amount of DCE was examined for the hydrogenation of gBTA. As a benchmark, gBTA was hydrogenated in DCM, since this metal complex has previously been reported therein, and showed good catalytic activity of unsubstituted olefins. [10] All reported conversions are an average of at least 2 reactions, which makes the results more reliable. The conversion in pure DCE (49%) is much lower than that observed in pure DCM (79%) (Table 5, entry 1,2). Reducing the volume percent DCE from 100-10% reduces the conversion from 49-<5% (Table 5, entry 1-6). Remarkably, at 20% DCE (v/v) in MCH there is a local optimum in conversion after which the conversion decreases below 20%.

A possible cause for the observed difference of catalytic activity between DCM and DCE is that DCE may compete with COD for the free binding space on iridium, as the structure of DCE is similar to COD. Thus when DCE binds to iridium an inactive catalytic species may be formed. Because MCH is a poor solvent to solubilize the transition states, they define the activation energy and thereby the rate of the catalyst, the catalytic reactivity is decreased when reducing the amount of DCE in the solvent mixture (Fig. 1.2).[9]

Next, we explored the influence of reducing the vol% DCE in the solvent mixture for the conversion in the hydrogenation of aagBTA. Since the goal is to optimize the reaction to conditions where BTAs self-assembles, we started the investigation at 20 vol% DCE in MCH. The vol% of DCE was decreased from 20-<5% (Table 5, entry 7-10). Opposite of gBTA, reducing the vol% DCE does not have a clear effect on conversion, but the conversion at 20% DCE (v/v) is lower for aagBTA (18%) then for gBTA (55%) (entry 5 and 7 respectively). For the same reaction conditions, reaction mixtures of aagBTA and gBTA should contain the same amount of inactive catalytic species. Relatively, this indicates that in aagBTA reaction mixtures less active catalyst is present as the catalytic loading in aagBTA (10 mol%) is lower compared to gBTA (30 mol%). This could account for the lower conversion observed for aagBTA compared to gBTA at 20% DCE (v/v).

As the objective of the screening is to determine the reaction condition were BTAs self-assembly, the lowest vol% DCE where IrCl/(*R*)-PHOX converted aagBTA and gBTA is selected to further optimize the reaction conditions. For aagBTA this was at 5% DCE (v/v) in contrast to gBTA were 20% DCE (v/v) was required.

4.3.4 Investigation of Best Performing Metal Complex

The second experiment in the screening was intended to find the most active metal complex. Determining what type of ligand e.g. P,P-type, N,P-type or atropisomeric could help identify a possible molecular structure which can be linked to the BTA core to form achiral ligand BTA. First, the activity of IrCl and Ru/Cl complexes (30 mol%) was investigated for gBTA in 20% DCE (v/v) in MCH. All IrCl complexes, except IrCl/(*R,R*)-MeduPhos (Table 6, entry 1), were found to be catalytically active but their activity differed significantly: 42% for IrCl/(*R*)-WalPhos, 50% for IrCl/(*S*)-Phanephos, $\sim$ 70% for IrCl/(*S*)-BINAP and IrCl/(*R*)-PHOX and 80% for IrCl/(*S,S*)-DIOP (Table 6, entry 2-6). In contrast for RuCl complexes which were not effective (<5%) (Table 6, entry 7-12). Because all RuCl complexes were not active these were excluded from the activity examination in the hydrogenation of aagBTA. A similar trend was observed in the hydrogenation of aagBTA with 10 mol% catalyst loading in 5% DCE (v/v) in MCH, IrCl/(*R,R*)-MeduPhos was not active (Table 6, entry 13) and the other complexes have good activity with observed conversions 12-25% (Table 6, entry 14-18). To verify if the catalytic activity can be attributed to the metal complex, the reactivity of only IrCl was investigated, which was found to be below detectable limit for both gBTA and aagBTA hydrogenation (Table 6, entry 19, 20). Thus the observed conversions are the result of the metal complexes.

Lower catalytic activity is observed for the same complexes in the case of aagBTA compared to gBTA, which might be attributed to the low amount of chlorinated solvent, which is only 5 vol% in the hydrogenation of aagBTA. Because, there is no coordinating group next to the olefinic bonds, which is necessary for good reactivity of such complexes, could explain low activity of all RuCl complexes.[10, 11]

The least active ligand, (*R,R*)MeduPhos, exhibits a small bite (85°), which could result in the low conversions observed, as there is stronger electron back-donating of donor atoms in metal complexes with a large bite angle, which increases reactivity of the metal complex.[5, 15] Moreover, less flexible phospholane moieties in combination with the rigid backbone in (*R,R*)MeduPhos induce

Table 5: *Influence of vol% DCE on reactivity of IrCl/(R)-PHOX catalyst for the enantioselective hydrogenation of gBTA and aagBTA.*

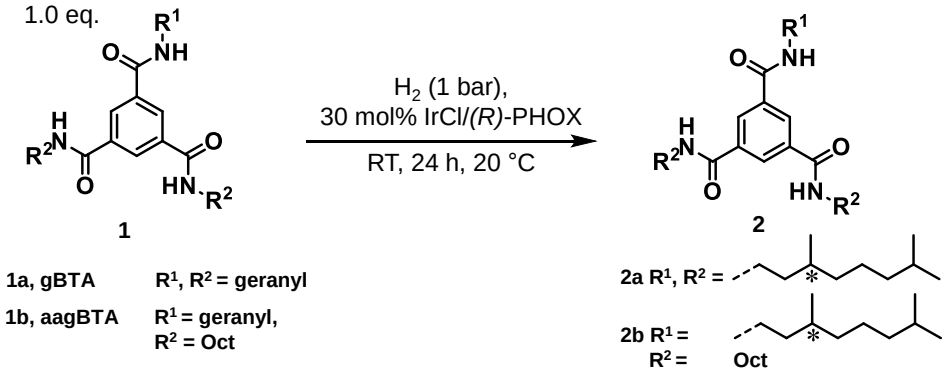

Entry	Substrate	Cat. loading (mol%)	Solv. A	Solv. B (vol%)	Conv. (%)[a]
1	**1a**	30	-	DCM (100)	76
2	**1a**	30	-	DCE (100)	49
3	**1a**	30	MCH	DCE (80)	46
4	**1a**	30	MCH	DCE (50)	42
5	**1a**	30	MCH	DCE (20)	55
6	**1a**	30	MCH	DCE (10)	<5[b]
7	**1b**	10	MCH	DCE (20)	18
8	**1b**	10	MCH	DCE (10)	16
9	**1b**	10	MCH	DCE (5)	18
10	**1b**	10	MCH	-	<5[b]

[a]The average conversion is listed, the full table can be found in Section 8.3 Table 16.

[b]Conversion of <5% indicates below detectable limit.

a high rotation barrier for the binding of phosphine atoms to the metal center, which can inhibit the degree of conformational freedom in transition state complexes, also reducing the reactivity.[15] The ferrocene backbone in (*R*)-WalPhos is known to be flexible, which can indicate a lack of preference for specific molecular structures in the transition state structures which decreases the rate of conversion.[6] The calculated natural bite angle (>103°) is widest for (*S*)-PhanePhos, which might clarify its poor reactivity.[16, 17] Most active ligands, (*S*)-BINAP, (*S,S*)-DIOP and (*R*)-PHOX, all have calculated bite angles between 90-100°.[7, 18, 19]

Because the best performing IrCl complexes all have ligands with a diphenylphosphine (PPh_2) we suggest that achiral ligands bearing such a group are good candidates to test after the optimization of the reaction conditions is completed. Because conversions reached for the best complexes in the hydrogenation of gBTA were not sufficient to decrease the vol% to 5%, the influence of counter-ion, pressure and catalytic loading were investigated.

4.3.5 Investigation of Coordinating Counter-Ion

With the optimized reaction conditions (IrCl/(*R*)-PHOX 10 mol% in 5% DCE (v/v) in MCH for aagBTA and 30 mol% in 20% DCE (v/v) in MCH for aagBTA), we examined a different coordinating counter-ion to improve the catalytic activity further. The coordinating counter-ion can range from weakly coordinating for example, hexafluorophosphate (PF_6^-), tetrafluoroborate (BF_4^-) to stronger coordinating like halides. Weaker coordinating counter-ions tend to increase catalytic activity.[9] A special non-coordinating counter-ion, is BAr_f^- which shows an increase in turn over frequency, which arises because BAr_f^- does not coordinate to the metal *via* π-coordination thus BAr_f^- will not be bonded to the metal.[10, 20] Furthermore, it is moisture and air stable, which increases the stability.

IrCl/(*R*)-PHOX complex hydrogenated the substrates with conversion (>5%; Table 7, entry 1, 3-4), opposed to the IrBAr$_f$/(*R*)-PHOX complex were no quantitative conversion (<5%; Table 7, entry 2, 5-6) was observed. This is inconsistent with the results reported in literature for a IrBAr$_f$/(*R*)-PHOX complex.[12–14, 21] Even though these complexes are more air stable, phosphorus can still be easily be oxidized, which prevents the ligand to bind Ir(I) causing inactivation of the catalyst.[22, 23] where an oxygen atom can act as nucleofile and attack the phosphine atom, which will make the phosphine atom positively charged.[7] This can be confirmed *via* ^{31}P-NMR spectroscopy. A

Table 6: *Investigation of the activity of catalysts IrCl/L and RuCl/L for the enantioselective hydrogenation of gBTA and aagBTA.*

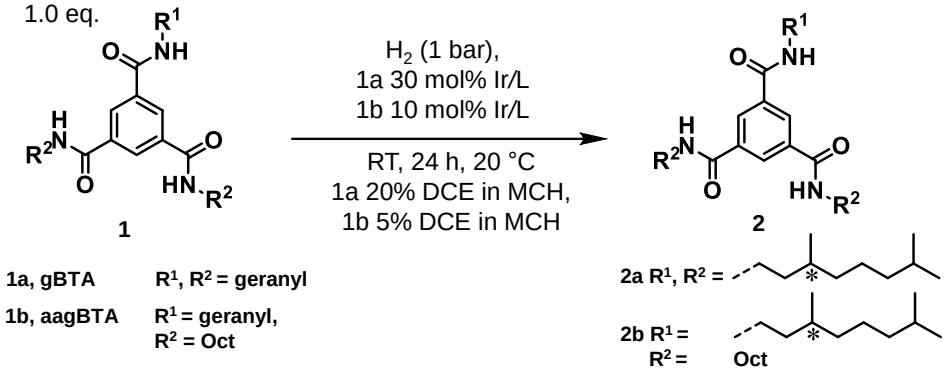

Entry	Sub.	Cat.	Conv. (%)[a,b]	Entry	Sub.	Cat.	Conv. (%)[a,b]
1	**1a**	IrCl/(*R,R*)-MeduPhos	<5	13	**1b**	IrCl/(*R,R*)-MeduPhos	<5
2	**1a**	IrCl/(*S*)-BINAP	69	14	**1b**	IrCl/(*S*)-BINAP	17
3	**1a**	IrCl/(*S*)-PhanPhos	50	15	**1b**	IrCl/(*S*)-PhanPhos	12
4	**1a**	IrCl/(*S,S*)-DIOP	80	16	**1b**	IrCl/(*S,S*)-DIOP	25
5	**1a**	IrCl/(*R*)-WalPhos	42	17	**1b**	IrCl/(*R*)-WalPhos	14
6	**1a**	IrCl/(*R*)-PHOX	70	18	**1b**	IrCl/(*R*)-PHOX	25
7	**1a**	RuCl/(*R,R*)-MeduPhos	<5	19	**1a**	IrCl	<5
8	**1a**	RuCl/(*S*)-BINAP	<5	20	**1b**	IrCl	<5
9	**1a**	RuCl/(*S*)-PhanPhos	<5				
10	**1a**	RuCl/(*S,S*)-DIOP	<5				
11	**1a**	RuCl/(*R*)-WalPhos	<5				
12	**1a**	RuCl/(*R*)-PHOX	<5				

[a]Average conversion is listed, the full table can be found in Section 8.3 Table 17.

[b]Conversion of <5% indicates below detectable limit.

phosphorus atom bonded to Ir(I) should have a shift around $\delta = 11$ ppm and bonded to oxygen a shift between $-5 > \delta > 20$ ppm is expected.[13, 24] Therefore, we examined the catalyst complex formation of IrCl/(*R*)-PHOX and IrBAr$_f$/(*R*)-PHOX and the complex preparation were investigated.

Samples were prepared by dissolving $\sim$ 1 mg of IrCl and $\sim$ 2 mg (*R*)-PHOX in 1 mL DCM, DCE or 5% DCE (v/v) in MCH and $\sim$ 1 mg of IrBAr$_f$ and $\sim$ 1 mg (*R*)-PHOX in 1 mL DCE. The group of Pflatz prepared their IrBAr$_f$/(*R*)-PHOX complexes by first dissolving IrCl and (*R*)-PHOX in DCM and stirring it at reflux temperature for 2 hours.[13] The same method was employed to investigate the difference in sample preparation on the oxidation of the phosphorus atom. All samples were stirred for 2 hours; heated samples were heated to 60 °C in a sand bath. Heating a sample before measurements or using BAr$_f^-$ as counter-ion both resulted in negative δ values (Table 8, entry 2,5), suggesting that the phosphorus atom is oxidized. Moreover, heating the sample gave rise to appearance of multiple peaks in the spectrum (entry 2), which might indicate the formation of numerous different species. The solvent has no influence on the ability of oxygen to oxidize the phosphorus atom, as for DCM, DCE and 5% DCE (v/v) in MCH positive δ values are observed (entry 1, 3 and 4 respectively). Samples measured after 24 hours indicated that no change in oxidation was observed (entry 1, 2 and 5). These findings were in accordance with the hydrogenation results, therefore the catalytic complex with BAr$_f^-$ was discarded for further research. All ^{31}P-NMR spectra can be found in Section 8.4.

4.3.6 Influence of Pressure

As a the reaction with IrBAr$_f$ at 1 bar gave only poor conversion (<5%) we aimed to improve the reactivity by increasing the hydrogen pressure. According to literature an increase in pressures should result in an increase in conversion.[12, 21, 25] To study if a higher H_2 pressure leads to an increase in conversion in our system, we compared the hydrogenation of aagBTA and gBTA under previously optimized conditions (IrCl/*R*-PHOX 30 or 10 mol% in 5% DCE (v/v) in MCH) at 1 and 50 bar H_2 pressure. For both substrates a increase in pressure increased the conversion to 38% for gBTA (Table 9) and 33% for aagBTA (Table 9).

Table 7: *Influence of the coordinating counter-ion $BAr_f{}^-$ and Cl^- for the enantioselective hydrogenation of aagBTA and gBTA.*

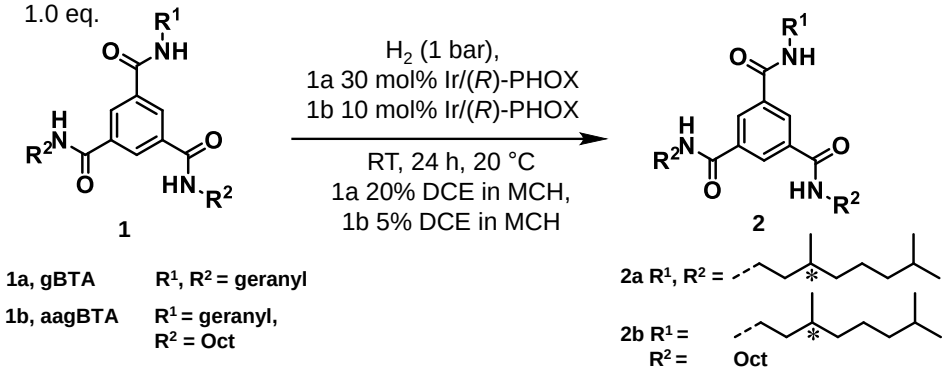

Entry	Sub.	Cat.	Solv. MCH/DCE (vol%)	Conv. (%)
1	**1a**	IrCl/(*R*)-PHOX	80/20	55
2	**1a**	RuCl/(*R*)-PHOX	80/20	<5[a]
3	**1b**	IrCl/(*R*)-PHOX	95/5	16
4	**1b**	IrCl/(*R*)-PHOX	95/5	23
5	**1b**	RuCl/(*R*)-PHOX	95/5	<5[a]
6	**1b**	RuCl/(*R*)-PHOX	95/5	<5[a]

[a]Conversion of <5% indicates below detectable limit.

Table 8: ^{31}*P-NMR chemical shifts of Ir/PHOX complexes with $BAr_f{}^-$ and Cl^-.*

Sample #	Anion	Solvent	Heating[a]	δ (ppm)
1 after 1 hour	Cl^-	DCM	No	14
1 after 24 hours	Cl^-	DCM	No	14
2 after 1 hour	Cl^-	DCM	Yes	14, -6
2 after 24 hours	Cl^-	DCM	Yes	-26[b]
3 after 1 hour	Cl^-	DCE	No	14
4 after 1 hour	Cl^-	5% DCE (v/v) in MCH %	No	14
5 after 1 hour	$BAr_f{}^-$	DCE	No	-6
5 after 24 hours	$BAr_f{}^-$	DCE	No	-6

All samples were stirred for one hour at room temperature after their preparation.
[a]Heated to 70 °C and stirred for 3 hours. [b]More peaks were observed, but this was most prominent.

There is no indication if the reaction is enantioselective by examining the conversion with ^{1}H-NMR spectroscopy, therefore the CD spectrum of the final mixture could be investigated. A Cotton effect indicative for the supramolecular polymer for (*S*)-BTA would support the hypothesis that (*S*)-BTA is formed. The samples were diluted 10 times to reach a concentration of 50 μM aagBTA, while the vol% DCE remained 5%. We measured the CD spectrum after 24 h of 4 samples which were hydrogenated at 1 bar: 'a1' and 'a2' with a ratio of IrCl/(*R*)-PHOX 1/2, catalyst loading of 30 mol% with conversion <5% and 50% respectively; 'b1' and 'b2' both with a ratio of IrCl/(*R*)-PHOX 1/2, catalyst loading of 10 mol%, with conversion of 15% and 13% respectively. Besides, two hydrogenations at 50 bar were investigated, 'c1' and 'c2' both with a ratio of IrCl/(*R*)-PHOX 1/2, catalyst loading of 10 mol%, with conversion of 33% and 36% respectively.

A positive cotton effect was observed for samples 'a1', 'a2', 'c2', indicated by a maximum at 270 nm and a minimum at 235 nm, while sample 'b2' and 'c1' show the same characteristics their spectra are inverted (Fig. 4.3a,b). Sample 'b1' shows no signal eventhough there is conversion (15%) After heating the samples to 80 °C and measuring at 20 °C, loss of CD signal was observed (Fig. 4.3a,b). This is unlike a 'typical' CD spectrum for (*S*)-BTA where a minimum at 223 nm is observed and the CD signal is recovered after heating to 80 °C (Fig. 4.3c).

Because the spectrum is not resembling a typical CD spectrum of (*S*)-BTA, it might be that a complex present in the final reaction mixture forms precipitated larger aggregates with a certain chirality.[26, 27] Such aggregates can be identified using linear dichroism, for which the LD spectrum should be similar to the shape of the CD spectrum. However, measuring LD spectra (Fig. 4.3d) showed no signal, implying that the signal which arises is due to another reason.

Table 9: *Influence of the pressure on the reactivity of catalysts IrCl/(R)-PHOX for the enantioselective hydrogenation of gBTA and aagBTA.*

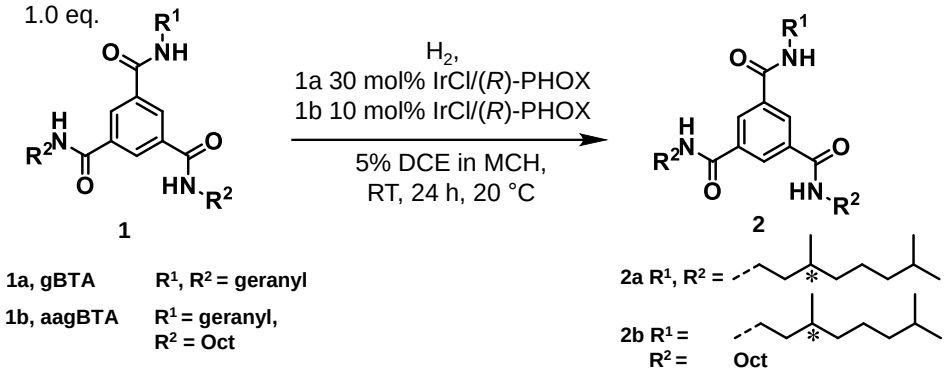

Entry	Substrate	Pressure (bar)	Conv. (%)[a]
1	**1a**	1	11
2	**1a**	50	59
3	**1b**	1	21
4	**1b**	50	35

[a] Average conversion is listed, the full table can be found in Section 8.3 Table 18.

The CD signal is often present when there is conversion, this might indicates formation of a type I chiral oligomeric species between IrCl, (*R*)-PHOX and hydrogenated aagBTA. Supporting this statement is the increased minimum at 235 mn and maximum at 2770 nm for 'a2' were the catalytic loading was increased from 10 to 30 mol% and the conversion increased to 50%. With higher conversion we expected more chiral oligomeric species and thus a higher signal intensity. Negative Cotton effect for 'b2' 'c1' can suggest a chiral species of opposite handedness. However, in experiment 'a1' no quantitative conversion was observed nonetheless a positive Cotton effect can be observed, which might indicate that Ir/Cl and (*R*)-PHOX can also form a type II chiral oligomeric species with aagBTA. A possible way to identify if the signal can be attributed a type II oligomeric species is by mixing aagBTA with Ir/Cl and (*R*)-PHOX in 5% DCE (v/v) in MCH. If after 24 h the signal is present this is indicative for a type II oligomeric species.

4.3.7 Influence of Catalytic Loading

The influence of catalyst loading and ratio between IrCl/(*R*)-PHOX on catalytic activity was investigated for aagBTA at 1 bar in 5% DCE (v/v) in MCH. Because IrCl is a dimer, it can bind two ligand molecules, thus normal catalyst loading was 10 mol% IrCl and 20 mol% (*R*)-PHOX. When the catalytic loading increased from 10 mol% to 30 mol% the conversion increased from 25% to 50 % (Table 10, entry 1,2). Halving the catalytic loading to 5 resulted in a decrease in the conversion to 7% (Table 10, entry 3). For a catalytic loading of 2 mol% the conversion was below the detectable limit (Table 10, entry 4).

An increase to 1/6 in the ratio of IrCl/(*R*)-PHOX was used to examine the influence of the ratio on the catalytic activity. When this complex was tested with the aforementioned conditions the catalytic activity was below the detectable limit (Table 10, entry 5). This suggests that an inactive catalytic complex is formed between IrCl and (*R*)-PHOX. The olefinic C = C bond is inserted at the position were COD is coordinated to Ir(I).[9, 23, 28] As COD is a weak coordinating ligand this exchange occurs relatively fast. (*R*)-PHOX on the other hand is bonded to Ir(I), thus if this molecule would also bind to Ir(I) at the free binding spot designed for the olefinic C = C bond, an inactive catalytic species would be formed. This implies that Ir(I) might also form an inactive species when it binds rather then coordinates the to geranyl side chain.

4.3.8 General Remarks and Conclusion on Reaction Optimization

In this screening never quantitative conversions (>99%) were reached, which might be ascribed to inactivation of the the catalytic complex. Metal complex IrCl/(*R*)-PHOX is similar to Crabtree's catalyst and inactivation of such catalysts, especially for hindered C = C bonds, has been described.[29] The cause is often attributed to formation of extremely stable inactive hydride-bridged trimers.[10, 30] Low temperature ^{1}H-NMR analysis can elucidate if such aggregates are present

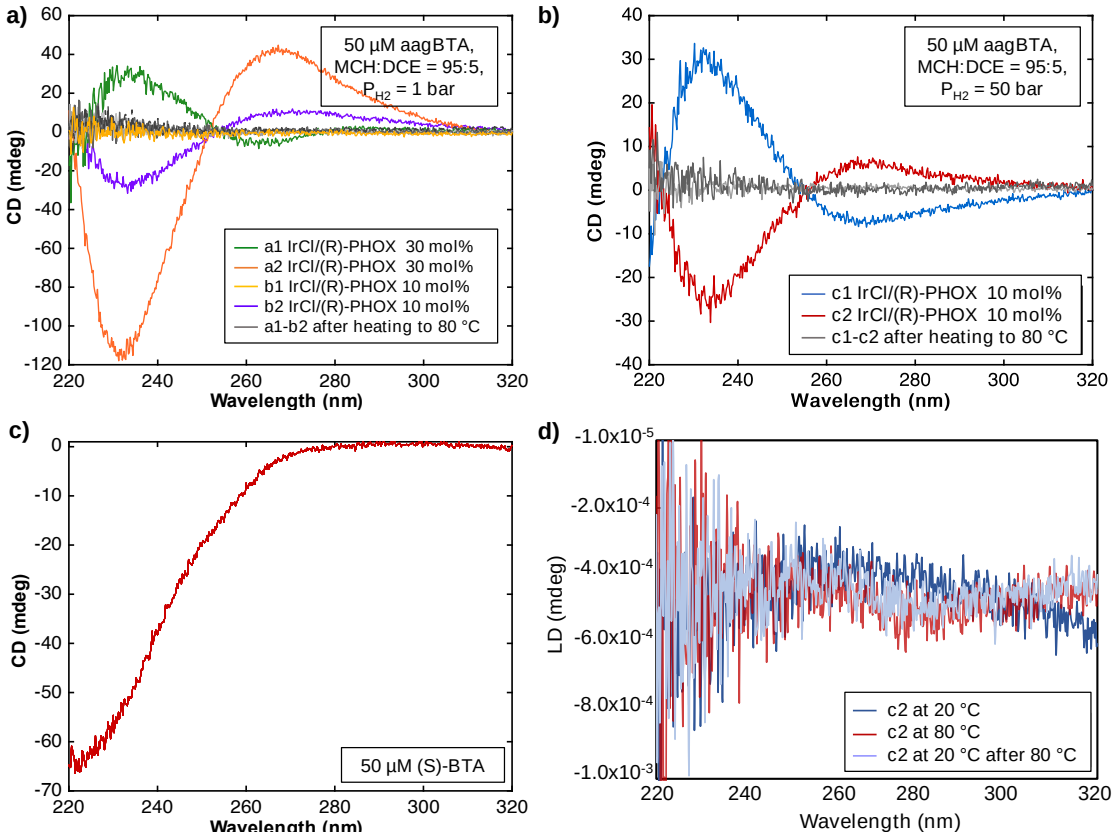

Figure 4.3: *CD spectra of 50 µM solutions of final hydrogenation of agBTA with IrCl/(R)-PHOX in 5% DCE (v/v) in MCH reaction mixtures at (a) 1 bar and (b) 50 bar. (c) Typical CD spectrum of (S)-BTA (d). LD spectrum of experiment 'c2' at different temperatures.*

in the sample. Besides, working under wet and oxygen rich conditions also reduces the catalytic activity.[10] Thus the conversion could be increased if the reaction are performed under dry and air free conditions.

The hydrogenation of aagBTA and gBTA was carried out with success. Throughout the screening several trends were observed. First, reducing the volume percentage of DCE decreased the conversion, excluding 20% (v/v) wherein the catalyst IrCl/(*R*)-PHOX performed better then in pure DCE. All RuCl complexes were ineffective in the hydrogenation of gBTA, while IrCl/ligand complexes except IrCl/(*R,R*)-MeduPhos can hydrogenate aagBTA and gBTA, where IrCl/(*S,S*)-DIOP and IrCl/(*R*)-PHOX showed highest catalytic activity. A rise in pressure and catalytic loading increased the conversion. RuBAr$_f$/(*R*)-PHOX complexes bearing BAr$_f$$^-$ as counter-ion were ineffective in the hydrogenation of aagBTA and gBTA, therefore this ion was not used in further research. In the end the optimized reaction conditions were found to be 50 bar H_2 pressure and 30 mol% IrCl/PHOX or 50 bar H_2 pressure and 10 mol% IrCl/PHOX for gBTA and aagBTA respectively. Under these conditions both substrates can be hydrogenated in a solvent mixture of 5% DCE (v/v) in MCH. In this solvent mixture the BTAs self-assemble into supramolecular stacks. This is essential for the final hydrogenation system where the catalytic activity en selectivity will be determined by supramolecular stacks.

4.4 Investigation of Achiral Ligands

The three complexes that showed very high catalytic activity, (*S*)-BINAP, IrCl/(*S,S*)-DIOP and IrCl/(*R*)-PHOX, all have a PPh_2 group and the group of Raynal demonstrated the good catalytic activity of an asymmetric BTA ligand in a supramolecular scaffold where one side chain contains a diphenhylphosphine group.[31, 32] Therefore, we assessed a commercially available achiral triphenylphosphine PPh_3 ligand as starting point for the exploration of possible molecular groups in the ligand BTA.

The catalytic activity was first examined for gBTA with IrCl/PPh_3 at 1 bar in DCM and DCE, which gave conversions above 40% for both solvents (Table 10, entry 1,2). In the screening we found that an increase in pressure, the vol% DCE can be reduced to 5% and still good catalytic

Table 10: *Influence of the catalyst loading on the reactivity of catalysts IrCl/(R)-PHOX for the enantioselective hydrogenation of aagBTA.*

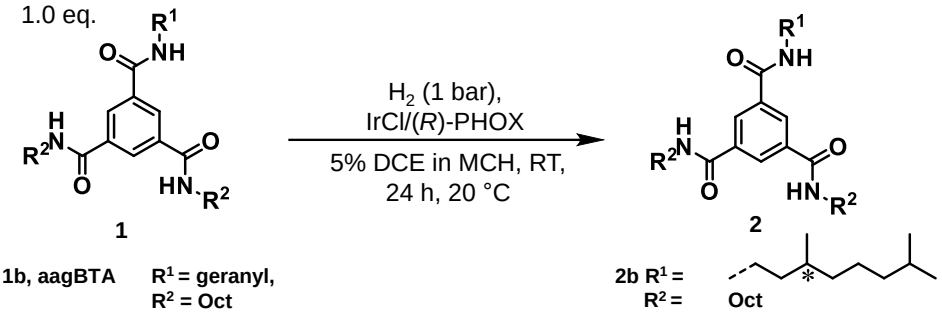

Entry	Cat. loading (mol%)	Conv. (%)[a]
1	30/60	50
2	10/20	24
3	5/10	7
4	2/4	<5[a]
5	10/60	<5[a]

[a]Average conversion is listed, the full table can be found in Section 8.3 Table 19.
[b]Conversion of <5% indicates below detectable limit.

activity is observed. Hence, the pressure was increased to 50 bar and the vol% DCE was decreased to 5% in MCH. Quantitative conversion of gBTA was observed in both solvents (Table 10, entry 3). These promising results indicated that an amine with a PPh_2 group could be a good candidate as achiral side chain in the asymmetric ligand-BTA.

Table 11: *Investigation of IrCl/PPh_3 and L-BTA for the enantioselective hydrogenation of gBTA and aagBTA*

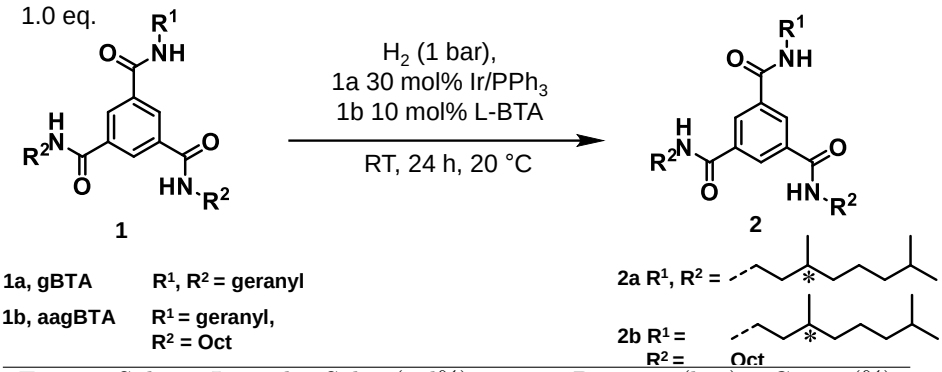

Entry	Subs.	Ligand	Solv. (vol%)	Pressure (bar)	Conv. (%)
1	**1a**	PPh3	DCM (100)	1	50[a]
2	**1a**	PPh3	DCE (100)	1	47[a]
3	**1a**	PPh3	MCH/DCE (95/5)	50	>99[a]
4	**1b**	L-BTA	MCH/DCE (95/5)	1	45
5	**1b**	L-BTA	MCH/DCE (95/5)	1	32

[a]The average conversion is listed, the full table can be found in Section 8.3 Table 20.

Subsequently, asymmetric ligand-BTA was synthesized with two (n)-octyl chains and a 2-(diphenylphosphino)-ethyl ($(Ph)_2PEt$) chain (Fig. 4.4), which will be referred to as L-BTA. However, oxidation is a known problem for these phosphine based ligands. Electron rich and donating side groups attached to the phosphine atom, in e.g. PPh_3, will stabilize this positive charge and as a result the phosphine will be less prone to oxidation.[22] In L-BTA the phosphine atom is only twice surrounded by a electron donating benzene ring, but also the nitrogen atom can donate electrons to stabilize the positive charge. However, expected was that $(Ph)_2PEt$ will be less stable then PPh_3. Thus ^{31}P-NMR spectra were measured throughout the synthesis and before hydrogenation to determine the amount of oxidized L-BTA. Oxidized phosphorus compounds have a chemical shift $\delta > 20$ and aliphatic phosphorus compounds will exhibit a chemical shift of $\delta < -5$.[24] In the final

pure L-BTA 19% of the phosphorus atoms were oxidized, the ^{31}P-NMR spectra can be found in Section 8.1.6.

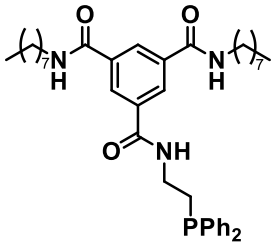

Figure 4.4: *Molecular structure of ligand BTA (L-BTA) with two (n)-octyl chains and one 2-(diphenylphosphino)ethyl chain.*

This L-BTA was tested without IrCl to investigate the catalytic activity of a BTA stack as supramolecular catalyst with an incorporated BTA ligand. In the optimized reaction conditions (10 mol% L-BTA in 5% DCE (v/v) in MCH) aagBTA was hydrogenated with a conversion of 37% (Table 11, entry 5,6). As $\sim$ 20% of L-BTA is oxidized, there was only 8 mol% of active ligand, showing that these preliminary results are extremely promising. However, more tests need to be conducted but the results are encouraging to investigate the selectivity of this L-BTA in a environment with a small enantio imbalance and of the results can be amplified in the presence of aBTA.

4.5 Conclusion

Hydrogenation of gBTA and aagBTA was successful with several metal complexes. After screening for the optimal reaction conditions the best results obtained for hydrogenation of aagBTA and gBTA was with IrCL and (*R*)-PHOX complexes. General trends in pressure, catalyst loading and volume percent DCE were observed, an increase in pressure, catalyst loading or vol % DCE (v/v) increased the conversion. At 50 bar both aagBTA and gBTA were hydrogenated with good conversion (38% and 35% respectively) in MCH 5% DCE (v/v).

Furthermore, investigation of achiral triphenylphosphine (PPh_3) as ligand yielded excellent results, with >99% conversion of gBTA at 50 bar. This result strengthened the idea to synthesize an asymmetric BTA with two (*n*)-octylamine linkers and a $(Ph)_2$PEtamine linker attached to the BTA core as ligand BTA. This ligand BTA was then tested as supramolecular catalyst and preliminary results indicated good reactivity for this complex. More experiments need to be conducted before statements regarding the reactivity are conclusive. This ligand BTA was found prone to oxidation, but more research needs to be conducted to analyze the nature of this instability. Working moisture and air free might solve or reduce this problem.

In future research this supramolecular catalyst should be tested in a chiral environment to determine the enantioselectivity, as the selectivity of this complex is determined by enantiomeric excess of the helices. If this supramolecular catalyst has both good enantioselectivity and reactivity, it should then be tested in the amplification of an asymmetric hydrogenation reaction.

4.6 Experimental Section

4.6.1 Materials and instrumentation

Solvents were purchased from Biosolve and deuterated solvents were obtained from Cambridge Isotopes Laboratories. BTAs were synthesized as described in Section 2.4 and used without any further purification.

^{1}H-NMR measurements were carried out on a Bruker 400 MHz Ultrashield spectrometer (400 MHz for ^{1}H. Proton chemical shifts are reported in ppm (δ) downfield from trimethylsilane (TMS). Splitting patterns are abbreviated as: singlet (s), doublet (d), triplet(t), quartet (q), multiplet (m), and broad singlet (br).

Circular dichroism (CD) and linear dichroism (LD) measurements were performed on a Jasco J-815 spectropolarimeter, for which the sensitivity, time constants, scan rates and temperature were chosen appropriately (sensitivity standard, response time 0.125s, band width 1 nm, scanning speed 100 nm/min, wavelength 220-320 nm, temperature 22 °C). Corresponding temperature depended measurements were performed with a Jasco PFD-425S/15 Peltier type temperature controller with a temperature range of 263–393 K and adjustable temperature slope. All spectroscopic measurements

were recorded in cells with an optical path length of 1 cm. The Spectrophotometer is equipped with a multi-cells holder for 6 samples and the temperature controlled was set on the holder station.

4.6.2 Methods

Hydrogenation
For reactions carried out at 1 bar a 20 mL Biotage Reaction Vial was used. Reaction mixtures of 500 μM 5 mL substrate were prepared in the reaction vial. The vial was closed by a cap with septum and air was removed thrice and replaced by argon. A balloon was filled with hydrogen and was then used to replace the argon atmosphere to hydrogen. The balloon was then disconnected from the vial and the reaction was stirred for 24 hours at room temperature. The solvent was removed under vacuo, the obtained mixture was subsequently dissolved in deuterated chloroform and the conversion was determined using ^{1}H-NMR spectroscopy. A total of 12 reactions could be run at the same time.

Reactions carried out at 50 bar were performed in a Parr 5521 HP Compact Reactor. With a Parr 4848 Reactor Controllor stirring was set to 400 rpm and temperature to 22 °C. Reaction mixtures of 500 μM 50 mL substrate were prepared and loaded in the reactor. The reactor was first flushed with nitrogen three times then the pressure was increased to 50 bar with hydrogen. The reaction mixture was stirred for 24 hours. A sample of 5 mL was taken from this reaction to analyze conversion. The solvent was removed under vacuo, the obtained mixture was subsequently dissolved in deuterated chloroform and the yield was determined using ^{1}H-NMR spectroscopy.

Jasco J-815 spectropolarimeter parameter settings
All CD and LD measurements were recorded with following parameters: sensitivity standard, response time 0.125s, band width 1 nm, scanning speed 100 nm/min, wavelength 220-320 nm, temperature 22 °C.

4.6.3 Synthetic Procedures

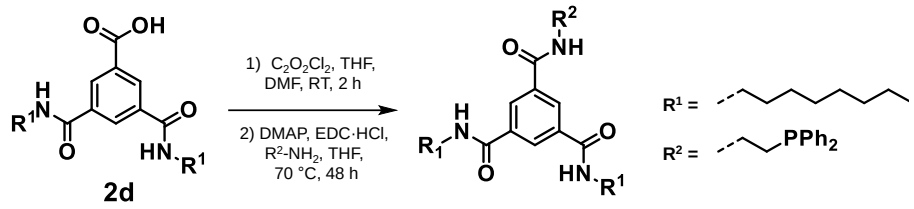

Scheme 4: *Synthetic route for L-BTA*

Synthesis of L-BTA
Details of the synthesis of ***2d*** *can be found in the Section 2.4.*
In a round bottom flask under argon **2d** (100 mg, 231 mmol, 1.0 eq.) was suspended in THF (10 mL). DMAP (42.3 mg, 347 mmol, 1.5 eq.), EDC· HCl (67.4 mg, 355 mmol, 1.5 eq.) and 2-(diphenylphosphino) ethylamine (62.0 mg, 270 mmol, 1.2 eq.) were added to the flask. The reaction mixture was stirred at reflux temperature for 48 hours. The reaction mixture was then cooled to RT and the solvent was evaporated under vacuo. DCM was added to the residue and the organic phase was washed three times with water (3 × 10 mL). The organic phase was dried over magnesium sulfate, filtrate was collected using a cellulose filter and the solvent was removed under vacuum which afforded the crude product. The crude product was purified by silica column choromatography (eluating with DCM:EtOAc 95:5-88:12 v/v) to afford final L-BTA as white powder (mg, % yield).

^{1}H-NMR (400 MHz, Chloroform-d) δ (ppm) = 8.32 (t, J = 1.7 Hz, 1H), 8.23 (d, J = 1.7 Hz, 2H), 7.55 – 7.28 (m, 10H), 6.61 (d, J = 7.0 Hz, 1H), 6.40 (d, J = 6.1 Hz, 2H), 3.76 – 3.56 (m, 2H), 3.46 (q, J = 6.7 Hz, 4H), 2.43 (t, J = 7.3 Hz, 2H), 1.48 – 1.13 (m, 24H), 0.99 – 0.79 (m, 6H). ^{31}P-NMR (162 MHz, Chloroform-d) δ (ppm) = -21.30.

References

(1) Helmchen, G.; Pfaltz, A. *Accounts of Chemical Research* **2000**, *33*, 336–345.

(2) Zhou, H. X. *FEBS Letters* **2013**, *587*, 394–397.

(3) Zhang, Y.; Rempel, C.; Mclaren, D., *Edible Coating and Film Materials: Carbohydrates*; Elsevier Ltd: 2013, pp 305–323.

(4) Pfaltz, A.; Drury, W. *Proceedings of the National Academy of Sciences of the United States of America* **2004**, *101*, 5723–5726.

(5) Dierkes, P.; van Leeuwen, P. N. M. *J. Chem. Soc., Dalton Trans.* **1999**, 1519–1529.

(6) Van Leeuwen, P. W.; Kamer, P. C.; Reek, J. N. *Pure and Applied Chemistry* **1999**, *71*, 1443–1452.

(7) Van Leeuwen, P. W.; Kamer, P. C.; Reek, J. N.; Dierkes, P. *Chemical Reviews* **2000**, *100*, 2741–2769.

(8) Bell, S.; Wu, B.; Kaiser, S.; Menges, F.; Netscher, T.; Pfaltz, A. *Science* **2006**, *311*, 642–645.

(9) Källström, K.; Munslow, I.; Andersson, P. *Chemistry - A European Journal* **2006**, *12*, 3194–3200.

(10) Roseblade, S.; Pfaltz, A. *Accounts of Chemical Research* **2007**, *40*, 1402–1411.

(11) Wang, A.; Wüstenberg, B.; Pfaltz, A. *Angewandte Chemie* **2008**, *120*, 2330–2332.

(12) Wang, A.; Fraga, R.; Hörmann, E.; Pfaltz, A. *Chemistry - An Asian Journal* **2011**, *6*, 599–606.

(13) Lightfoot, A.; Schnider, P.; Pfaltz, A. *Angewandte Chemie - International Edition* **1998**, *37*, 2897–2899.

(14) Schumacher, A.; Bernasconi, M.; Pfaltz, A. *Angewandte Chemie* **2013**, *125*, 7570–7573.

(15) Mwansa, J. M.; Page, M. I. *Catalysis Science and Technology* **2020**, *10*, 590–612.

(16) Czerwieniec, R.; Kowalski, K.; Yersin, H. *Journal of the Chemical Society. Dalton Transactions* **2013**, *42*, 9826–9830.

(17) Dyer, P. W.; Dyson, P. J.; James, S. L.; Martin, C. M.; Suman, P. *Organometallics* **1998**, *17*, 4344–4346.

(18) Lemouzy, S.; Jean, M.; Deplante, F.; Albalat, M.; Lemouzy, S.; Jean, M.; Deplante, F.; Albalat, M.; Hérault, D.; Lemouzy, S.; Jean, M.; Deplante, F.; Albalat, M.; Hérault, D. *ChemistrySelect, Wiley* **2018**, *3*, 12281–12286.

(19) Giereth, R.; Mengele, A. K.; Frey, W.; Kloß, M.; Steffen, A.; Karnahl, M.; Tschierlei, S. *Chemistry - A European Journal* **2020**, *26*, 2675–2684.

(20) Strauss, S. H. *Chemical Reviews* **1993**, *93*, 927–942.

(21) Smidt, S.; Zimmermann, N.; Studer, M.; Pfaltz, A. *Chemistry - A European Journal* **2004**, *10*, 4685–4693.

(22) Van Leeuwen, P., *Homogeneous Catalysis: Understanding the Art*, 2004.

(23) Brandt, P.; Hedberg, C.; Andersson, P. *Chemistry - A European Journal* **2003**, *9*, 339–347.

(24) Kutzelnigg, W.; Fleischer, U.; Schindler, M. In *The IGLO-Method: Ab-initio Calculation and Interpretation of NMR Chemical Shifts and Magnetic Susceptibilities*, 1990; Vol. 23, pp 234–238.

(25) Brandt, P.; Hedberg, C.; Andersson, P. G. *Chemistry - A European Journal* **2003**, *9*, 339–347.

(26) Desmarchelier, A.; Caumes, X.; Raynal, M.; Vidal-Ferran, A.; Van Leeuwen, P.; Bouteiller, L. *Journal of the American Chemical Society* **2016**, *138*, 4908–4916.

(27) Li, Y.; Bouteiller, L.; Raynal, M. *ChemCatChem* **2019**, *11*, 5212–5226.

(28) Fan, Y.; Cui, X.; Burgess, K.; Hall, M. *Journal of the American Chemical Society* **2004**, *126*, 16688–16689.

(29) Crabtree, R. *Accounts of Chemical Research* **1979**, *12*, 331–337.

(30) Xu, Y.; Mingos, D.; Brown, J. *Chemical Communications* **2008**, *44*, 199–201.

(31) Li, Y.; Hammoud, A.; Bouteiller, L.; Raynal, M. *Journal of the American Chemical Society* **2020**, *142*, 5676–5688.

(32) Raynal, M.; Portier, F.; Van Leeuwen, P. W. N. M.; Bouteiller, L. *Journal of the American Chemical Society* **2013**, *135*, 17687–17690.

5 Reproducibility Problems in Supramolecular Assemblies

5.1 Introduction

Trivial features which seem unimportant at first may cause significant changes. Sometimes the procedure for a chemical compound bought by scientists might have slightly changed when ordering the same compound again at same manufacturer.[1] This may leave traces of other chemicals which can cause different results. Another issue may arise when the precise compositions of a chemical compound differs between manufacturers.[2] A key example can be found in inorganic catalysis, where only traces of undesired metals present in the catalyst changed the outcome of entire experiments.[3–6] As a result scientists often analyse catalysts they use for traces of other metals and if present these metals are written on publications to prevent reproducibility issues. To handle reproducibility as a consequence of these influences seems difficult but can be achieved carefully analyzing and reporting each component of an experiment.

Recently, supramolecular chemistry encountered more and more reports on reproducibility issues.[7] This can be attributed to the weak interactions that govern supramolecular assemblies. Moreover, cooperativity, which is often observed in supramolecular polymers, can lead to amplification of small stimuli – ultimately interfering with the polymer. This chapter describes irreproducibility problems encountered in this thesis.

5.2 Solvent-Solute Interactions

Solvent-solute interactions play a crucial role governing solubility, reactivity and structure of a supramolecular assembly.[8] Solubility of monomers affects their tendency to assembly as supramolecular polymers in the first place.[9] In a bad solvent monomers will stay in their unbound state not assembling at all. In a good solvent the monomers assemble, but, depending on the solvent it might occur via different mechanisms. Because in different solvents the strength of supramolecular interaction differs, the interplay between strong and weak interactions differs, influencing the structure and stability of supramolecular polymers.[10] Moreover, the balance between solubilizing ability of the solvent while accommodating the noncovalent interactions between solute monomers to form a supramolecular polymer is crucial. For instance, solvents that possess competitive interactions can stabilize the disassembled state and thereby decrease the supramolecular association.[9]

Water can greatly influence the assembly either by altering the helical screw-sense creating different helical states or biasing the net helicity and therefore the observed enantiomeric excess.[11] The water content in solvents might fluctuate even without knowing, hereby causing irreproducibilities. While all these effects are already hard to predict for pure solvents, it becomes even more challenging to predict and control supramolecular assembly in solvent mixtures. The addition of cosolvent might adjust the morphology of the supramolecular assembly or the exchange dynamics between monomeric moieties and supramolecular polymer.[12–14]

5.2.1 Solubility of Monomers and Supramolecular Assemblies

Finding a good solvent for gBTA was difficult. A quick solubility check indicated that gBTA can be dissolved in decalin. To study the solubilizing properties of decalin the same method was applied as described in Section 3.2. However, performing three experiments under the same conditions resulted in three completely different dissasembly-assembly curves (Fig. 5.1a,b). This suggested that there were either contaminants such as impurities or water in the bottle or that or that the relative ratio of *cis*- and *trans*-decalin in the mixture used caused these problems. Therefore new bottles were purchased one with pure *cis*-decalin and one with pure *trans*-decalin.

Analyzing solubility of gBTA in the three decalin solvents showed extremely different absorption spectra for gBTA in each solvent (Fig. 5.1a-e), while the absorption spectra should be almost identical. This is most likely due to impurities as a result from e.g. the decalin synthesis. Decalin is produced by reduction of naphthalene and different catalysts are needed for *cis* versus *trans*. Hence, it is possible that either side products, starting material or reagents are still in small amounts in the solvent, which cause the different absorption spectra. Another problem with these solvents is that the maximum absorption exceeds the detectable limit of the spectrometer. Impurities in the solvent absorb UV-light, which cause different absorption intensity for the same compound, this hampers the possibility to study the thermodynamic behavior. Besides, no clear transition can be observed between the monomeric phase, at high temperature, and supramolecular polymeric phase, at low temperature, which also complicates the thermodynamic measurements. However, in all heating and cooling curves of gBTA no hysteresis is observed.

To overcome these complications anhydrous decalin as solvent for the thermodynamic measurement was exploited. It has two clear advantages: the water content in the solvent bottle is defined and low and it and it is available in spectroscopic grade eliminateing most impurities that could harm the measurement. To study the thermodynamics often the wavelength characteristic for assembly is followed as function of temperature. When this wavelength is close or equal to the maximum of the solvent, the absorption of the solvent will interfere with the measurement. The maximum absorption of gBTA in anhydrous decalin was below the detectable limit but hysteresis was again observed for heating and cooling curves of gBTA (Fig. 5.1f). Because all absorption spectra measured in decalin were either irreproducible or the absorption was above detectable limit, MCH/DCE mixtures were investigated.

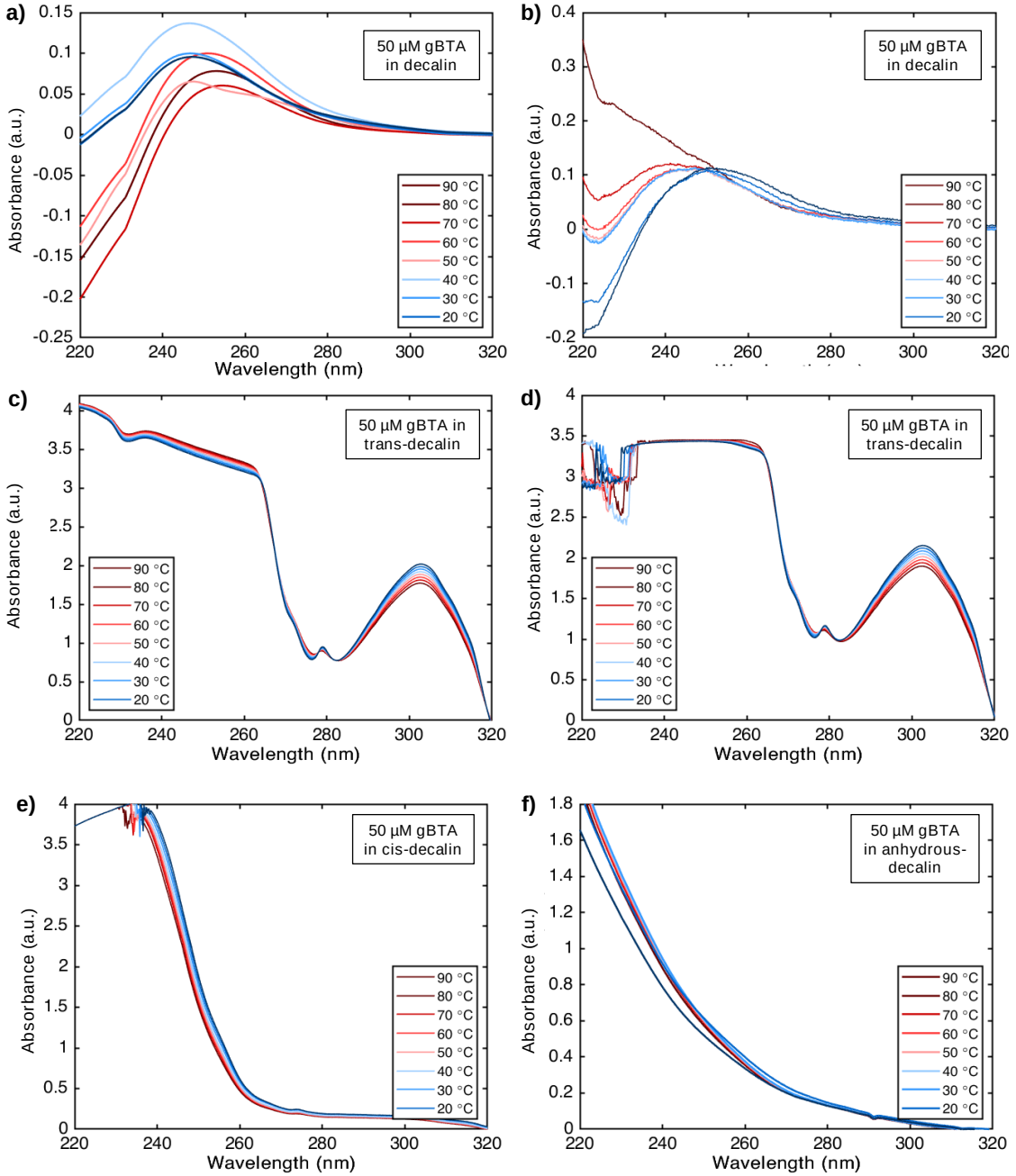

Figure 5.1: *Melting curves measured by UV/vis spectroscopy, to identify assembled and disassembled state of 50 µM gBTA in different solvents, a-c) decalin, d) cis-decalin, e) trans-decalin and f) anhydrous decalin.*

As gBTA is not soluble in pure MCH, we explored solvent mixtures of MCH and DCE which have been previously used for BTA systems. Adding DCE should resolve the low solubility of gBTA in MCH, however for lower volume percentages of DCE ($< 5\%$) this problem remained. Two characteristics were observed which are an indication of poor solubility. The first, non superimposing absorption spectra for heating and cooling curves, which is marked by the curves having similar

shape but their absolute values differ or are shifted. Second is the detection of different spectral shapes for a compound in the same solvent. Both characteristics are present for solutions with 1 and 3% DCE (v/v) (Fig. 5.2), but for higher mol% DCE both disappear.

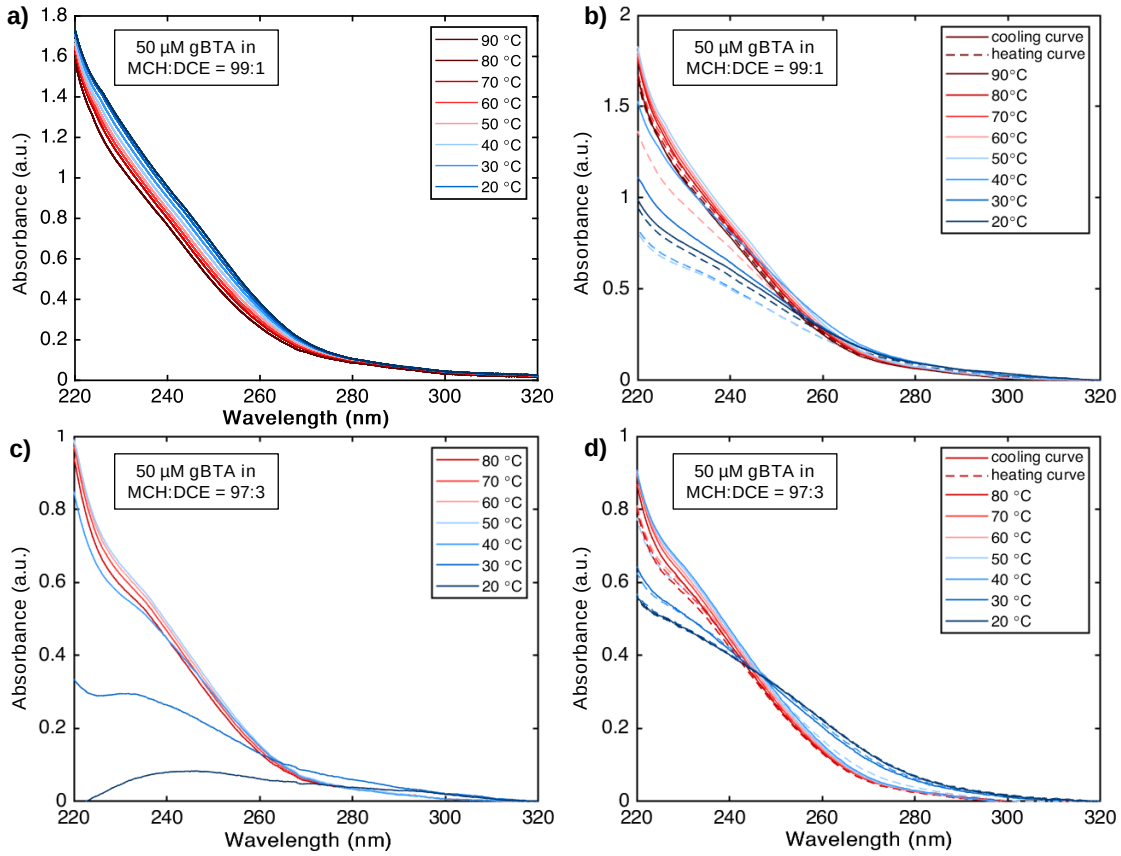

Figure 5.2: *Melting curves measured by UV/vis spectroscopy, to identify assembled and disassembled state of 50 µM gBTA in MCH with a-b) 1% DCE (v/v) and c-d) 3% DCE (v/v).*

5.2.2 Solvent Contamination

From previous research in this group the maximum absorption for 50 μM (S)-BTA in MCH is determined to be approximately -50 millidegrees (mdeg). Therefore, we expected that the absorption of 50 μM solution of (S)-BTA in MCH with 5% DCE (v/v) should be around the same value. In Section 3 circular dichroism spectra are only measured when S&S principle was investigated. Therefore it was not until this stage that small contaminants in the MCH solvent bottle were detected. First measurements with (S)-BTA in MCH bottle no. 1 gave "normal" results, indicated by an absorption of -40 mdeg (solid blue line in Fig. 5.3a). When these experiments were repeated a second time, not even two weeks later, the signal had completely disappeared (blue dotted line). No contaminants could be identified by NMR-spectroscopy, which might interfere with the self-assembly of (S)-BTA causing the absence of CD signal.

A new bottle, MCH bottle no. 2 was employed, to study if this bottle was not contaminated as well, a 50 μM solution of (S)-BTA was measured (solid red line). After 1.5 months this bottle was tested again to see if the same problem had reoccurred. Once more, the CD signal had completely disappeared (red dotted line). Accumulation of contaminants over time is believed to hinder the self-assemble of (S)-BTA, causing loss of CD signal.

Over time water content in the solvent will fluctuate if no accurate measures are taken. As a result absorption, IR or CD spectra of a compound can unexpectedly look offbeat if the time between measurements is long enough. Tthe effect of water has been investigated for (S)-BTA in MCH, barely an effect was observed, but for other BTAs an effect was observed.[9, 15] So, such an effect might also be present in MCH/DCE mixtures and for gBTA, as this side chain has not been investigated.

In order to explore the potential effect of water on the assembly of gBTA in MCH two sample vials were prepared, one pure MCH with molecular sieves of 4 Å (dry MCH) and one with 50%

demi-water (v/v) in MCH (wet MCH). After 72 hours the absorption spectrum of gBTA was inspected in dry and wet MCH to study the role water molecules have in the self-assembly of gBTA. These spectra were measured at 20 °C, because at this temperature all gBTA has assembled into supramolecular stacks. The spectra overlap almost perfectly (Fig. 5.3b), thus it is unlikely that water was the source for the different spectra observed in the solvent-solute study. Nonetheless, it is important to be aware of water and what kind of influence it might have on compounds.

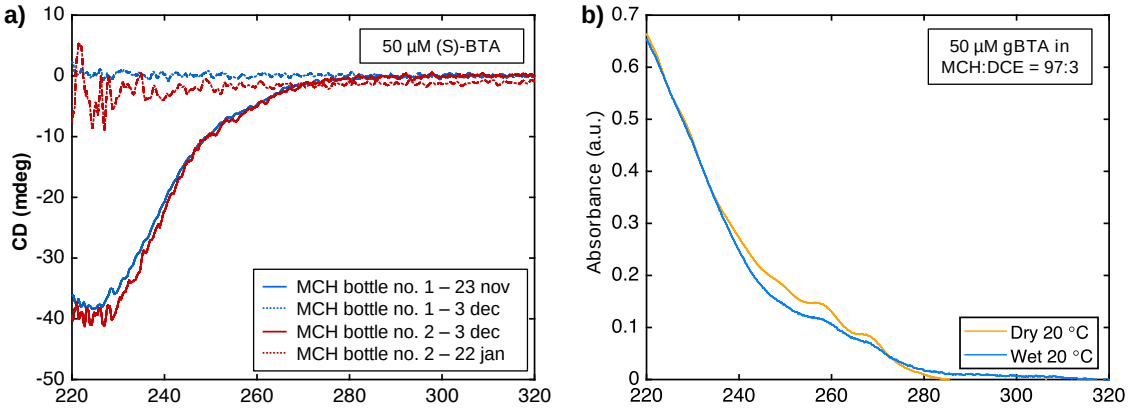

Figure 5.3: *a) CD spectrum of 50 µM (S)-BTA in MCH 1% DCE (v/v). The MCH is contaminated over time, indicated by a loss of CD signal. b) absorption spectra of 50 µM gBTA in wet (blue line) and dry (orange line) MCH 1% DCE (v/v).*

5.3 Experimental Hydrogenation Set-Up

Hydrogenations performed at 1 bar were extremely challenging, the conversion varied each time even when the same set of reaction conditions were applied. For example, the hydrogenation of gBTA with IrCl/(*R*)-PHOX (Section 4.1) in a solvent mixture of 20% DCE (v/v) in MCH gave conversions between 0-64% (Table 12, entry 1a-e). Even for hydrogenations performed with the same conditons but in pure DCM the conversion ranged between 0-88% (Table 12, 2a-e). To find the cause for this variation a systematic study was performed on all factors which might influence the hydrogenation: 1) sample preparation (addition of DCE or MCH first and the addition of premixed catalyst or separately add the metal precursor and ligand) 2) sample volume, 3) vial size 4) hydrogen source.

The solvent surface is critical for hydrogenation as this is the interface at which the hydrogen enters the solution to react with the substrate.[16] Therefore, we expected that the origin of all irreproducible conversions was caused by the hydrogenation set-up. The set-up used before optimization was as follows: vials were 10 mL and were filled with a sample volume was 5 mL, a hydrogen balloon was the source of hydrogen. The air in the sample was first removed and changed to argon and then to hydrogen by the use of the hydrogen balloon. This balloon was connected to a cap with septum *via* a syringe with a needle.

In entry 3a and 3b in Table 12, gBTA, IrCl and (*R*)-PHOX (30 mol%) were first dissolved in DCE before MCH was added to reach a solvent mixture of 20% DCE (v/v) in MCH. This, in contrast to entry 3c and 3d were first all components were added to MCH before DCE was added. Nonetheless, no difference was observed as the conversion was in both cases low (<15%). To investigate if the second and third factor influenced the conversion, the same conditions were used and for the vial size no clear effect was observed. All conversions were below the detectable limit (entry 4a-c), but using a vial size of 20 mL the conversion increased to 15% (entry 5). As a larger vial size increased the conversion, the examination of hydrogen source were carried out in vials of 20 mL.

Table 12: *Investigation of reproducibility with IrCl and (R)-PHOX or triphenylphosphine (PPh_3) on the conversion of gBTA.*

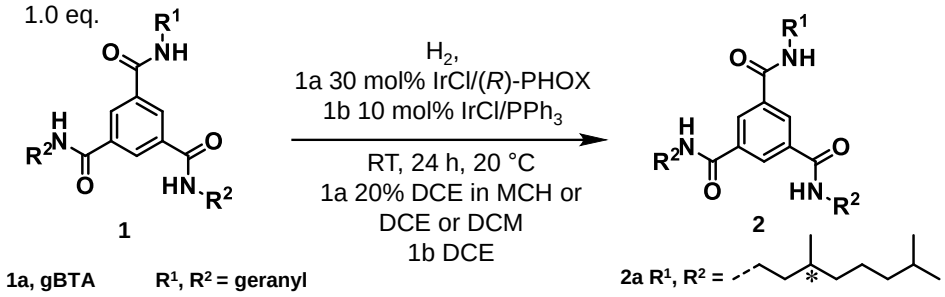

Entry	Solv. (vol%)	Ligand	Sample volume (mL)	Vial size (mL)	Hydrogen source	Conv. (%)
1a	MCH/DCE (80/20)	(*R*)-PHOX	5	10	Balloon	64
1b	MCH/DCE (80/20)	(*R*)-PHOX	5	10	Balloon	<5[a]
1c	MCH/DCE (80/20)	(*R*)-PHOX	5	10	Balloon	30
1d	MCH/DCE (80/20)	(*R*)-PHOX	5	10	Balloon	<5[a]
1e	MCH/DCE (80/20)	(*R*)-PHOX	5	10	Balloon	23
2a	DCM (100)	(*R*)-PHOX	5	10	Balloon	10
2b	DCM (100)	(*R*)-PHOX	5	10	Balloon	19
2c	DCM (100)	(*R*)-PHOX	5	10	Balloon	<5[a]
2d	DCM (100)	(*R*)-PHOX	5	10	Balloon	88
2e	DCM (100)	(*R*)-PHOX	5	10	Balloon	<5[a]
3a	MCH/DCE (80/20)	(*R*)-PHOX	5	10	Balloon	15
3b	MCH/DCE (80/20)	(*R*)-PHOX	5	10	Balloon	<5[a]
3c	MCH/DCE (80/20)	(*R*)-PHOX	5	10	Balloon	<5[a]
3d	MCH/DCE (80/20)	(*R*)-PHOX	5	10	Balloon	15
4a	MCH/DCE (80/20)	(*R*)-PHOX	3	10	Balloon	<5[a]
4b	MCH/DCE (80/20)	(*R*)-PHOX	5	10	Balloon	<5[a]
4c	MCH/DCE (80/20)	(*R*)-PHOX	7	10	Balloon	<5[a]
5	MCH/DCE (80/20)	(*R*)-PHOX	5	20	Balloon	15
6a	DCE (100)	PPh3	5	20	H_2 volume	34
6b	DCE (100)	PPh3	5	20	H_2 volume	25
6c	DCE (100)	PPh3	5	20	Balloon	<5[a]
7a	DCM (100)	(*R*)-PHOX	5	20	H_2 volume	54
7b	DCM (100)	(*R*)-PHOX	5	20	H_2 volume	86
7c	DCM (100)	(*R*)-PHOX	5	20	H_2 volume	88
8a	DCE (100)	(*R*)-PHOX	5	20	H_2 volume	45
8b	DCE (100)	(*R*)-PHOX	5	20	H_2 volume	44
8c	DCE (100)	(*R*)-PHOX	5	20	H_2 volume	29
9a	DCE (100)	PPh3	5	20	H_2 volume	50
9b	DCE (100)	PPh3	5	20	H_2 volume	52
9c	DCE (100)	PPh3	5	20	H_2 volume	62

[a]Conversion below detectable limit.

To reduce the influence of solvent on the hydrogenation all next reactions were executed in one solvent, either DCM or DCE. When the empty volume in the vial was filled with hydrogen instead of attaching a balloon, the catalysts IrCl/PPh_3 (30 mol%) converted gBTA in DCE with 30% conversion (entry 6a,6b). As a reference the hydrogenation was once performed with a hydrogen balloon, which gave a conversion <5% (entry 6c). Two elements are believed cause the low conversions observed for the hydrogenation where a hydrogen balloon is attached. Air molecules can diffuse into the balloon and during the reaction form a heavy layer of air on top of the solvent, which can prevent interaction of H_2 molecules and catalytic complex thus lowering the conversion. Besides, the solvents used are not dry and glassware was not dried in the oven prior to use, thus the content of residual water in reaction mixtures is always different. From literature we know that water can influence the reactivity of IrCl/(*R*)-PHOX complexes to below <5%, so traces of water might be present in reaction mixtures were the conversion is low.[17, 18]

Several reactions mixtures of gBTA in DCM or DCE were hydrogenated with IrCl/ligand complex (30 mol% at 1 bar) to verify that the hydrogen balloon was the source for the irreproducible results. Ligands (*R*)-PHOX and PPh_3 were used to exclude any influence of the ligand itself. The hydrogenation of gBTA was reproducible, in DCM (entry 7a-c) and DCE (entry 8,9) and high conversions were obtained (76% and 40% respectively). Also hydrogenation with PPh_3 resulted in reproducible results with a conversion of 55% (entry 9a-9c). After this finding each reaction was run at least two times to manage the fluctuations in conversions, the hydrogen balloon was no longer used and reproducible results were obtained for each experiment.

5.4 Conclusion

There can be many factors that cause irreproducibilities in organic chemistry. After examination of possible factors it was found that solvent-solute interactions were the origin for the changing absorption spectra of gBTA. Impurities in solvent are most likely to cause loss of CD signal. The source of irreproducibilities in the hydrogenation of aagBTA and gBTA was the experimental 1 bar set-up. The vial size and hydrogen source were dominant factors which influenced the conversion in these reactions. To overcome such challenges in the future it is crucial to proper analyse chemicals and report procedures.

5.5 Experimental Section

5.5.1 Materials and instrumentation

Solvents were purchased from Biosolve and deuterated solvents were obtained from Cambridge Isotopes Laboratories. BTAs were synthesized as described in Section 2.4 and used without any further purification.

UV/Vis and circular dichroism (CD) measurements were performed on a Jasco J-815 spectropolarimeter, for which the sensitivity, time constants, scan rates and temperature were chosen appropriately. Corresponding temperature depended measurements were performed with a Jasco PFD-425S/15 Peltier type temperature controller with a temperature range of 263–393 K and adjustable temperature slope. All spectroscopic measurements were recorded in cells with an optical path length of 1 cm. The Spectrophotometer is equipped with a multi-cells holder for 6 samples and the temperature controlled was set on the holder station.

5.5.2 Methods

Sample preparation
Weighing enough material of each component to make a stock solution of roughly 1 mM in the solvent selected for each measurement. Samples were then prepared by diluting the stock solution to give the desired concentration.

Jasco J-815 spectropolarimeter parameter settings
Melting curves were recorded with following parameters: sensitivity standard, response time 0.125s, band width 1 nm, scanning speed 100 nm/min, wavelength 220-320 nm, temperature gradient 1.0 °C/min, halt temperature ramping during measurement.

All CD and LD measurements were recorded with following parameters: sensitivity standard, response time 0.125s, band width 1 nm, scanning speed 100 nm/min, wavelength 220-320 nm, temperature 22 °C.

References

(1) Bergman, R. G.; Danheiser, R. L. *Angewandte Chemie - International Edition* **2016**, *55*, 12548–12549.

(2) Baker, M. *Nature* **2017**, *548*, 485–488.

(3) Gonda, Z.; Tolnai, G. L.; Novák, Z. *Chemistry - A European Journal* **2010**, *16*, 11822–11826.

(4) Thomé, I.; Nijs, A.; Bolm, C. *Chemical Society Reviews* **2012**, *41*, 979–987.

(5) Buchwald, S. L.; Bolm, C. *Angewandte Chemie - International Edition* **2009**, *48*, 5586–5587.

(6) Leadbeater, N. E. *Nature Chemistry* **2010**, *2*, 1007–1009.

(7) Preuss, M. D.; Schnitzer, T.; Vantomme, G.; Meijer, E. W.

(8) Marcus, Y. *Chemical Society Reviews* **1993**, *22*, 409–416.

(9) Mabesoone, M. F.; Palmans, A. R.; Meijer, E. W. *Journal of the American Chemical Society* **2020**, *142*, 19781–19798.

(10) Satake, A. *ChemPlusChem* **2020**, *85*, 1542–1548.

(11) Van Zee, N. J.; Adelizzi, B.; Mabesoone, M. F. J.; Meng, X.; Aloi, A.; Zha, R. H.; Lutz, M.; Filot, I. A. W.; Palmans, A. R. A.; Meijer, E. W. *Nature* **2018**, *558*, DOI: 10.1038/s41586-018-0169-0.

(12) Denkova, A. G.; Bomans, P. H. H.; Coppens, M. O.; Sommerdijk, N. A. J. M.; Mendes, E. *Soft Matter* **2011**, *7*, 6622–6628.

(13) Gillissen, M. A. J.; Koenigs, M. M. E.; Spiering, J. J. H.; Vekemans, J. A. J. M.; Palmans, A. R. A.; Voets, I. K.; Meijer, E. W. *Journal of the American Chemical Society* **2014**, *136*, 336–343.

(14) Lafleur, R. P. M.; Lou, X.; Pavan, G. M.; Palmans, A. R. A.; Meijer, E. W. *Chemical Science* **2018**, *9*, 6199–6209.

(15) Van Zee, N. J.; Mabesoone, M. F. J.; Adelizzi, B.; Palmans, A. R. A.; Meijer, E. W. *Journal of the American Chemical Society* **2020**, *142*, 20191–20200.

(16) Van Leeuwen, P., *Homogeneous Catalysis: Understanding the Art*, 2004.

(17) Smidt, S.; Zimmermann, N.; Studer, M.; Pfaltz, A. *Chemistry - A European Journal* **2004**, *10*, 4685–4693.

(18) Lightfoot, A.; Schnider, P.; Pfaltz, A. *Angewandte Chemie - International Edition* **1998**, *37*, 2897–2899.

6 Conclusions and Future Perspective

In this thesis we presented steps towards a new strategy to amplify enantiomeric excess by employing a supramolecular catalyst in an asymmetric hydrogenation reaction. Preliminary steps were taken to validate this new strategy. In our design the supramolecular catalyst is composed of several different BTA moieties: achiral substrate (aagBTA or gBTA), achiral comonomer (aBTA), chiral product ((*S*)-BTA) and achiral ligand (L-BTA).

We worked with a multi component system which is extremely complex. As a result subtle changes in the system composition play a role as irreproducibility factors. However, careful analysis and experiment reports allowed us to understand those issues and establishing a reproducible reaction protocol for both the assembly and the hydrogenation reaction.

The system components, aagBTA, gBTA, aBTA and (*S*)-BTA were successfully synthesized, characterized and their assembly properties were analyzed by UV/vis and CD spectroscopy. Investigation of mixtures of MCH/DCE demonstrated the trade-off between solubilizing capacities of the solvent and intermolecular hydrogen bonding strength. Higher volume percent of chlorinated solvent reduces hydrogen bond strength but increases solubility of gBTA. Below 5% DCE (v/v) solubility of gBTA is very poor and as consequence aggregates are formed. The optimal ratio between MCH and DCE was found to be 5% (v/v) for all compounds. VT-IR spectroscopy was used to investigate the formation of intermolecular hydrogen bonding in this solvent mixture further. Thermodynamic analysis revealed a cooperative assembly mechanism for the homopolymerization of these BTAs. Finally, we analyzed the monomers as soldiers in a S&S experiment, as this function is crucial for the amplification in the hydrogenation reaction. Both aBTA and aagBTA show a clear S&S effect with (*S*)-BTA, a net helicity of 1 was reached when 0.1 fraction of sergeant was added. For gBTA no S&S effect was observed because (*S*)-BTA could not direct the handedness of gBTA stacks at 20 °C. When the temperature was first increased to 80 °C, (*S*)-BTA and gBTA coassemble and (*S*)-BTA can stir the screw-sense of the stack to its preferred handedness. This increased the non-linear relation between fraction of sergeant and net helicity, but remained for higher fractions (>0.65) linear.

Lastly, the catalytic performance of several chiral ligands and metal precursors was studied. Reaction optimization provided - in terms of conversion - ($[Ir(COD)Cl]_2$)/(*R*)-PHOX as the best performing catalyst in the asymmetric hydrogenation of aagBTA and gBTA. Moreover, relations between conversion and MCH/DCE ratio, pressure, catalyst loading and coordinating counter-ion were established. Higher pressure, volume percent of chlorinated solvent and catalytic loading all increased the conversion. The ratio between metal and ligand is very important, we found that a ratio of 1/6 deactivated the catalyst completely. Reactions carried out in DCM gave better conversion then DCE, which might be attributed to the formation of inactive catalytic complex between DCE/Ir(I). Investigation of $BAr_f{}^-$ and Cl^- as coordinating counter-ion showed that $[Ir(COD)]_2BAr_f$ with (*R*)-PHOX are ineffective in the hydrogenation of both aagBTA and gBTA, which could be caused by oxidation of the phosphorus atom in $[Ir(COD)]_2BAr_f$/(*R*)-PHOX complexes. Triphenylphosphine was investigated as achiral ligand and showed very good catalytic performance at 1 and 50 bar (25% and >99% respectively). The obtained results suggested that a diphenylphosphine would be a good candidate in the ligand BTA. Therefore, L-BTA with two (*n*)-octylamine chains and one 2-(diphenylphosphino) ethylamine chain was synthesized and characterized. Its catalytic activity in the hydrogenation of aagBTA was tested with success (38% conversion, 10 mol% L-BTA, 5% DCE (v/v)in MCH).

We suggest the advance of the steps presented in this thesis - we identified the components essential for amplification of an asymmetric hydrogenation reaction and ultimately showed the catalytic activity of a supramolecular BTA scaffold - towards the new strategy to amplify enantiomeric excess of an asymmetric hydrogenation reaction. The promising early result for L-BTA confirmed that a supramolecular BTA catalyst can hydrogenate aagBTA and gBTA. This catalyst was tested in absence of chiral stimulus thus there was no stereoselectivity. To observe amplification in our new proposed strategy, the product should be formed in some enantiomeric excess. Therefore testing the supramolecular catalyst in presence of chiral stimulus, which creates a racemic mixuture of *M*- and *P*-helices, is crucial. If the product is then formed in a slight enantiomeric excess, amplification of this initial small enantio imbalance could be observed over several rounds.

However, before we reach a system were amplification of enantiomeric excess is observed several milestones need to be reached. First of all, the synthesized ligand BTA should be more extensively tested to confirm the results reported in this thesis. Second, a method to determine the enantiomeric excess of product needs to be established. We envision two possible methods to determine the enantiomeric excess. The first method would include separation of stereoisomers with

a chiral high-performance liquid chromatography (HPLC). But, this might proof challenging as the interaction with the chiral stationary phase in the HPLC columns will only minutely differ between the two enantiomers - formed after hydrogenating aagBTA - as those are very apolar and mainly consist of aliphatic chains. Furthermore, we envision that cleavage of the amides and separation, by chiral HPLC, of the correspond chiral amines will be more promising. Optical rotation is another possibility to determine the enantiomeric excess. This has two disadvantages, the optical rotation of enantiopure aa(S)-BTA must be identified, thus this compound should be synthesized, and this method is only conclusive when high concentrations are measured. Both methods would specify the enantiomeric excess. Following the hydrogenation over time with CD spectroscopy would quantify if chiral product is enantioselectivly formed but would not determine the exact enantiomeric excess.

7 Acknowledgement

Na ruim 12 maanden met genoegen en veel enthousiasme in de MST groep gewerkt te hebben, rond ik hierbij mijn master thesis af. In het begin, vanwege COVID-19, mochten we alleen halve weken in het lab aanwezig zijn, gelukkig duurde dat niet al te lang. Want het is niet alleen prettiger werken, maar ook was het heel fijn om iedereen te leren kennen die in de vakgroep zit. Zonder al deze mensen zou mijn thesis niet zijn geworden wat het nu is. Daarom wil ik graag iedereen bedanken voor alle hulp.

Firstly, Tobi, I would like to express my deep gratitude for your guidance throughout this project, your patience, always asking if I needed help with anything in the lab, writing or with any presentation and explaining how I could improve. For striving to reach the best, there was always something where I could advance. You showed me, how little it may seem, it does matter. You explained to me that you want people to realize how much time and effort you spent on something and to achieve that you must pay attention to the details. But most of all, your inexhaustible enthusiasm when it comes to chemistry. When something did not work out the way we both hoped, you were always there to say: 'but this is interesting because why would it behave like that?'. You facilitated a really nice working atmosphere, especially before the Christmas holiday when I could hear ABBA already playing in the hallway and so knew you were also working in the lab. In the end you really sparked my interest in science. Without you, I really believe, my thesis would not be near what I hoped it would be after 12 months of working.

Daarnaast, Bert ik wil u graag bedanken voor de mogelijkheid dit project te doen in de MST groep. Net voor de zomervakantie van 2020 hadden wij een gesprek en u zei dat het misschien wel een goed idee was om een fundamenteel project te kiezen; het zou lastiger zijn maar ik zou waarschijnlijk ook meer leren. Ik ben heel erg blij dat ik voor dit project heb gekozen en onderweg zo ontzettend veel nieuws heb mogen doen en veel nieuwe mensen heb leren kennen. Daarnaast, was het gemakkelijk te praten over de hobbels die ik tijdens dit traject ben tegengekomen. Door het erover te hebben heeft u echt een hoop onzekerheid weggenomen. Dan wil ik graag nog benoemen met wat voor enthousiasme u jonge onderzoekers inspireert en wat u allemaal voor hen doet en betekent. Van het creëren van een fijne werksfeer, tot een deur die bijna altijd open staat. Daarom wil ik u bedanken dat ik dit project in deze vakgroep heb mogen doen en het vertrouwen dat u in mij gesteld heeft.

Ook Anja wil ik graag bedanken voor uw expertise omtrent 'vreemde' CD signalen maar ook voor de goede tips tijdens de lunchgroupmeetings. De opbouwende kritiek was altijd erg welkom en heeft me geholpen me steeds te verbeteren. En natuurlijk voor het deelnemen in mijn afstudeercommissie.

Ivo Filot wil ik graag bedanken voor het deelnemen in mijn afstudeercommissie.

I want to thank Ghislaine for the always happy 'good morning' in the hallway and asking me how the project was going and if I needed help with anything. Besides, I would like to thank Ghislaine and Anja for the opportunity to supervise the practical course.

Dan zou ik graag nog Bas de Waal bedanken voor alle hulp met de 50 bar Parr reactor. Dit was de eerste keer dat de hydrogenering werkte en dat we eindelijk bevestiging kregen dat het project kans hadte slagen.

A special thanks to all the members of Lab 1 for the nice working atmosphere. En hier zou ik in het bijzonder Jolanda willen bedanken. Voor de vele tips en tricks die u me heeft geleerd en voor alle hulp tijdens de syntheses. Het was ontzettend prettig om naast iemand te mogen werken die zo veel ervaring heeft.

I would like to thank the lunchgroup, for showing me what there is to learn during your PhD, which is definitely not restrained to doing only research. Besides, all the feedback you gave after my presentations during the lunchgroupmeeting really helped.

Natuurlijk wil ik ook graag mijn mede masterstudenten bedanken. Hoewel we allemaal met een heel ander onderwerp bezig waren, was het heel prettig om het met gelijkgestemden over problemen te kunnen hebben. Zeker Piers, die óók voor zijn midway de boodschap had 'waarschijnijk moet ik iets anders gaan proberen', de koffiepauzes waren super.

Als laatste zou ik graag mijn familie en vrienden bedanken voor hun steun en interesse. Mijn ouders die hun uiterste best hebben gedaan om te snappen waar ik me het afgelopen jaar mee bezig heb gehouden. Mijn vrienden die soms niet snapten wat het betekende als ik een slechte dag in het lab had gehad, maar die wel altijd met veel geduld mijn verhaal aanhoorden.

8 Appendix

8.1 Characterization of Compounds

8.1.1 (*S*)-BTA

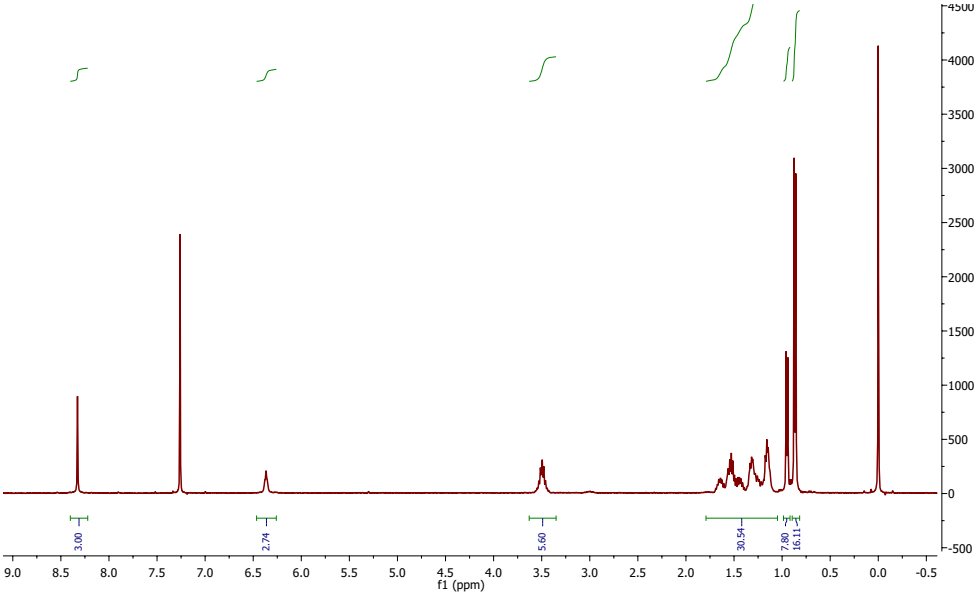

(a)

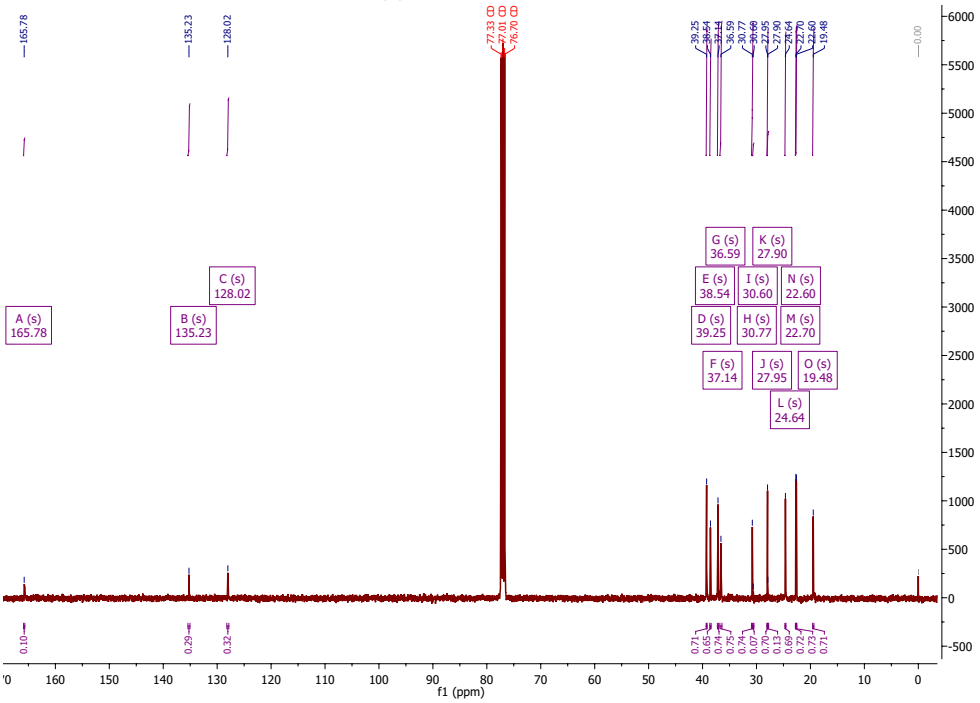

(b)

Figure 8.1: *(a)* ^{1}*H-NMR and (b)* ^{13}*C-NMR spectrum of (S)BTA*

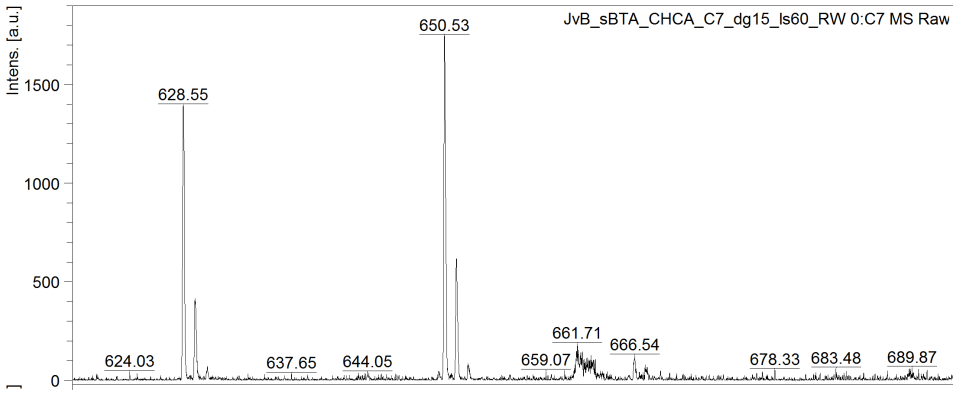

Figure 8.2: *MALDI-TOF MS spectrum of gBTA*

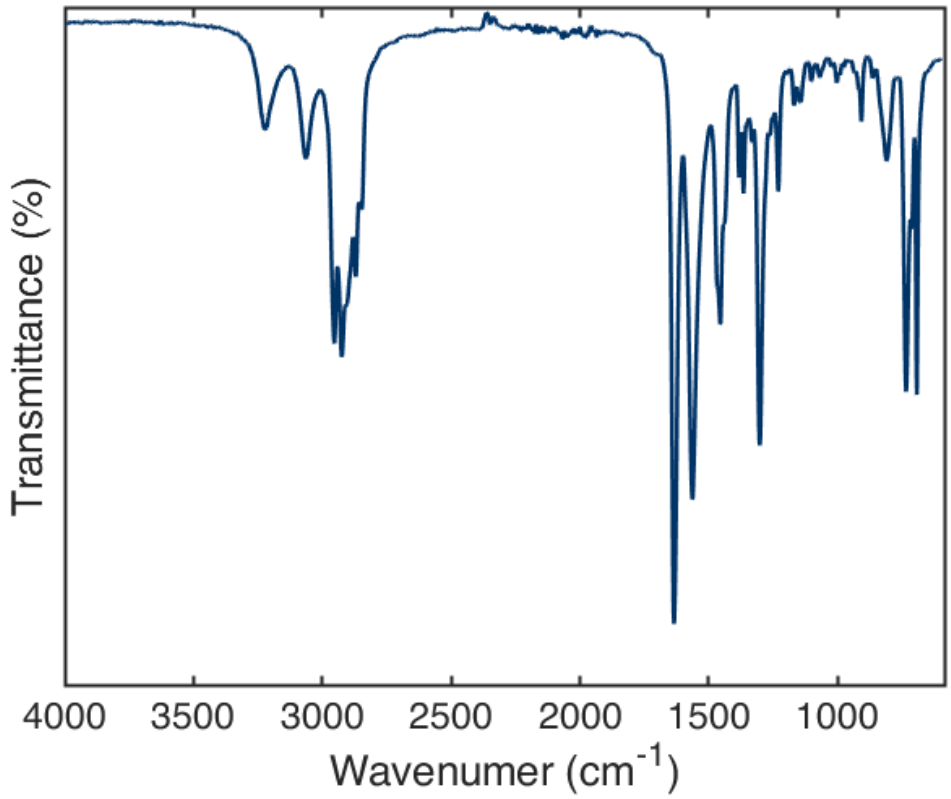

Figure 8.3: *FT-IR spectrum for a solid sample of (S)-BTA at 25 °C*

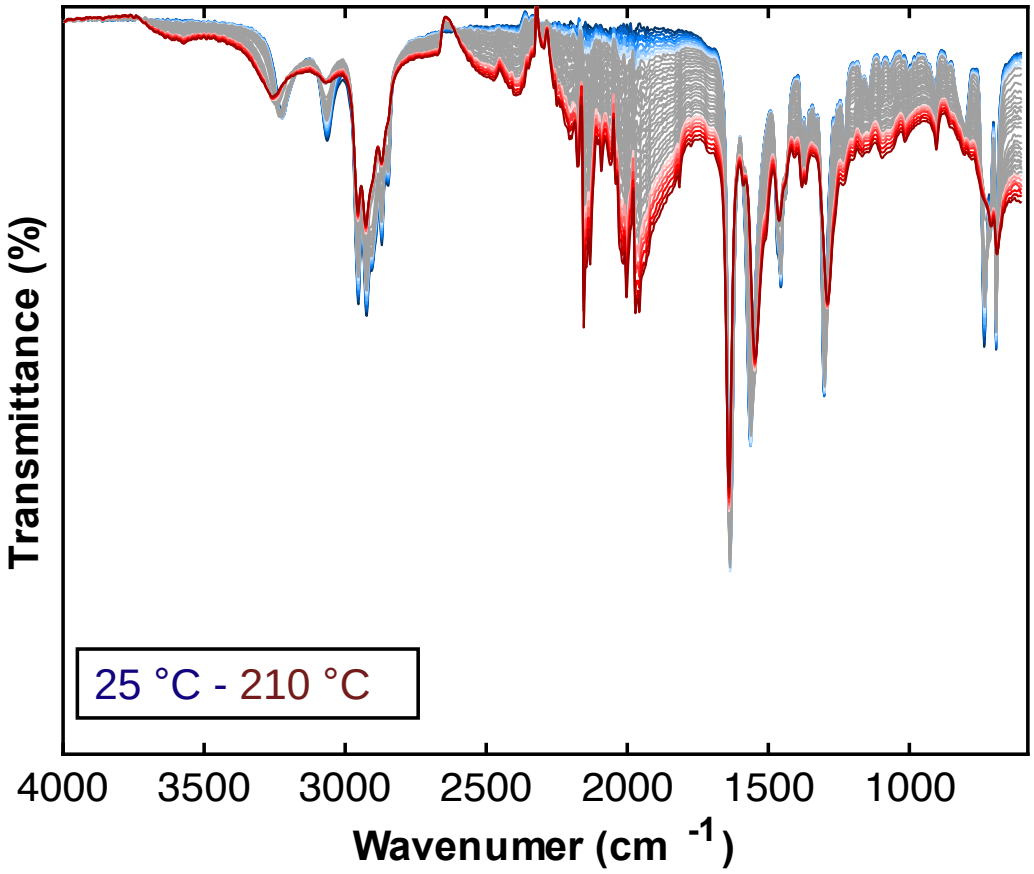

Figure 8.4: *VT-IR spectrum for a sample of (S)-BTA starting at 25 °C till 210 °C, measured every 5 °C.*

8.1.2 aBTA

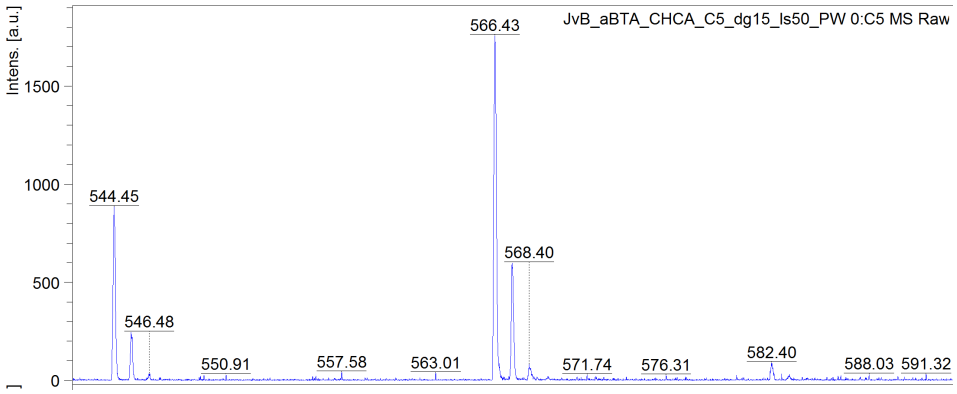

Figure 8.5: *MALDI-TOF MS spectrum of aBTA*

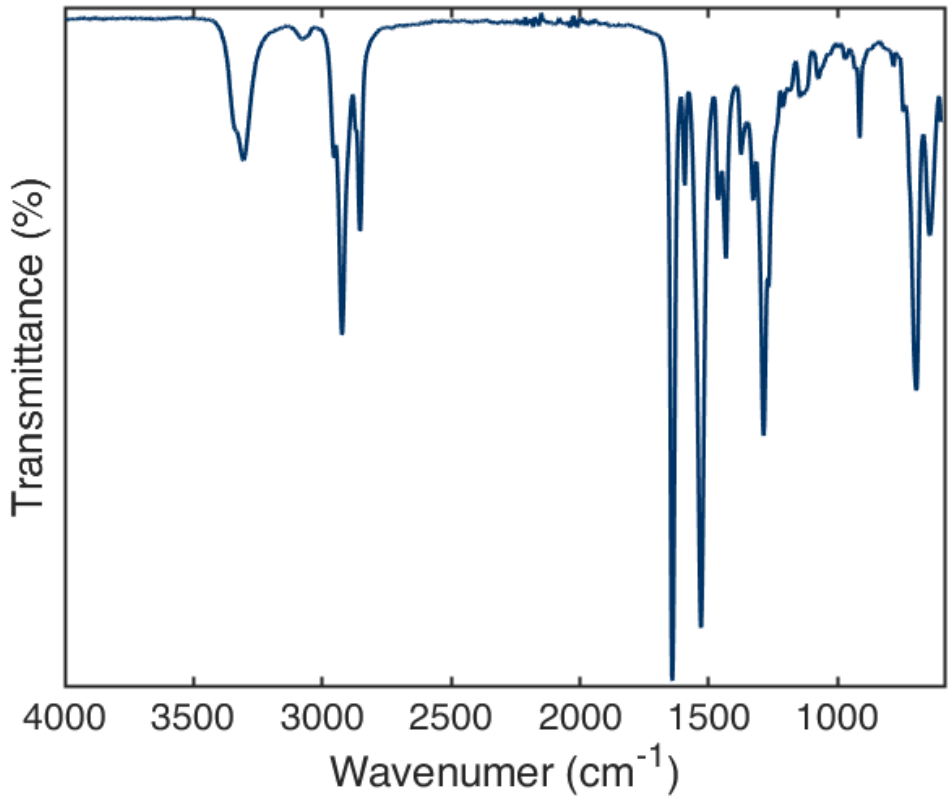

Figure 8.6: *FT-IR spectrum for a solid sample of aBTA at 25 °C*

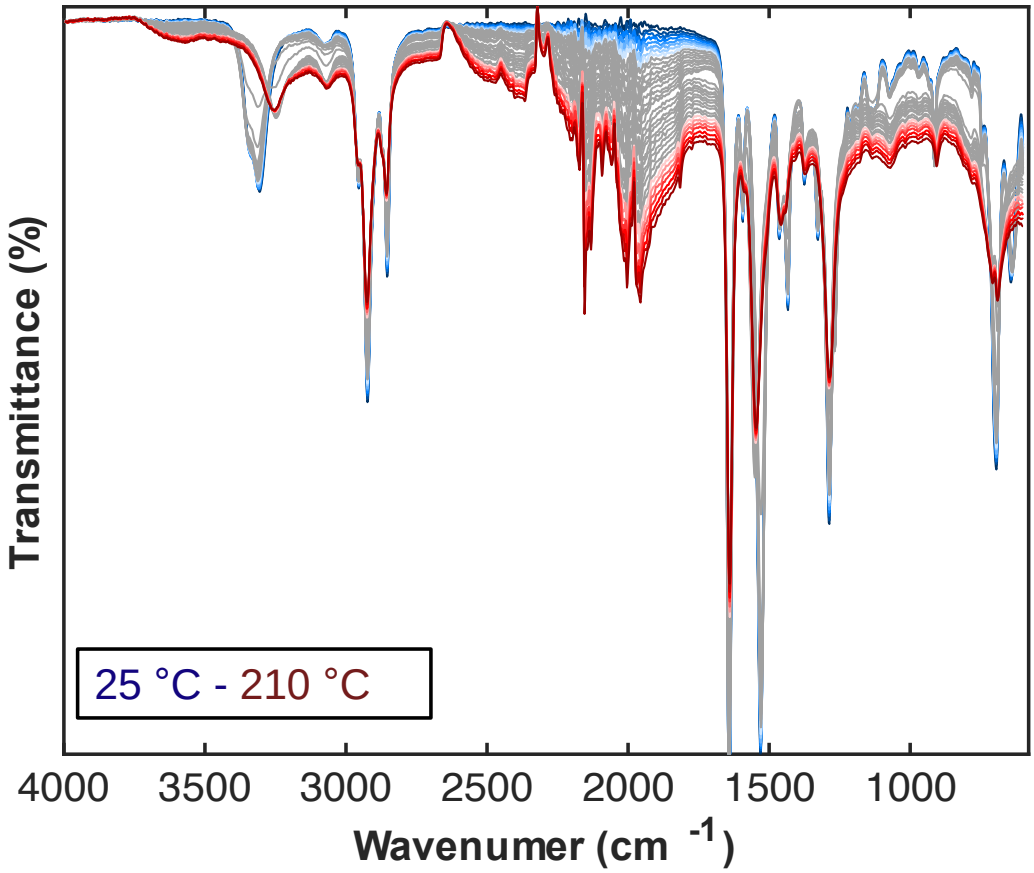

Figure 8.7: *VT-IR spectrum for a sample of aBTA starting at 25 °C till 210 °C, measured every 5 °C.*

8.1.3 gBTA

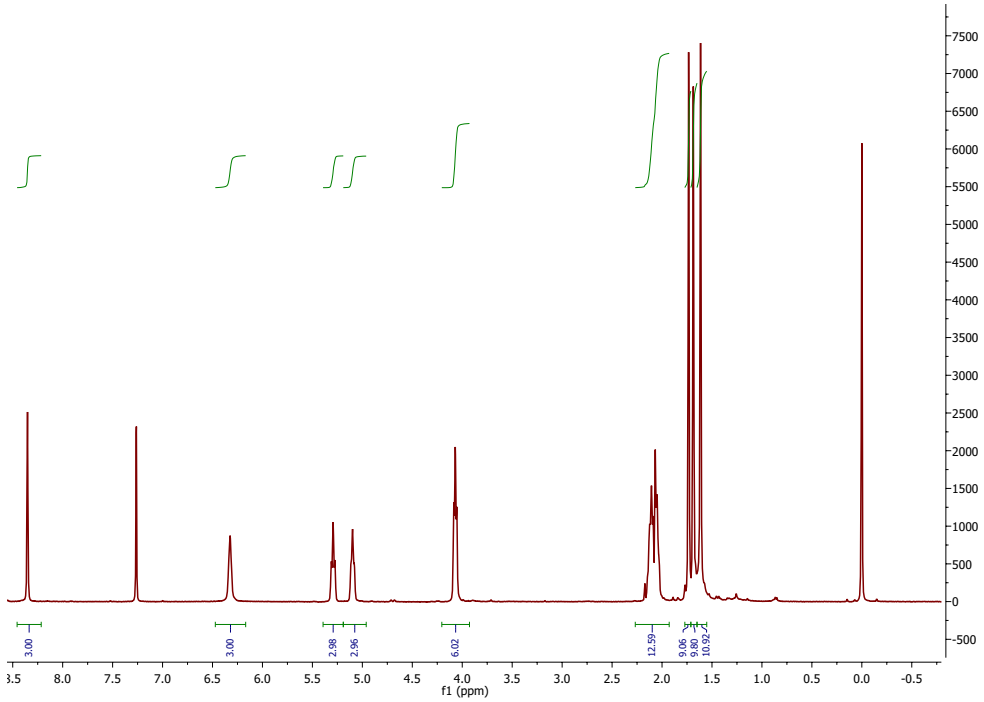

(a)

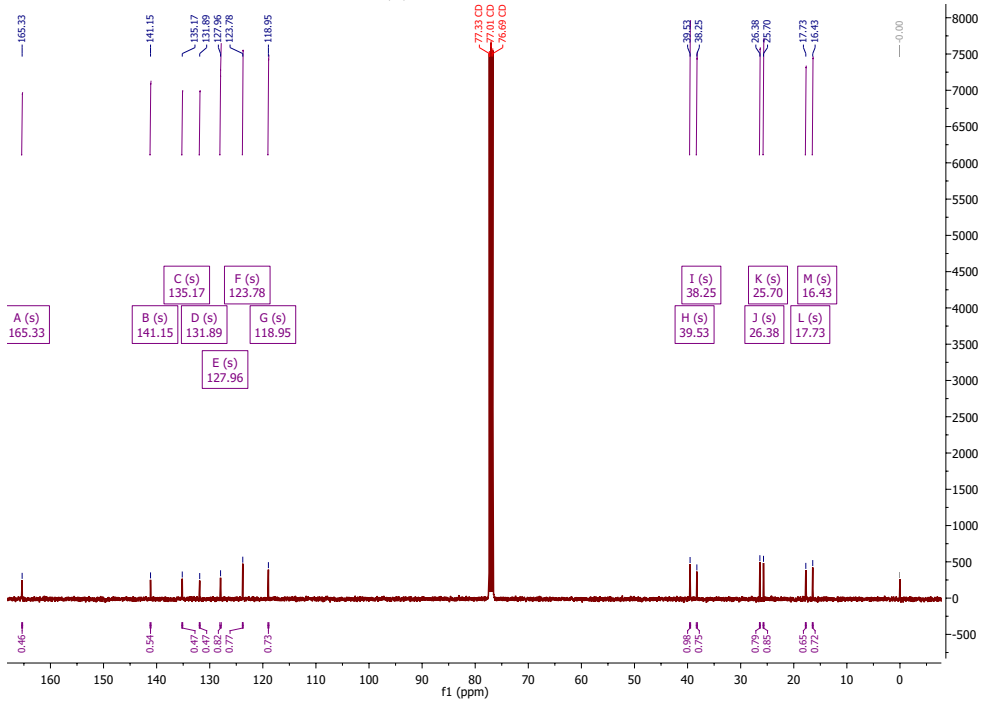

(b)

Figure 8.8: *(a)* ^{1}*H-NMR and (b)* ^{13}*C-NMR spectrum of gBTA*

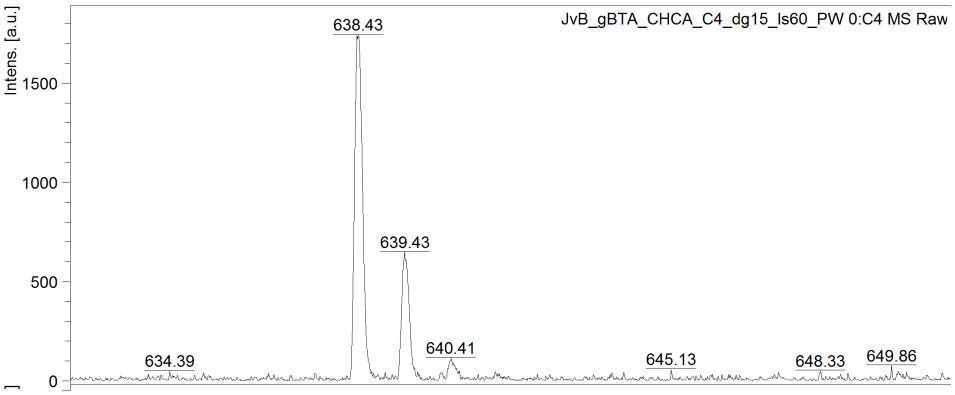

Figure 8.9: *MALDI-TOF MS spectrum of gBTA*

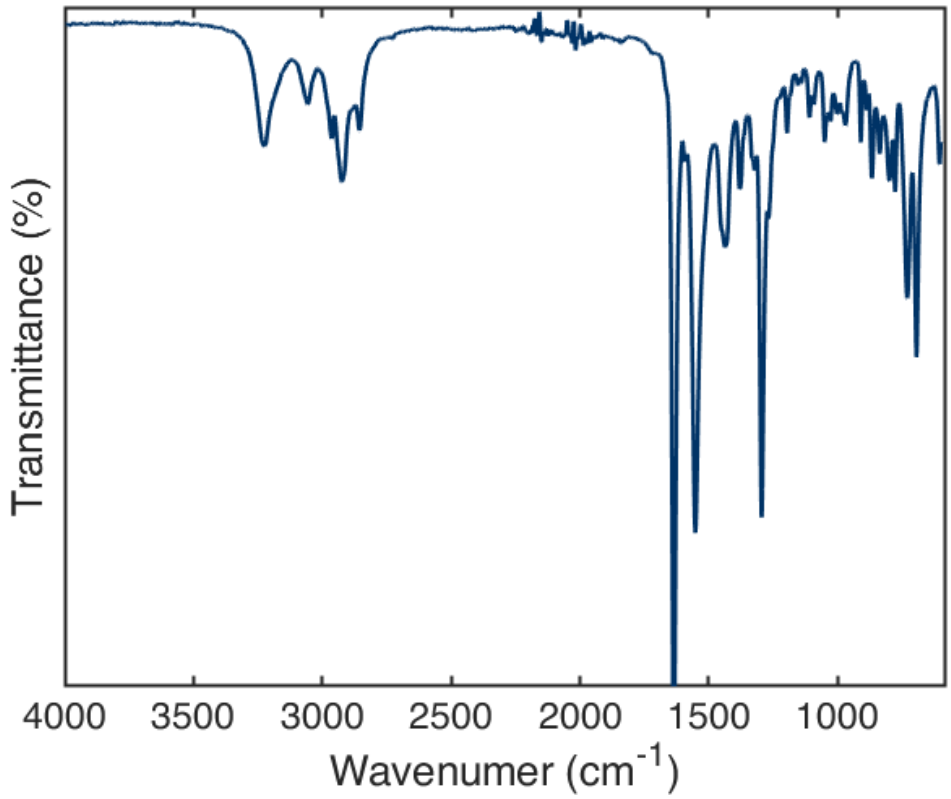

Figure 8.10: *FT-IR spectrum for a solid sample of gBTA at 25 °C*

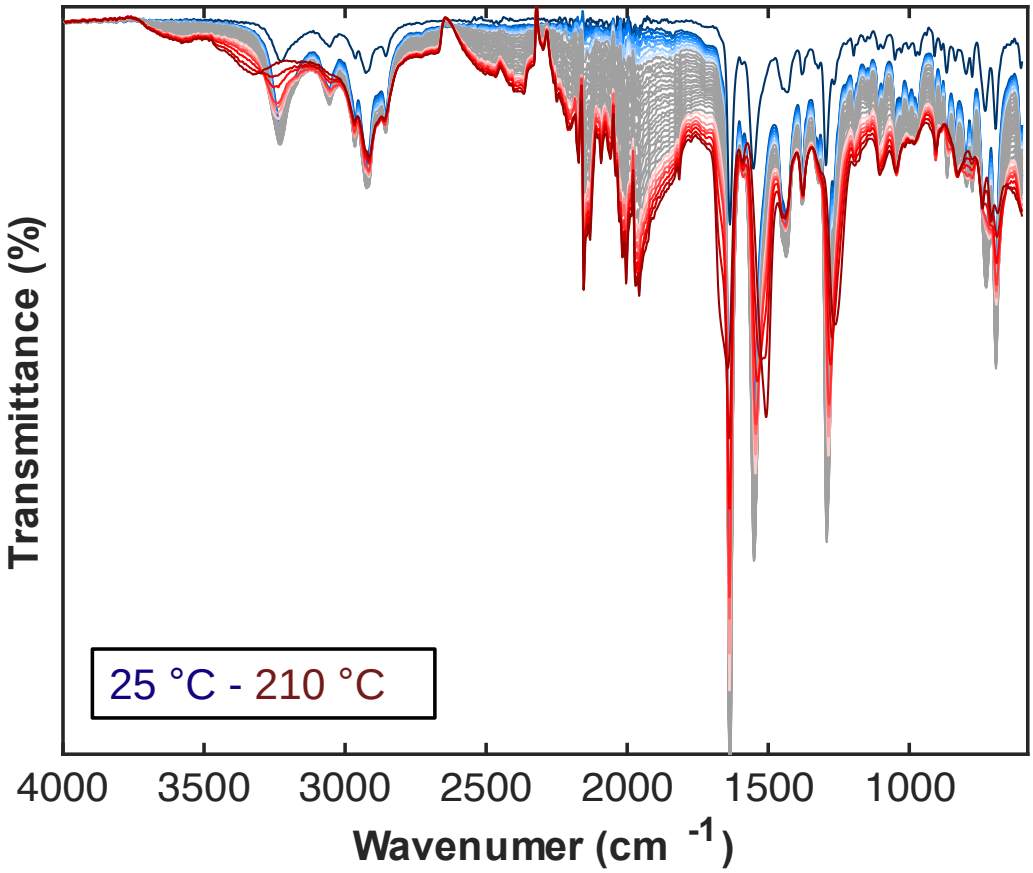

Figure 8.11: *VT-IR spectrum measured for a sample of gBTA starting at 25 °C till 210 °C, measured every 5 °C.*

8.1.4 Intermediate Compounds

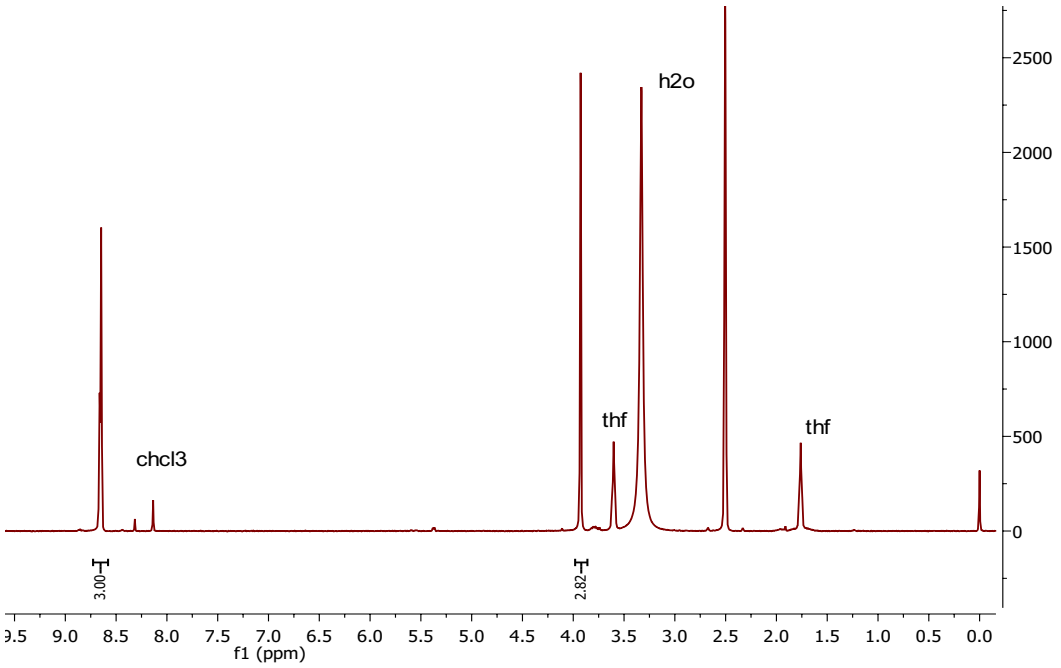

Figure 8.12: ^{1}*H-NMR spectrum of 5-(methoxycarbonyl)isophthalic acid (2b)*

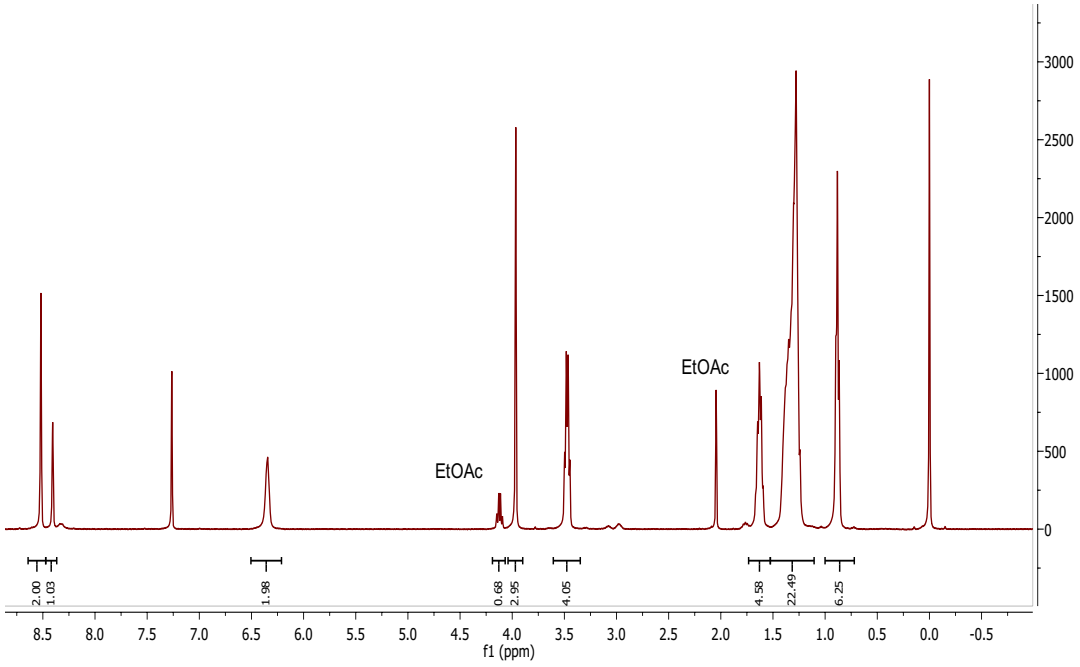

Figure 8.13: ^{1}*H-NMR spectrum of 3,5-bis((octyl)carbamoyl)benzoic methyl ester (2c)*

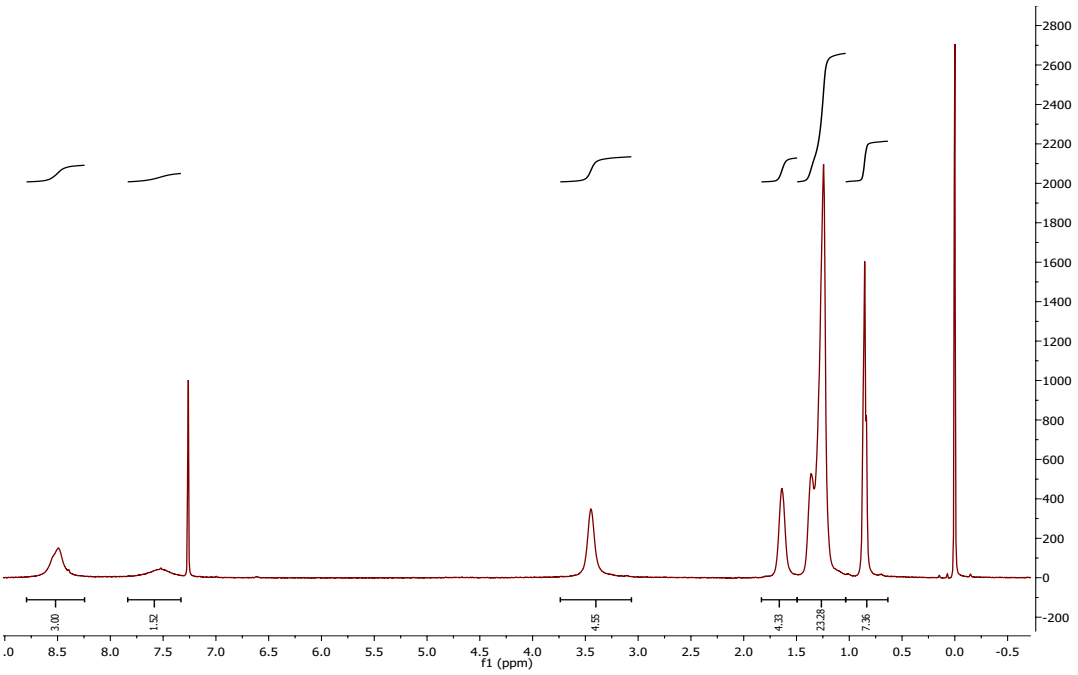

Figure 8.14: ^{1}*H-NMR spectrum of 3,5-bis((octyl)carbamoyl)benzoic acid (2d)*

8.1.5 aagBTA

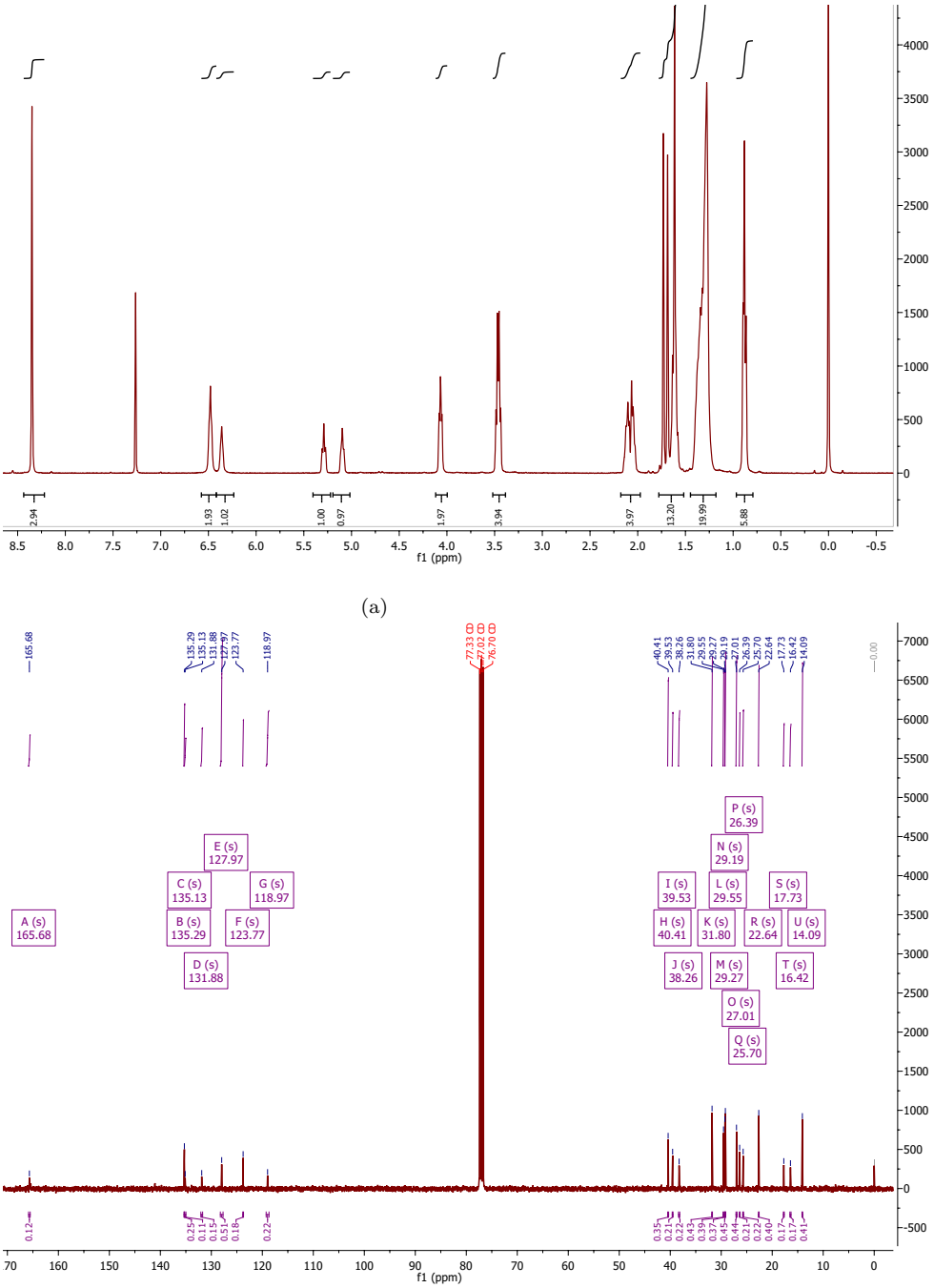

(a)

(b)

Figure 8.15: *(a)* ^{1}*H-NMR and (b)* ^{13}*C-NMR spectrum of aagBTA*

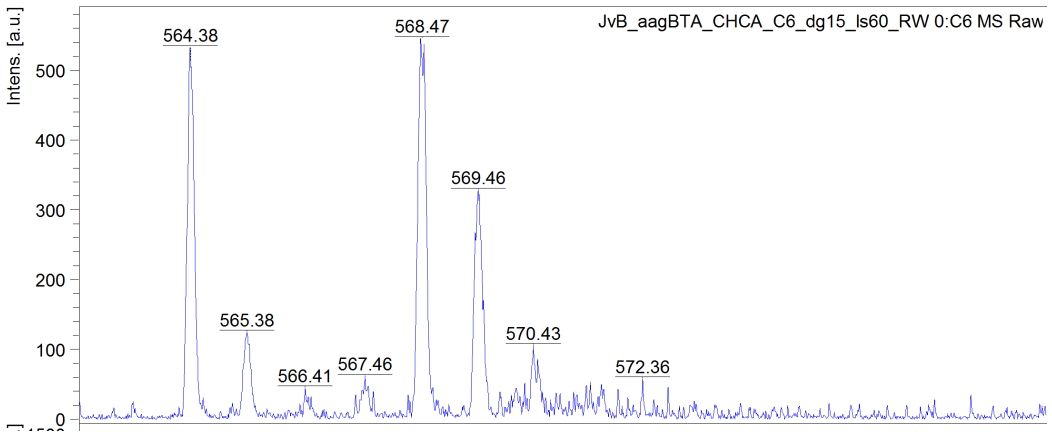

Figure 8.16: *MALDI-TOF MS spectrum of aagBTA*

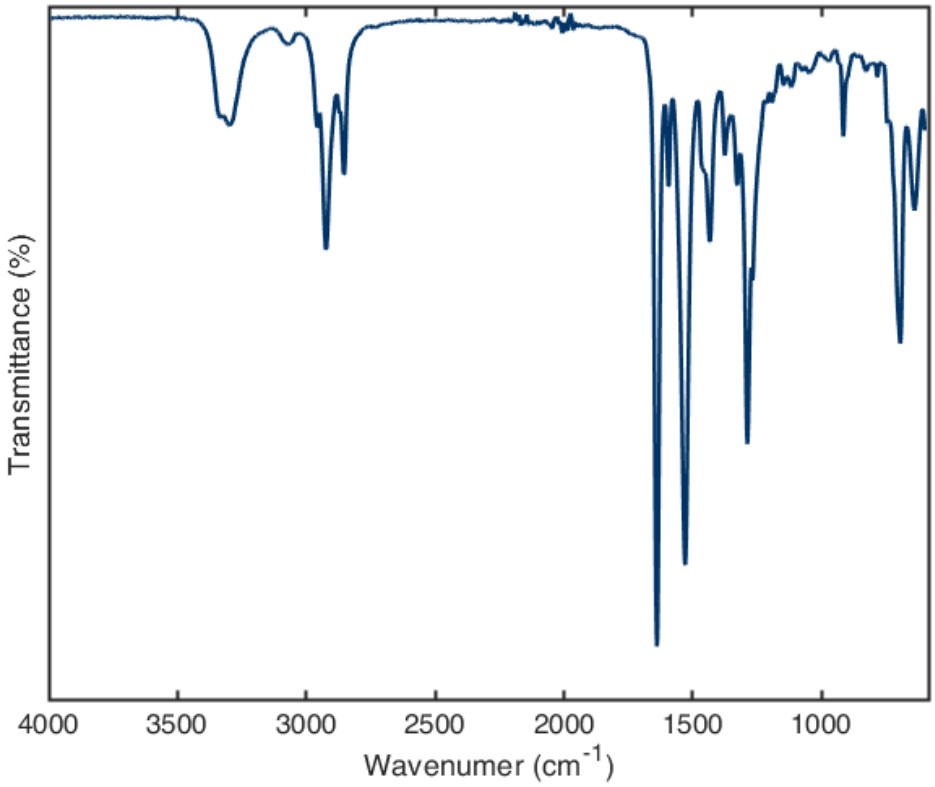

Figure 8.17: *FT-IR spectrum for a solid sample of aagBTA at 25 °C*

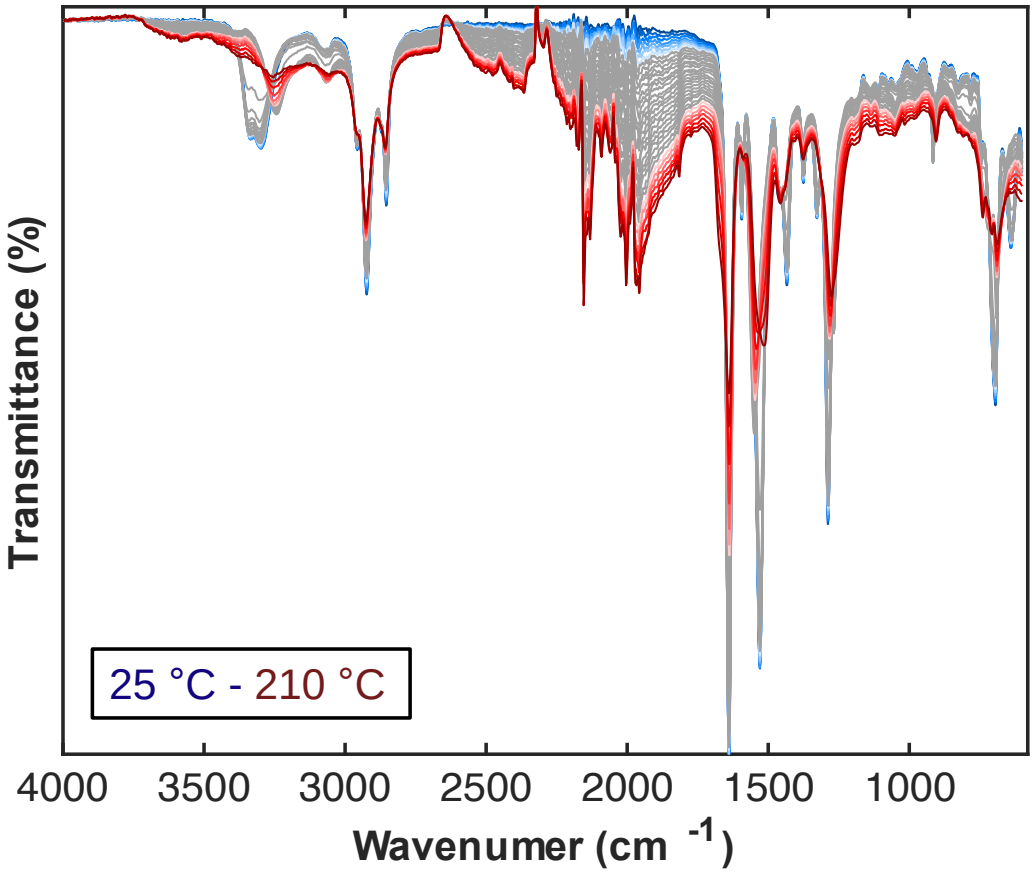

Figure 8.18: *VT-IR spectrum measured for a sample of aagBTA starting at 25 °C till 210 °C, measured every 5 °C.*

8.1.6 L-BTA

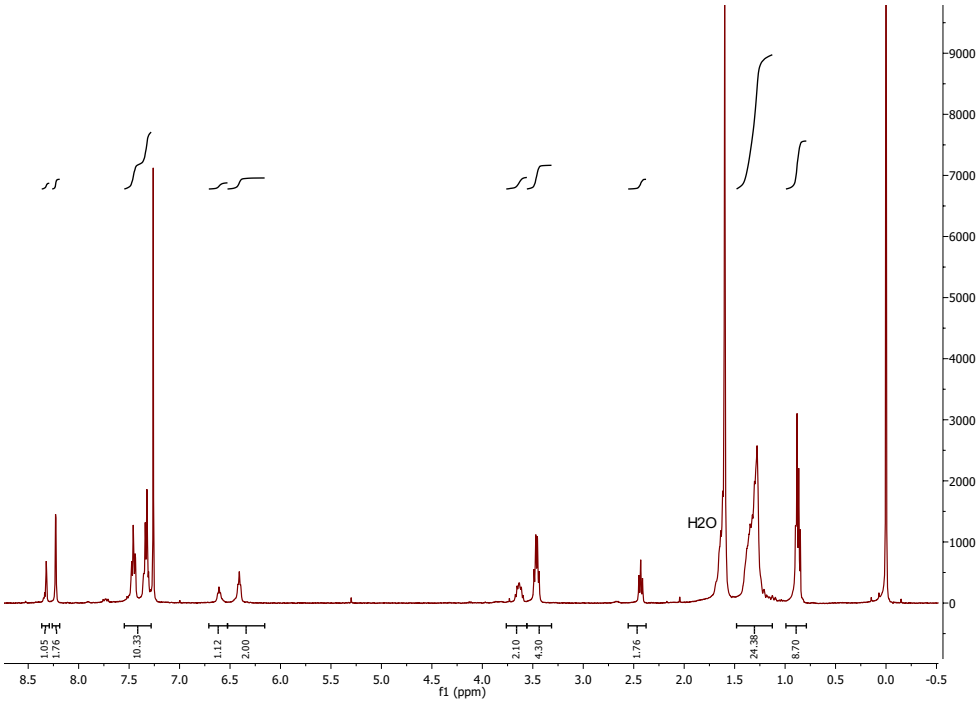

Figure 8.19: ^{1}H-*NMR spectrum of L-BTA*

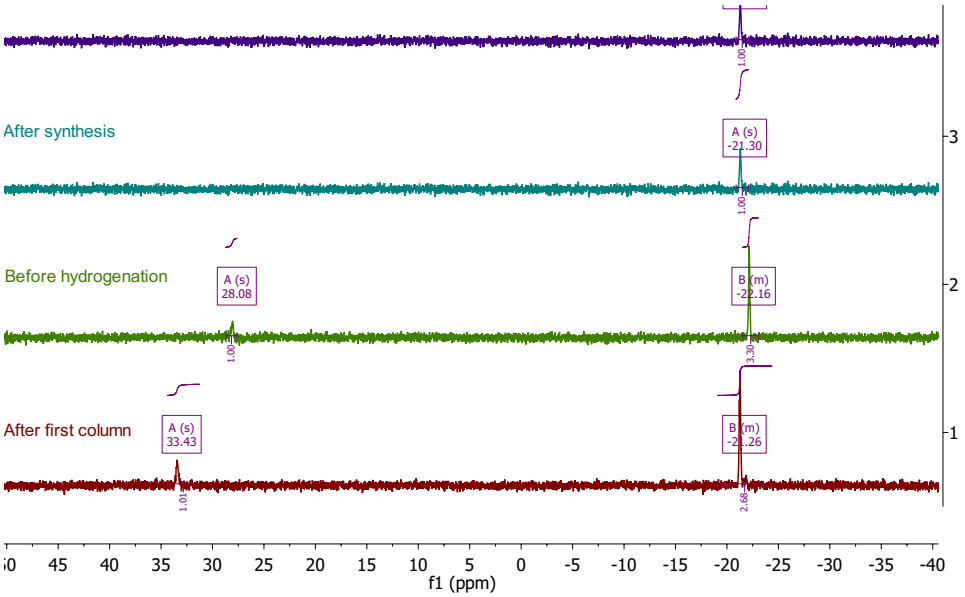

Figure 8.20: ^{31}P-*NMR spectrum of L-BTA*

8.2 Thermodynamic Analysis

8.2.1 One-Component Equilibrium Model

The thermodynamic parameters can be determined using a one-component equilibrium model which is implemented in a MatLab model. The model represents the self-assembly of the system as a one-dimensional linear aggregate. It determines the thermodynamic parameters by fitting the best curve to the experimental data. For better estimation of equilibrium constants and energy terms multiple concentrations are measured. Frequently the ΔS_e and ΔS_n are taken as equal value to simplify the fitting. For that same reason often enthalpy and entropy are set to be independent of temperature. Correspondingly, the ΔG_n and ΔG_e can be extracted from the fit. As a result the K_n, K_e and σ can be calculated.

The matlab model used to determine the thermodynamic parameters was designed by Charley Schaefer. The following general equations were used. M represents a monomer, D the nucleation dimer, P_i a polymer of length i, P_{i+1} a polymer of length i plus one monomer and ΔH^0_{np} is the nucleation penalty.

Nucleation step

$$\mathrm{M} + \mathrm{M} \underset{\mathrm{K}_{n-1}}{\overset{\mathrm{K}_n}{\rightleftharpoons}} \mathrm{D}$$

$$\mathrm{K}_n = \exp\left(-\frac{\Delta \mathrm{G}^0_\mathrm{n}}{\mathrm{RT}}\right), \quad \Delta \mathrm{G}^0_\mathrm{n} = \Delta \mathrm{H}^0_\mathrm{n} - \mathrm{T}\Delta \mathrm{S}^0$$

Elongation step

$$\mathrm{P}_i + \mathrm{M} \underset{\mathrm{K}_{e-1}}{\overset{\mathrm{K}_e}{\rightleftharpoons}} \mathrm{P}_{i+1}$$

$$\mathrm{K}_e = \exp\left(-\frac{\Delta \mathrm{G}^0_\mathrm{e}}{\mathrm{RT}}\right), \quad \Delta \mathrm{G}^0_\mathrm{e} = \Delta \mathrm{H}^0_\mathrm{e} - \mathrm{T}\Delta \mathrm{S}^0$$

Cooperativity paramter and elongation temperature

$$\sigma = \frac{\mathrm{K}_n}{\mathrm{K}_e} = \exp\frac{\Delta \mathrm{H}^0_\mathrm{np}}{\mathrm{RT}}, \quad \Delta \mathrm{H}^0_\mathrm{np} = \Delta \mathrm{H}^0_\mathrm{e} - \Delta \mathrm{H}^0_\mathrm{n}$$

$$1 = \mathrm{c}_\mathrm{tot}\mathrm{K}_e = \mathrm{c}_\mathrm{tot} \exp\left(-\frac{\Delta \mathrm{G}^0_\mathrm{e}}{\mathrm{RT}_\mathrm{e}}\right)$$

8.2.2 Thermodynamic Parameters

The complete table of the thermodynamic parameters and the fitted melting curves.

	(S)-BTA ABS	(S)-BTA CD	aBTA	aagBTA	gBTA
chi square	3.06	6.16	2.60	2.07	2.50
ΔH_e (kJ mol^{-1})	-54.6	-53.9	-53.2	-85.1	-123.0
SD_{He}	1.18	1.32	0.31	2.30	7.11
ΔH_{nuc} (kJ mol^{-1})	-21.5	-26.3	-33.2	-68.6	-105.2
SD_{He}	9.87	4.45	0.32	0.76	1.84
ΔH_{np} (kJ mol^{-1})	-33.1	-27.6	-20.0	-16.4	-17.8
S_0 (J mol^{-1} K^{-1}	-88.1	-85.9	-79.0	-196	-310
SD_{S0}	3.78	4.22	0.97	7.80	23.5
ΔG_e (kJ mol^{-1})	4.31	-1.16	-10.1	-11.2	-14.3
ΔG_n (kJ mol^{-1})	-28.8	-28.7	-30.1	-27.6	-32.2
σ	1.55E-06	1.45E-05	3.12E-04	2.40E-03	1.04E-03
T_e (K) at 50 μM	320.6	-	329.9	311.6	309.8
T_e (K) at 40 μM	317.1	-	326.1	309.5	308.3
T_e (K) at 30 μM	312.8	-	321.4	306.9	305.5
T_e (K) at 20 μM	306.9	-	315.0	303.2	

Table 13: *Thermodynamic parameters describing the supramolecular self-assembly of (S)-BTA, aBTA, aagBTAand gBTA in MCH 5% DCE (v/v). Parameters were obtained by analyzing data obtained from UV spectroscopy experiments with a model of supramolecular polymerization. Changes in Gibbs free energy are reported for 293 K.*

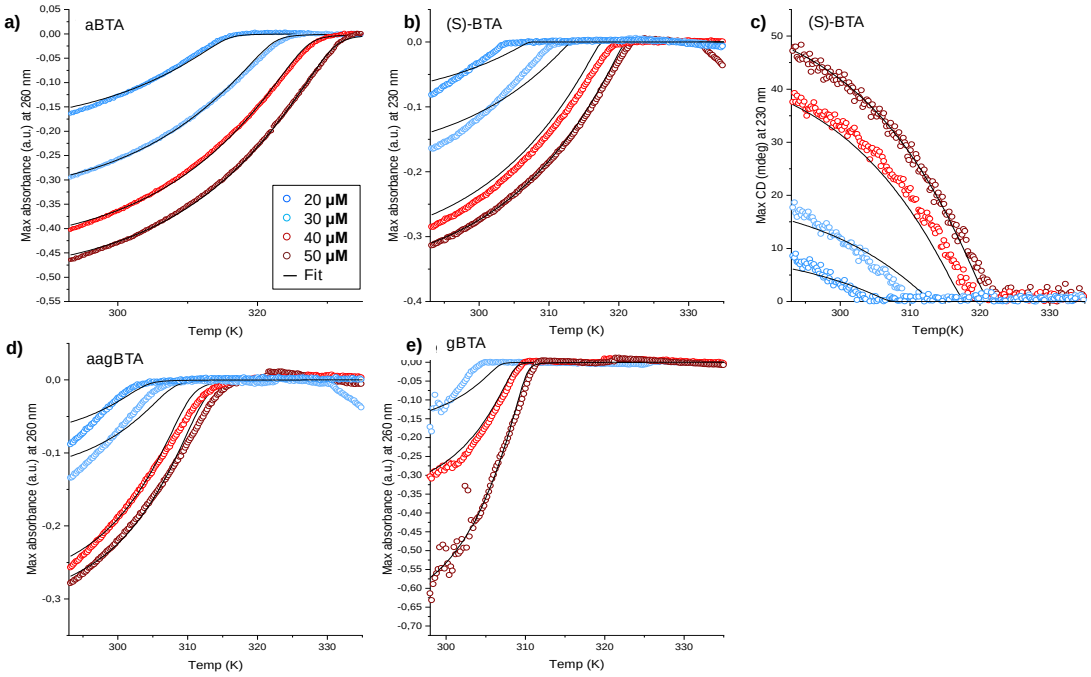

Figure 8.21: *Relative change in absorbance as a function of temperature measured for solution of different concentrations for a) aBTA b) (S)-BTA d) aagBTA and e) gBTA in MCH 5% DCE (v/v). Relative change in CD as a function of temperature measured for solution of c) (S)-BTA. Data and fit represented by open circles and black line respectively.*

8.3 Hydrogenation Table

The full hydrogenation tables of the presented results in Section 4.

Table 14: *Investigation of the reactivity of catalysts IrCl/L and RuCl/L for the enantioselective hydrogenation of gBTA*

Entry	Cat.	Conv.(%)[a]	Entry	Cat.	Conv.(%)[a]
1a	IrCl/(*R,R*)-MeduPhos	<5	7a	RuCl/(*R,R*)-MeduPhos	<5
1b	IrCl/(*R,R*)-MeduPhos	<5	7b	RuCl/(*R,R*)-MeduPhos	<5
2a	IrCl/(*S*)-BINAP	<5	8a	RuCl/(*S*)-BINAP	<5
2b	IrCl/(*S*)-BINAP	<5	8b	RuCl/(*S*)-BINAP	<5
3a	IrCl/(*S*)-PhanPhos	<5	9a	RuCl/(*S*)-PhanPhos	<5
3b	IrCl/(*S*)-PhanPhos	9	9b	RuCl/(*S*)-PhanPhos	<5
4a	IrCl/(*S,S*)-DIOP	10	10a	RuCl/(*S,S*)-DIOP	<5
4b	IrCl/(*S,S*)-DIOP	<5	10b	RuCl/(*S,S*)-DIOP	<5
5a	IrCl/(*R*)-WalPhos	<5	11a	RuCl/(*R*)-WalPhos	<5
5b	IrCl/(*R*)-WalPhos	<5	11b	RuCl/(*R*)-WalPhos	<5
6a	IrCl/(*R*)-PHOX	<5	12a	RuCl/(*R*)-PHOX	<5
6b	IrCl/(*R*)-PHOX	<10	12b	RuCl/(*R*)-PHOX	<5

[b]Conversion of <5% indicates below detectable limit.

Table 15: *Investigation of the reactivity of catalysts IrCl/(R)-PHOX with Et_3SiH as hydrogen donor in the enantioselective hydrogenation of gBTA*

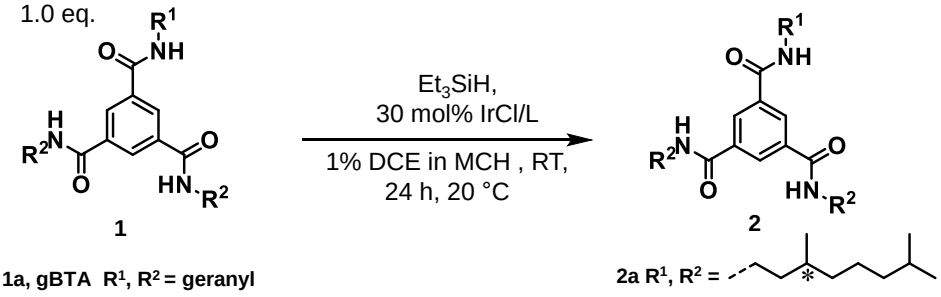

Entry	Cat.	Conv.(%)[a]	Entry	Cat,	Conv.(%)[a]
1a	IrCl/(*R,R*)-MeduPhos	<5	4a	IrCl/(*S,S*)-DIOP	<5
1b	IrCl/(*R,R*)-MeduPhos	<5	4b	IrCl/(*S,S*)-DIOP	<5
2a	IrCl/(*S*)-BINAP	<5	5a	IrCl/(*R*)-WalPhos	<5
2b	IrCl/(*S*)-BINAP	<5	5b	IrCl/(*R*)-WalPhos	<5
3a	IrCl/(*S*)-PhanPhos	<5	6a	IrCl/(*R*)-PHOX	<5
3b	IrCl/(*S*)-PhanPhos	<5	6b	IrCl/(*R*)-PHOX	<5

[a]Conversion of <5% indicates below detectable limit.

Table 16: *Influence of vol% DCE on reactivity of IrCl/(R)-PHOX catalyst for the enantioselective hydrogenation of gBTA and aagBTA.*

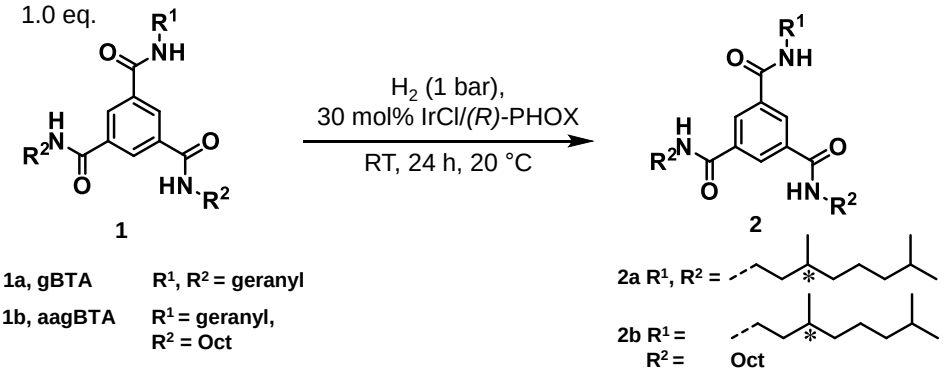

Entry	Substrate	Cat. loading (mol%)	Solv. A	Solv. B (vol%)	Conv. (%)
1a	**1a**	30	-	DCM (100)	54
1b	**1a**	30	-	DCM (100)	86
1c	**1a**	30	-	DCM (100)	88
2a	**1a**	30	-	DCE (100)	61
2b	**1a**	30	-	DCE (100)	63
2c	**1a**	30	-	DCE (100)	44
3a	**1a**	30	MCH	DCE (80)	45
3b	**1a**	30	MCH	DCE (80)	47
3c	**1a**	30	MCH	DCE (80)	39
4a	**1a**	30	MCH	DCE (50)	39
4b	**1a**	30	MCH	DCE (50)	45
4c	**1a**	30	MCH	DCE (50)	39
5a	**1a**	30	MCH	DCE (20)	43
5b	**1a**	30	MCH	DCE (20)	67
5c	**1a**	30	MCH	DCE (20)	64
6a	**1a**	30	MCH	DCE (10)	10
6b	**1a**	30	MCH	DCE (10)	$<5^a$
7a	**1b**	10	MCH	DCE (20)	20
7b	**1b**	10	MCH	DCE (20)	16
8a	**1b**	10	MCH	DCE (10)	16
8b	**1b**	10	MCH	DCE (10)	16
9a	**1b**	10	MCH	DCE (5)	13
9b	**1b**	10	MCH	DCE (5)	25
10a	**1b**	10	MCH	-	$<5^a$
10b	**1b**	10	MCH	-	$<5^a$

[a]Conversion of <5% indicates below detectable limit.

Table 17: *Investigation of the activity of catalysts IrCl/L and RuCl/L for the enantioselective hydrogenation of gBTA and aagBTA.*

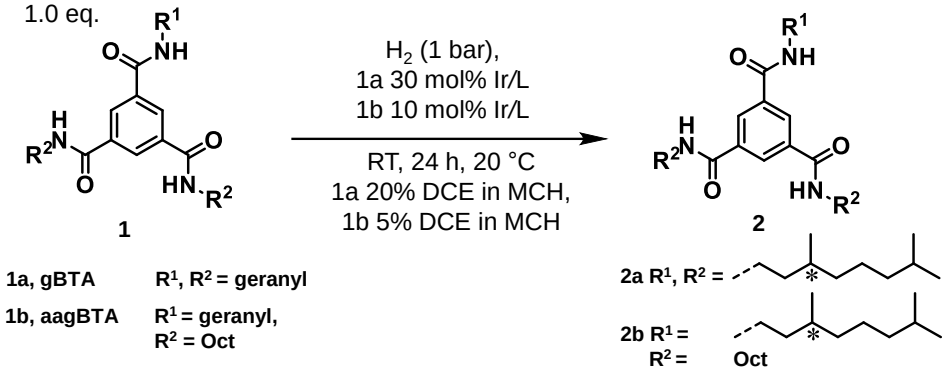

Entry	Sub.	Cat.	Conv. (%)[a]	Entry	Sub.	Cat.	Conv. (%)[a]
1a	**1a**	IrCl/(*R,R*)-MeduPhos	<5	13a	**1b**	IrCl/(*R,R*)-MeduPhos	<5
1b	**1a**	IrCl/(*R,R*)-MeduPhos	<5	13b	**1b**	IrCl/(*R,R*)-MeduPhos	10
2a	**1a**	IrCl/(*S*)-BINAP	51	14a	**1b**	IrCl/(*S*)-BINAP	17
2b	**1a**	IrCl/(*S*)-BINAP	87	14b	**1b**	IrCl/(*S*)-BINAP	17
3a	**1a**	IrCl/(*S*)-PhanPhos	47	15a	**1b**	IrCl/(*S*)-PhanPhos	10
3b	**1a**	IrCl/(*S*)-PhanPhos	52	15b	**1b**	IrCl/(*S*)-PhanPhos	13
4a	**1a**	IrCl/(*S,S*)-DIOP	79	16a	**1b**	IrCl/(*S,S*)-DIOP	14
4b	**1a**	IrCl/(*S,S*)-DIOP	81	16b	**1b**	IrCl/(*S,S*)-DIOP	35
5a	**1a**	IrCl/(*R*)-WalPhos	28	17a	**1b**	IrCl/(*R*)-WalPhos	13
5b	**1a**	IrCl/(*R*)-WalPhos	55	17b	**1b**	IrCl/(*R*)-WalPhos	15
6a	**1a**	IrCl/(*R*)-PHOX	71	18a	**1b**	IrCl/(*R*)-PHOX	24
6b	**1a**	IrCl/(*R*)-PHOX	69	18b	**1b**	IrCl/(*R*)-PHOX	25
7a	**1a**	RuCl/(*R,R*)-MeduPhos	<5	19a	**1a**	IrCl	<5
7b	**1a**	RuCl/(*R,R*)-MeduPhos	<5	19b	**1a**	IrCl	<5
8a	**1a**	RuCl/(*S*)-BINAP	<5	20a	**1b**	IrCl	<5
8b	**1a**	RuCl/(*S*)-BINAP	<5	20b	**1b**	IrCl	<5
9a	**1a**	RuCl/(*S*)-PhanPhos	<5				
9b	**1a**	RuCl/(*S*)-PhanPhos	<5				
10a	**1a**	RuCl/(*S,S*)-DIOP	<5				
10b	**1a**	RuCl/(*S,S*)-DIOP	<5				
11a	**1a**	RuCl/(*R*)-WalPhos	<5				
11b	**1a**	RuCl/(*R*)-WalPhos	<5				
12a	**1a**	RuCl/(*R*)-PHOX	<5				
12b	**1a**	RuCl/(*R*)-PHOX	<5				

[a]Conversion of <5% indicates below detectable limit.

Table 18: *Influence of the pressure on the reactivity of catalysts IrCl/(R)-PHOX for the enantioselective hydrogenation of gBTA and aagBTA.*

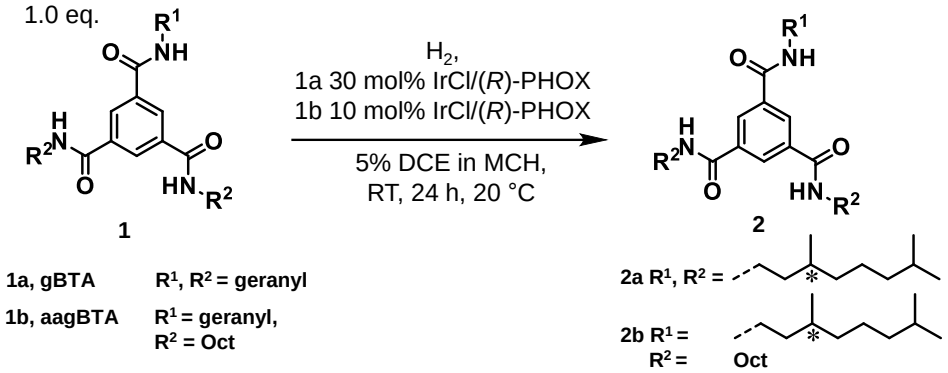

Entry	Substrate	Pressure (bar)	Conv. (%)[a]
1a	**1a**	1	<5
1b	**1a**	1	22
1c	**1a**	1	<5
2a	**1a**	50	38
2b	**1a**	50	79
3a	**1b**	1	17
3b	**1b**	1	23
3c	**1b**	1	24
4a	**1b**	50	33
4b	**1b**	50	37

[a] Average conversion is listed, the full table can be found in Section 8.3

Table 19: *Influence of the catalyst loading on the reactivity of catalysts IrCl/(R)-PHOX for the enantioselective hydrogenation of aagBTA.*

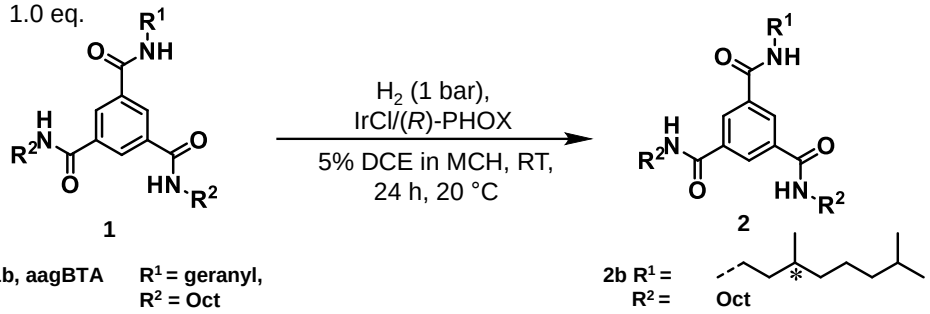

Entry	Cat. loading (mol%)	Conv. (%)
1a	30/60	52
1b	30/60	49
2a	10/20	24
2b	10/20	23
2c	10/20	25
3a	5/10	7
3b	5/10	6
4a	2/4	$<5^b$
4b	2/4	$<5^b$
5a	10/60	$<5^b$
5b	10/60	$<5^b$

[b]Conversion of <5% indicates below detectable limit.

Table 20: *Investigation of IrCl/PPh$_3$ and L-BTA for the enantioselective hydrogenation of gBTA and aagBTA*

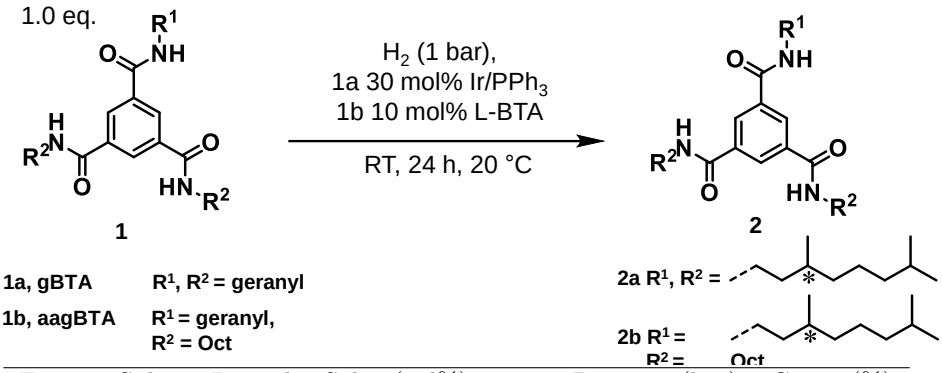

Entry	Subs.	Ligand	Solv. (vol%)	Pressure (bar)	Conv. (%)
1a	**1a**	PPh3	DCM (100)	1	41
1b	**1a**	PPh3	DCM (100)	1	64
1c	**1a**	PPh3	DCM (100)	1	45
1d	**1a**	PPh3	DCM (100)	1	50
2a	**1a**	PPh3	DCE (100)	1	62
2b	**1a**	PPh3	DCE (100)	1	53
2c	**1a**	PPh3	DCE (100)	1	66
2d	**1a**	PPh3	DCE (100)	1	36
2e	**1a**	PPh3	DCE (100)	1	34
3a	**1a**	PPh3	MCH/DCE (95/5)	50	>99
3b	**1a**	PPh3	MCH/DCE (95/5)	50	87
3c	**1a**	PPh3	MCH/DCE (95/5)	50	>99
3d	**1a**	PPh3	MCH/DCE (95/5)	50	>99

8.4 Investigation for Oxidation of (*R*)-PHOX

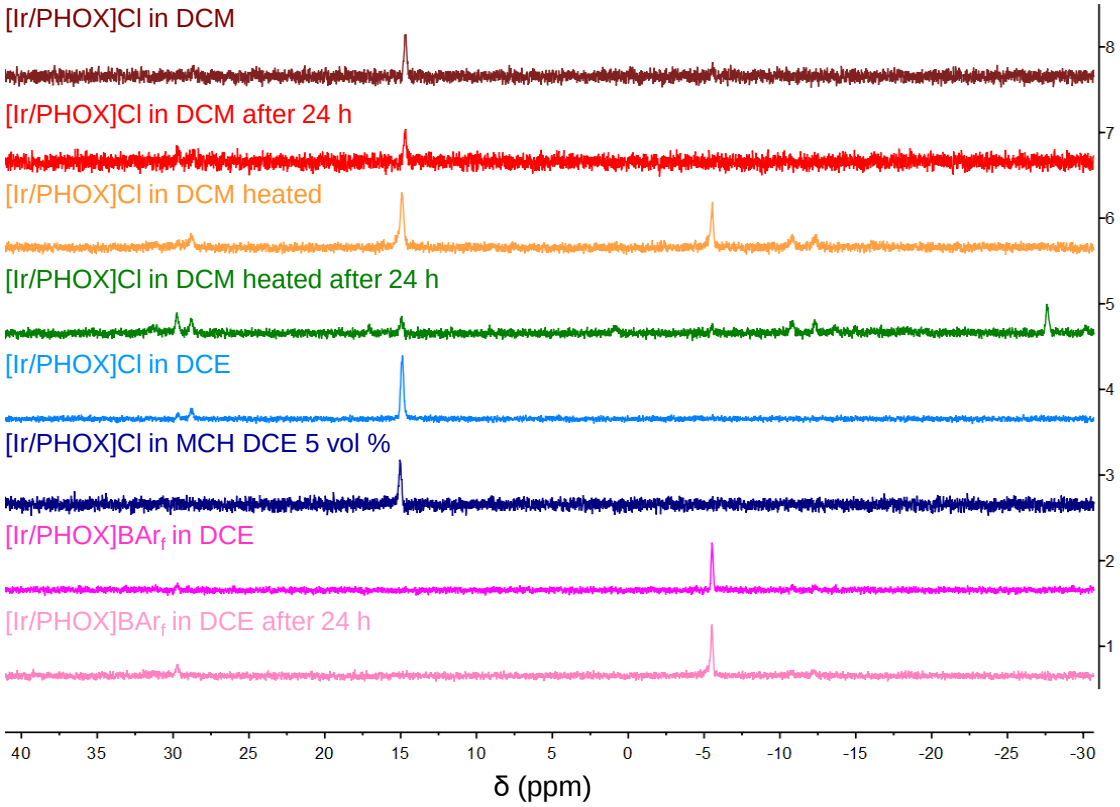

Figure 8.22: ^{31}*P-NMR spectrum of R-PHOX. A signal* $\delta < 0$ *implies that the phosphor atom is bonded to iridium. Where a signal* $\delta > 0$ *implies that phosphor atom is oxidized.*

8.5 MCH Contamination

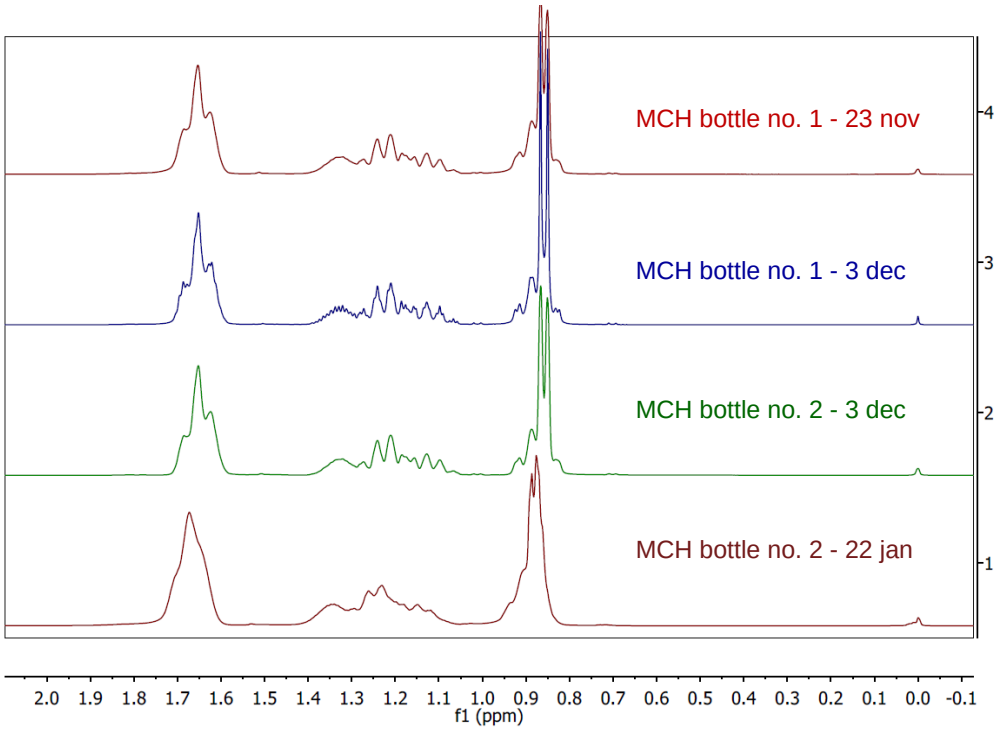

Figure 8.23: ^{1}*H-NMR spectrum of crude mixture of MCH and* $CDCl_3$.